TECHNICAL UNIVERSITY OF LIBEREC
UNIVERSITY PAUL SABATIER TOULOUSE III

Faculty of Mechatronics and Interdisciplinary Engineering Studies

Center for Plasma Physics and Applications in Toulouse

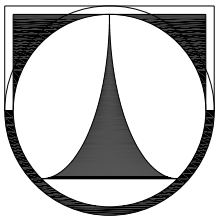

ELECTRIC CONDUCTIVITY MODEL OF DISCHARGE LAMPS

2007

Jan Koprnický

Electric Conductivity Model of Discharge Lamps

Ph.D. thesis in the branch of Technical Cybernetics

Jan Koprnický

Technical University of Liberec

Faculty of Mechatronics and Interdisciplinary Engineering Studies

University Paul Sabatier Toulouse III

Center for Plasma Physics and Applications in Toulouse

2007

Name of the thesis: Electric Conductivity Model
of Discharge Lamps

Doctoral Candidate: Ing. Jan Koprnický
Study programme: 2612V Electrical Engineering and Computer Science
Specialization area: 2612V045 Technical Cybernetics
Department: Institute of Mechatronics and Technical Informatics
Faculty of Mechatronics and Interdisciplinary
Engineering Studies
Technical University of Liberec

Center for Plasma Physics and Applications
in Toulouse
University Paul Sabatier Toulouse III

Supervisors: Prof. Ing. Aleš Richter, CSc. (FM TUL)
Prof. Dr. Georges Zissis (CPAT UPS)

Poděkování

Tato práce vznikla pod trpělivým vedením Prof. Ing. Aleše Richtera, CSc., kterému bych rád poděkoval za mnohé rady, připomínky a nezbytné materiální a organizační zajištění v průběhu studia.

Rád bych též poděkoval přátelskému kolektivu katedry elektrotechniky jmenovitě pak Mírovi Novákovi, Honzovi Václavíkovi, Leoši Beranovi, Jiřímu Kubínovi, Tomáši Slukovi, Honzovi Krausovi, Patrikovi Endlerovi, Petrovi Přívratskému, Martinovi Diblíkovi, Pepovi Černohorskému, Honzovi Vodolanovi, Tomáši Mikolandovi, s kterými jsem sdílel slasti i strasti výuky a s nimiž jsem často v plodných diskusích nalézal mnohé odpovědi nejen na technické otázky.

Na tomto místě bych také rád poděkoval přátelům, kteří mi vždy vyšli vstříc, zvláště pak Pavlovi Herajnovi a Honzovi Alešovi, neboť jsou podivuhodní.

Děkuji úterním podvečerům a společnosti, která mne provázela celým mým studiem.

Největší dík však patří mé rodině a přítelkyni, bez jejichž podpory a porozumění bych se neobešel.

Acknowledgement

I would like to sincerely thank my advisor at CPAT, prof. Georges Zissis, for his guidance and support throughout this work.

I would like to extend my sincerely thanks to colleagues of CPAT Bruno Laffitte, Adrian Harabor, Sounil Bhosle, David Buso, Jasmine Legere and others for their valuable discussions, hospitality and friendly atmosphere at CPAT and outside.

Special thanks to Dr. ir. Pascal Dupuis, whose advises and collaboration gave me a lot.

At last I would like to thank to coordinator of bilateral cooperation between TUL and UPS Mrs. Josiane Poque for her kindness in organisation and official matters.

This work has been supported by the EU COST action n°529 - Efficient Lighting for the 21^{st} Century and by the Ministry of Education of Czech Republic (Project Code MSM 242200002).

Liberec, April 2007

Anotace

Tato dizertační práce se zabývá modelováním světelných výbojů pro popis elektrických obvodů. Nejedná se o modelování plazmatu, ve smyslu modelování jeho vnitřních dějů, ale o využití rovnice elektrické vodivosti světelného výboje, která však vychází z jeho fyzikálního rozboru.

Parametry vodivostního modelu jsou určeny z naměřených napěťových a proudových charakteristik v praxi běžně používaných výbojek bez znalosti technologických dat od výrobce. Zpracování naměřených dat $u(t), i(t)$, aplikace idetifikačního algoritmu a simulace elektrických obvodů je provedena v prostředí Matlab, resp. Matlab Simulink.

Výsledky simulace jsou porovnány s naměřenými údaji. Model je ověřen v simulacích nízkotlakých i vysokotlakých výbojek v zapojení s elektromagnetickými předřadníky.

Klíčová slova: dynamický vodivostní model, identifikace parametrů, model v Matlabu, nelineární zátěž, simulace elektrických obvodů, světelené zdroje, výbojky.

Annotation

This Ph.D. thesis deals with light discharges modelling for description of electric circuits. It is not modelling of internal behaviour of a plasma, but its equivalent conductivity.

The parameters of conductivity model are determined from measured voltage and current characteristics of discharge lamps. This model does not require any technological data from lamp producers. The Matlab/Matlab Simulink is used for data processing of $u(t), i(t)$, application of identification algorithms and electric circuits simulation.

The simulated results are compared with measurements. The model is tested in simulations of low and high pressure discharge lamps in circuits with magnetic ballasts.

Key words: discharge lamps, dynamic conductivity model, light sources, Matlab model, nonlinear load, parameter estimation, simulation of electric circuits.

Annotation[1]

Cette thèse de doctorat est consacrée à la modélisation de décharges luminescentes pour la description de circuits électriques. L'objet n'est pas la modélisation du comportement interne d'un plasma, mais de sa conductivité équivalente.

Les paramètres de la conductivité sont déterminés à partir des caractéristiques de tension et de courant de lampes à décharges. Ce modèle ne requiert aucune donnée technologiques de la part des fabricants de lampe. L'environnement Matlab/Matlab Simulink est utilisé pour le traitement de $u(t), i(t)$, l'exécution des algorithmes d'identification et la simulation en termes de circuits électriques équivalents.

Les résultats des simulations sont comparés avec les données mesurées. Le modèle de conductance est testé dans des simulations de lampes à décharge à basse et haute pression, alimentées par ballast magnétique.

Mots Clés: lampes à décharges, modèle de conductance dynamique, sources d'éclairage, modèle MatLab, charge non-linéaire, estimation de paramètres, simulation de circuits électriques.

[1] translated by Pascal Dupuis

Contents

List of Figures

List of Tables

List of Symbols

Term	Unit	Definition
a_{1-6}		Lamp model parameters eq. (3.21), (3.24), (3.25), (3.26)
a_2	J^{-1}	Lamp model parameter eq. (1.1)
A	$s^5A^2m^{-4}kg^{-2}$	Lamp model parameter eq. (3.14)
A		Lamp model parameter eq. (3.3)
A_{1-4}		Lamp model parameters eq. (3.10)
$A_p(P_{lamp})$		Lamp model power function eq. (3.2)
A, B, C, D		Lamp model parameters eq. (3.21)
b_1	Hz	Thermal losses and the number of elastic collisions eq. (3.33)
b_2	$V^2A^{-2}s^{-1}$	Radiation losses eq. (3.33)
b_k		Lamp model constant eq. (1.1)
B		Lamp model parameter eq. (3.3)
B	s^{-1}	Lamp model parameter eq. (3.14)
B_{1-4}		Lamp model parameters eq. (3.10)
$B_p(P_{lamp})$		Lamp model power function eq. (3.2)
C	F	Capacitance
C		Lamp model parameter eq. (3.14)
C_{1-4}		Lamp model parameters eq. (3.11)
d	m	Distance between electrodes
D		Lamp model parameter eq. (3.11)
D		Lamp model parameter eq. (3.14)
e	C	Electron charge
E	Vm^{-1}	Scalar of electric field intensity
$\mathbf{E}$	Vm^{-1}	Vector of electric field intensity
f	Hz	Frequency
F	$kgA^{-2}s^{-3}m^{-1}$	Lamp model parameter eq. (3.8)
g	S	Instantaneous value of electric conductivity

Term	Unit	Definition
$\mathbf{g}$	S	Oscillogram (vector) of measured lamp conductivity
$\mathbf{g}_M$	S	Oscillogram (vector) of simulated lamp conductivity
g_s	Sm	Electric conductivity eq. (3.29)
G	S	Electric conductivity
G^k	S^k	k^{th} power of electric conductivity
h	m	Distance
h	Js	Planck's constant
i	A	Instantaneous value of electric current
i_{lamp}	A	Instantaneous value of lamp current
$\mathbf{i}_{lamp}$	A	Oscillogram (vector) of lamp current
$i_{lampNDC}$	A	Instantaneous value of lamp electric current without DC value
I	A	Electric current
$\mathbf{I}$	A	Complex current
$\bar{I}(t)$	A	Time-varying phasor of current
I_n	A	n^{th} harmonic of current
$\mathbf{I}_{lamp}$	A	Phasor of lamp current
I_{rms}	A	RMS value of current
$\mathbf{j}$	Am^{-2}	Vector of electric current density
$\mathbf{j}_e$	Am^{-2}	Vector of electron current density
$\mathbf{j}_i$	Am^{-2}	Vector of ion current density
$J(\mathbf{x})$		Criterion
k		Lamp model parameter eq. (3.4)
k		Mathematical parameter
k	JK^{-1}	Boltzmann's constant
$K_{1,2,3}$		Lamp model parameters eq. (3.7)
L	H	Inductance
L	m	Length of discharge channel eq. (3.32)
n_e	m^{-3}	Electron density
p	Pa	Pressure
P	W	Real power
p_{Ar}	Pa	Pressure of argon gas
P_{ball}	W	Ballast real power
P_{con}	W	Thermal conduction loss
P_{def}	W	Deformation power
P_{in}	W	Input power
P_{lamp}	W	Lamp imput power

Term	Unit	Definition
P_{rad}	W	Radiation loss
qu		Criterion number
Q	VAr	Reactive power
Q_{ball}	VAr	Ballast reactive power
Q_1	VAr	Reactive power of the first harmonic
r	m	Radius of tube of discharge lamp
R	Ω	Resistance
$\mathcal{R}$	Ω	Discharge resistance
R_{diff}	Ω	Differential resistance
R_{eq}	Ω	Lamp model equivalent resistance eq. (3.7)
R_s	Ω	Lamp model parameter eq. (3.7)
S	m^2	Cross-section
S	VA	Complex power
S_{ball}	VA	Ballast complex power
t	s	Time
T	K	Temperature
T	s	Period of harmonic and inharmonic signal
T_0	K	Temperature of arc tube wall eq. (3.25)
T_c	K	Temperature of hot zone
T_{CS}	K	Cold-spot temperature
T_e	K	Electron temperature
T_g	K	Gas (heavy particle) temperature
THD A	%	Total harmonic distortion in current
THD V	%	Total harmonic distortion in voltage
T_p	K	Temperature around hot zone
u_{ball}	V	Instantaneous value of ballast voltage
u_{lamp}	V	Instantaneous value of lamp voltage
$\mathbf{u}_{lamp}$	V	Oscillogram (vector) of lamp voltage
U	V	Voltage
$\mathbf{U}$	V	Complex voltage
$\mathbf{U}_{lamp}$	V	Phasor of lamp voltage
$\bar{U}(t)$	V	Time-varying phasor of voltage
U_{ef}	V	RMS value of voltage
U_l	V	Voltage drop
U_n	V	n^{th} harmonic of voltage
U_{net}	V	Mains voltage
U_{rms}	V	RMS value of voltage
U_s	V	Lamp model parameter eq. (3.7)
$v(t)$	V	Supply voltage eq. (3.20)

Term	Unit	Definition
V_{ele}	V	Electrode voltage drop
W_{con}	J	Heat conduction dissipation
W_{ele}	J	Input electric power
W_{dif}	J	Diffusion of particles from discharge
W_h	eV	Energy of higher energetic state
W_l	eV	Energy of lower energetic state
W_{rad}	J	Radiation dissipation
W_{sheath}	J	Dissipations at electrodes
x		Mathematical function of a lamp model
$\mathbf{x}$		Vector of parameters
$\bar{x}$		Mean Value
y	S	Mathematical function of a lamp model eq. (3.10)
$y(t)$		Output signal of a real system
$y_M(t)$		Output signal of a model system
$\mathbf{Z}$	Ω	Complex impedance
α	$\mathrm{s^2 m^{-5} kg^{-1}}$	Lamp model parameter eq. (3.8)
β	$\mathrm{s^{-1}}$	Lamp model parameter eq. (3.8)
$\Delta U_{electrodes}$	V	Voltage drop on electrodes
ΔW	eV	Energy difference
Δy		Difference of output signals
η	$\mathrm{lm\ W^{-1}}$	Luminous efficacy
λ	nm	Wavelength
λ		Virtual power factor
μ_e	$\mathrm{A\,s^2\,kg^{-1}}$	Electron mobility
ν	$\mathrm{s^{-1}}$	Frequency of electromagnetic radiation
π		Ludolph's number
ϱ_e	Ωm	Electric resistance
σ		Standard deviation
σ	$\mathrm{Sm^{-1}}$	Electric conductance of a discharge eq. (3.32)
σ_e	$\mathrm{Sm^{-1}}$	Electric conductance of a discharge eq. (2.4)
σ_e	S	Electric conductance of a discharge eq. (3.9)
σ_e	S	Electric conductivity of a discharge eq. (3.17)
σ_e	$\mathrm{Sm^{-2}}$	Electric conductance of a discharge eq. (3.26)
ξ		Mathematical parameter eq. (3.30)
ψ_{ion}	$\mathrm{s^{-1}}$	Ionization function eq. (3.18)
ψ_{dif}	$\mathrm{s^{-1}}$	Diffusion function eq. (3.19)
ω	$\mathrm{s^{-1}}$	Angular velocity (frequency)

List of Acronyms

Institutions

COST	European Cooperation in the field of Scientific and Technical Research
CPAT	Centre de Physique des Plasmas et de leurs Applications de Toulouse
DIEECS	Departamento de Ingeniería Eléctrica, Electrónica, de Computadores y Sistemas
ESAT	Departement Elektrotechniek
ELECTA	Elektrische energie & computerarchitecturen
FM	Fakulta mechatroniky (Faculty of Mechatronics)
KAM	Katedra měření (Department of Measurement)
KEL	Katedra elektrotechniky (Department of Electrical Engineering)
KU	Katholieke Universiteit
STSM	Short Term Scientific Mission
TUL	Technická univerzita v Liberci (Technical University of Liberec)
UPS	Université Paul Sabatier

AC	Alternate Current
Ar	Argon
AVG	Average Value
CAD	Computer Aided Design
CFL	Compact Fluorescent Lamp
CMH	Ceramic Metal Halide Lamp
CRI	Colour Rendering Index
CCT	Corelated Colour Temperature
DC	Direct Current

EB	Electronic Ballast
EMU-2	Ethernet Multifunction Unit
HF	High Frequency
Hg	Mercury
HID	High Intesity Discharge lamp
HMI	Hydrargyrum Medium-arc Iodide (mercury-halogen lamp)
Ho	Holmium
HPL	High Pressure Lamp
HPML	High Pressure Mercury Lamp
HPSL	High Pressure Sodium Lamp
FL	Fluorescent Lamp
In	Indium
IR	Infra Red light
Kr	Krypton
LED	Light Emitting Diode
LPSL	Low Pressure Sodium Lamp
LS	Least Squares
MB	Magnetic Ballast
MHL	Metal Halide Lamp
MLN	Mini-lighting Network
Na	Sodium
Ne	Neon
OLED	Organic Light Emitting Diode
PC	Positive Column
PCA	Polycrystalline Alumina
QR	Eigenvalue algorithm
RMS	Root Mean Square
Sc	Scandium
SI	The International System of Units
SOX	Sodium OXide Lamp
T8	Tubular fluorescent lamp with $\varnothing 26\,\mathrm{mm}$
THD	Total Harmonic Distortion
Tl	Thallium
TL	Tubular Lamp
TLS	Total Least Squares
UV	Ultraviolet light
V-I	Voltage-current
Xe	Xenon

Introduction to the COST Action no. 529 "Efficient Lighting for the 21^{st} century"

European Cooperation in the field of Scientific and Technical Research is the intergovernmental framework for coordination of nationally funded research on a European level.

It is based on Actions, which cover basic and pre-competitive research as well as activities of public utility. COST has 35 member countries and enables scientists to collaborate in a wide range of scientific and technological domains (*e.g.* Chemistry, Physics, Forestry, Materials ...).

Funding COST is basically used to cover coordination costs such as contributions to workshops/conferences, travel costs for meetings, contributions to publications and Short term scientific missions of researchers to visit other laboratories [COSa].

Our COST Action 529 "Efficient Lighting for the 21^{st} century" was concerned with the light source science and technology.

The main objective of the Action at both the basic breakthrough and the pre-competitive research levels, was to seek new concepts and materials for the lighting industry which avoid any known environmentally harmful substances through the study of the feasibility of high efficacy, novel light source technologies.

Other objective was building up a database of existing knowledge in given field, compiling and transferring the existing information such as experimental results and numerical simulation codes – generally the fundamental data necessary for forthcoming specific and more focused studies.

This Action enabled the creation of an interdisciplinary expert panel which acts as a consulting body for the industry as well as between specialists from different fields. This concept seems to be valuable especially when one considers the fact that the nature of total light systems (of which the lamp is only one of many elements) is in itself highly interdisciplinary. It includes

knowledge from several major domains such as electrical engineering, plasma physics and chemistry, chemistry and materials science [COSb, Kop05b].

Department of electrical engineering could, thanks to this Action, collaborate with plasma physicists from CPAT at University of Paul Sabatier in Toulouse, France; electrical engineers from DIEECS at University of Oviedo, Spain, and from ESAT/ELECTA at KU Lueven, Belgium.

In the frame of this action were realized number of STSMs, workgroup meetings or workshops, where were presented results of our laboratory and personally consulted with partners. We participated on the international 10^{th} Light Symposium in Toulouse in 2004 and other actions.

Chapter 1

Preface

It might be said that the life without the artificial light is nowadays hardly imaginable. It is now a long time since we stayed in dark and waited for the sunlight to come. The artificial light has become practically omnipresent all across the developed world. It is mainly the product of the electric energy which is transformed into the light by various electrical light sources. Approximately 25 % of the worldwide electricity production is consumed by these light sources [LLLG04]. There are numerous types of electric light sources and they could be classified *e.g.* according to the way of the light emission [Hab95, Miš79, Zis05]:

- In solid states
  - incandescent
    - vacuum light bulbs,
    - light bulbs filled by gas – conventional, and halogen;
  - luminescence
    - light-emitting diodes,
    - organic light-emitting diodes.
- In gases and in metal vapours
  - arc discharge
    - low pressure – fluorescent, sodium, sulphur lamps *etc.*,
    - high pressure – mercury, sodium, metal halide lamps, xenon lamps *etc.*
  - glow discharge
    - low pressure – glow-lamps.

It has been estimated that 80 % of electric light sources which are used for indoor commercial, industrial, institutional, and retail applications, is fluorescent. The discharge lamps significantly prevail compared to the other types, mainly due to their efficiency of electrical energy conversion into light [Way71].

Discharge lamps are based on plasma emitting light in visible or invisible luminous spectrum. The principle is very complex and due to it can exist many types of arc discharge tubes. These light sources do not work directly from the mains electricity as the light bulbs do, but rather over special circuits called *ballasts*. They are required for the lamp starting, arc-current limiting in the steady-state operation and relighting each half cycle (for alternate current operation). The ballast must provide these functions with minimum consumption of electric power, no adverse effect on lamp life and with no negative influence to the mains supply.

To solve such problem is the multidisciplinary task. The luminary system lamp-ballast is the product of many scientific/technical disciplines: plasma physics, chemistry, materials, optics, electrical engineering, electronics ... *etc.* [COSb, WWRN03].

The electrical point of view is the main interest of this work. The problem confines then to the field of electrical engineering especially to the electric circuit design, where the most interesting characteristic for the ballast designer is lamp terminal characteristic as an electrical load. This highly nonlinear part of the circuit should be described by the simplified model usable in various CAD systems.

1.1 State of the art

Specialists who focus on discharge lamps is aware of the fact that there is the strong tie between the source and the lamps characteristics, the former having the influence on the parameters of the latter, such as color temperature, operating power or luminous flux. However, there are hardly any analytic models linking the lamps characteristics with their electrical properties.

Numerical simulations must therefor take into account a number of coupled phenomenon: fluid motion and convection, heat dissipation, chemical reactions, electric and magnetic field computation ... *etc.* Fundamental data like the species cross section (*e.g.* [LC04]) or the chemical reactions occurring at this range of temperatures and pressures are not well known and are subject of the discussion among specialists.

Lister *et al.* [LLLG04] recently wrote a review of the physics of discharge

lamps and discussed the modelling of gas discharge. Schematically, this topic can be subdivided into two main branches:

- models based on the plasma equations,
- semiphysical or black box models.

The first one is about solving numerically the plasma equations. So far, numerous groups are working on various aspects of the discharge lamp simulations, like the influence of the electrode on the discharge column [BD04, ABN00, Ben00, Ben01], or the plasma properties inside the lamp [Lis92]. This approach is based upon Finite Elements discretization and delivers results as local variables like ions and electrons densities, temperatures, velocities, *etc.*

Due to its complexity and computational heftiness, such approach is not suitable for simpler tasks like electric circuits modelling, ballast design, influence of discharge lamps (electric load) evaluation, *etc.* In this case, semiphysical or black box models are applied, with parameters identified from real lamp data. This approach is said *global*, as the result is directly expressed in terms of the global electrical properties like voltage and current.

Those models are useful in specialised environments, like *e.g.* SPICE or Matlab [ZD02]. They are mainly based upon approximation of:

1. non-linear voltage-current characteristics,
2. equivalent conductivity/resistance.

The first approach makes use of a fixed *negative* resistance describing the negative slope of the voltage-current curve [BYSG02, BYSL02, CFS+01, VLH+98, NG01]. Such approach is better suited for high frequency operating mode, as the lamp starts behaving as a linear, constant load. But at mains frequencies, the time scale permits a significant variation of the plasma properties, leading thus to a time-varying formulation as a function of various easily measurable lamp parameters.

For low pressure fluorescent lamps, such conductance variation can readily be obtained from the Francis equation [Fra48] complemented by various relationships between electrons density, temperature, mobility and discharge parameters like current, gas properties, thermal emissivity, ... *etc.* [LMT+04, LSTD05, MT04c, MT04a, MT04b]. This leads to analytical and often nonlinear models suitable for circuit simulators.

Herrick [Her80] extrapolated the Francis model to HID[1] discharges, applied on data obtained from Hg and Na lamps. Based upon a black box approach, he expressed a Taylor developement of the time derivative of the conductance as a polynomial of the lamp current and conductance.

Other authors [SBY99, ABF+02b, ABF+02a, ABV+04, Sta84, TPP+04] followed the same path with various adjustments to the basic structure.

The model used for our study specified below by (1.1) belongs to this family, and it can be recognised that some function of the conductivity was approximated by a polynomial in the conductivity.

1.2 Aims of the thesis

The aim of the work is to describe discharge lamp (different types) as an electric load for the electric circuits simulation. Such model can be used in light net model to observe the behavior and influence onto mains electricity supply and for design of new electronic ballasts.

The lamp will be described by the G-model based on the electric conductivity $G(t)$ of the plasma proposed by Zissis *et al.* [ZD02]:

$$\frac{\mathrm{d}G}{\mathrm{d}t} = a_2 i^2 + \sum_{k=1}^{N} b_k G^k, \tag{1.1}$$

and other lamp models based on description of equivalent conductivity *eg.* from works [ABF+02b, ABF+02a].

The optimal structure of lamp models with its parameters will be determined. Such model will be used as the block in Matlab Simulink and verified against experimental results.

1.3 Outline of the thesis

The theory of the electric discharge is briefly explained in the first part of the thesis and the light production principles of different types of discharge lamps are introduced. The summary of widely used discharge lamps is given. Then the presentation of a necessary electric circuit for their operation – *ballast* follows.

[1] High Intensity Discharge or high pressure discharge lamps contain compact arc tubes, which enclose various gases and metal salts. They operate at relatively high pressures and temperatures. HID is a general term for mercury, metal halide, high pressure sodium lamps and less common, xenon short-arc lamps (more in sec. 2.4).

Second part deals with mathematical modelling of discharge lamps for lighting. It focuses on electrical description modelling of discharge lamps, on their simulation in electric circuits especially. The calculation and modification of G-model is noted.

The part with the presentation of experiments deals with measurements on different discharge lamps and their circuits. This step represents the data acquisition (oscillograms of lamp voltage and current $u_{lamp}(t), i_{lamp}(t)$) for model verification.

The next chapter describes the process of lamp model identification which is followed by simulation part where the applications of models in the luminary system models are shown.

In the conclusion, the advantages and disadvantages of used methods are discussed and perspectives of electrical modelling approaches are summarized.

Chapter 2

Electric discharge lamps

Electric discharge lamps are the most important electric light sources. They are used in virtually all areas of modern lighting technology. They could be found in households as well as in the offices (fluorescent lamps, compact fluorescent lamps), in industry (high intensity discharge lamps), public lighting (high pressure mercury, sodium lamps, metal halide lamps, low pressure sodium lamps), monument lighting (HIDLs), in medicine (germicidal lamps), automotive headlights (HIDLs), for commercial (neon lamps, HIDLs), for projection (special HID lamps – xenon and HMI), and many more. Their short list with the family of electric light sources is mentioned above.

Discharge lamps, as the artificial sources of visible[1] white light, are produced in wide rage of powers with different levels of luminous efficacy[2] η. According to figure 2.1 it is evident that incandescent lamps (light bulbs) have low efficacy while all discharge lamps have much higher efficacy than the former schematically sketched the evolution in lamp efficiency of discharge lamps against incandescent lamp over the years. From figure 2.1 is evident low efficacy of incandescent lamps (light bulbs) and much more higher efficacy of all discharge lamps (*e.g.* low pressure sodium lamp is up to now the most efficient artificial light source).

Unfortunately the quality characteristics of light sources can not be based on luminous efficacy only. There are other requirements on lamps, which are more or less important, depending on the application. Nevertheless it is possible to summarize how the "good lamp" should look like [Zis05]:

1. have a high efficiency;

[1] Visible light has wavelength λ in range 380 to 780 nm.

[2] The luminous efficacy is defined as the luminous flux related to the electrical power input to a light source – lm/W.

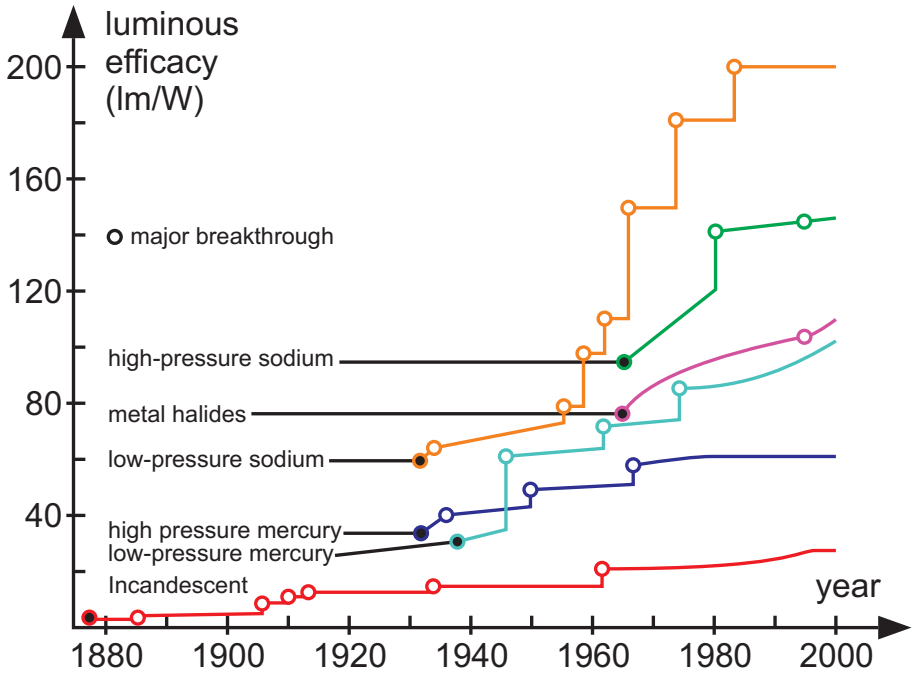

Figure 2.1: Evolution of luminous efficacy of discharge lamps compared to the incandescent lamp [Gen].

2. have a high CRI[3];
3. have a long life;
4. produce a stable light level during its lifetime;
5. avoid flickering;
6. produce its nominal flux instantaneously when turned on;
7. be exchangeable with other types of lamps;
8. be compact and light;
9. avoid harmonic distortion feedback effect to the electric network;
10. avoid environmental harmful materials;

[3]The general Colour Rendering Index is one of the main characteristic of a light source. It is a measure of how well the light source reproduce the colours of any object in comparison to a standard illuminant. The scale is from 0 (monochromatic) to 100 (white).

11. avoid electromagnetic interference with any other electronic equipment;
12. avoid excessive heat and UV[4] rejection;
13. be recyclable;
14. be inexpensive.

As an example could be taken a LPS lamp against incandescent lamp. Although LPSL win on the field of luminous efficacy with its 200 against 20 lm/W, completely lose with CRI almost 0 to 100.

2.1 Physics of discharge lamps

All electric discharge lamps convert electrical energy into the light by transforming electrical energy into the kinetic energy of moving electrons, which in turn is converted into electromagnetical radiation as a result of some kind of collision process with atoms of gas (vapours) or their mixture.

Some moving electrons make such energetic impacts on atoms that the atoms internal state changes (inelastic collisions). These changes can be of two types : *excitations* or *ionizations*.

The excitation collisions excited the atomic electrons from the lower energetic state to a higher energetic state. This transient state may takes some time ranging from few picoseconds to few seconds in the case of *forbidden transitions*, usually it takes around 1 nanosecond. The excited atomic electron then loses the energy by dropping into the lower energy state. The quantum of energy is emitted as an electromagnetic radiation of a frequency ν. Equation 2.1 shows that the product $h\nu$ is proportional to the energetical difference between higher and lower energetical states:

$$\Delta W = W_h - W_l = h\nu, \tag{2.1}$$

where h is Planck's constant.

Each atom allows specific transitions between energetic states, the specific frequency ν of emitted electromagnetic radiation. Therefore the radiation spectrum is formed as the separated *spectral lines* of atoms.

The ionization collisions generate pairs of electron-ions. This intimate mixture of positive ions and negative electrons is called a *plasma*. The motion of charged particles in plasma between electrodes positive *anode* (+) and negative *cathode* (−)[5], is oriented for electrons from cathode to anode and

[4] Ultraviolet light has wavelength λ in the range 100 to 380 nm.

[5] If the lamp operates on AC supply electrodes acts alternatively during each half cycle.

for positive ions from anode to cathode (c.f. figure 2.2). The electrons move randomly at high speed and the electron cloud drifts in the electric field[6]. The electric current is than given by the sum of the current of both particles and its orientation is the same as the motion of positive ions. The electrons

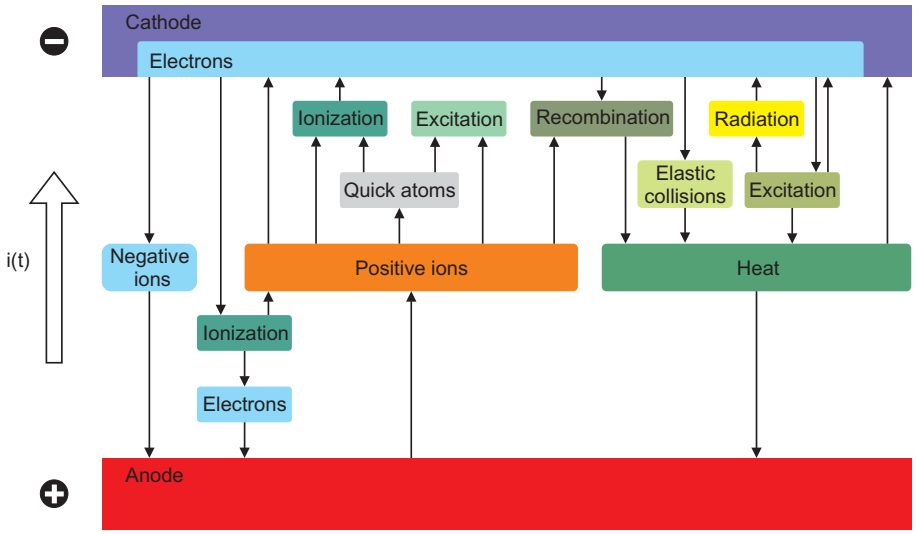

Figure 2.2: Interaction between plasma and electrodes [Gro67].

are much more mobile than the ions which can be regarded as stationary. So the ions flow is only the small fraction of whole current approximately 0.1 to 1 %.

The type of the electromagnetic radiation of the plasma depends on atoms (filling of a discharge tube) which are possible to be excited by electrons.

2.1.1 Power balance in a discharge

The total input electric power W_{ele} in all gas discharge lamps dissipates specially through radiation[7] W_{rad}, thermal conduction W_{con}, acceleration of ions in the sheaths at the walls and electrodes W_{sheath}, and diffusion of particles from the discharge W_{dif}, *i.e.*,

$$W_{ele} = W_{rad} + W_{con} + W_{dif} + W_{sheath}. \tag{2.2}$$

[6]Imagine of swarm of bees drifting along in gentle breeze is not far from the true [Wha00a].

[7]The light radiation in visible spectrum.

2.1.2 Starting and steady states of a discharge

At first, there must be few electrons at the cathode for a discharge to incept. Two approaches of electrons emission are used in discharge lamps.

- thermionic emission;
- high-field emission.

Two types of cathodes can be defined then. A *hot cathode* that uses thermionic emission and it is typical for arc discharges. A *cold cathode* operates with high-field emission (autoemission), which is specific for glow discharges.

Free electrons accelerated by electric field gains enough energy for new electrons production during inelastic collisions (ionization) with atoms.

An important factor for a discharge is *starting voltage* (*breakdown voltage*). It depends on the gas and discharge tube composition, the gas pressure, electrode's materials and their distance, and applied electric field. The efficiency of ion and electron production is reduced by increasing of the pressure p either electrodes distance d.

The electric discharge is now in steady-state mode of operation. Its form can be changed by the couple of voltage and current. In figure 2.3 a voltage-current characteristics of self-sustained discharges[8] is sketched. Note that

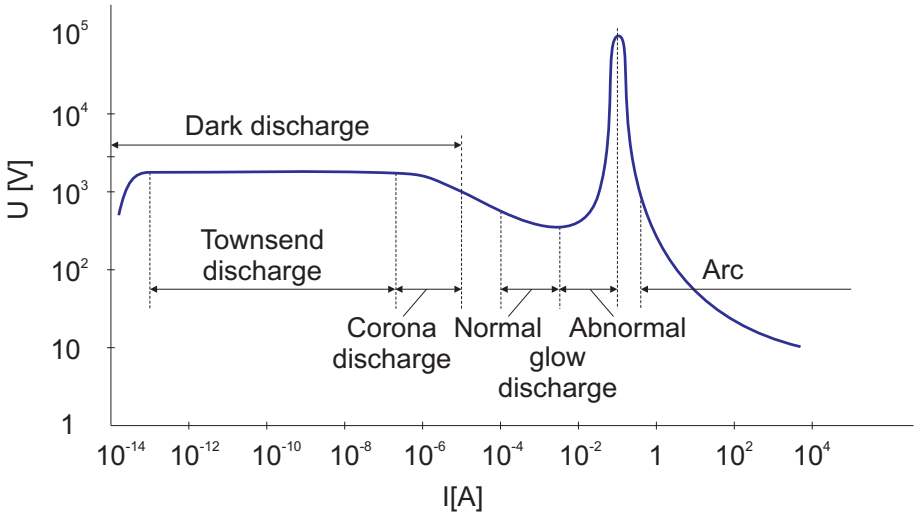

Figure 2.3: The general voltage-current characteristics for self-sustained discharges with schematic current regions, redrawn from reference [Gro67].

[8]Self-sustained discharges do not need external ionizator in the strong electric field.

ranges of currents and voltages are merely illustrative and depends on many factors. In the characteristics are three main regions divided by currents into

- dark discharge;
- glow discharge;
- arc discharge.

The *dark discharge* includes Townsend and Corona discharges which are given by low currents up to 10^{-4} A and high voltages over kilovolts. They do not come out by significant luminance.

The *glow discharge* (normal and abnormal) mode owes its name to the fact that the plasma is luminous. The gas glows because the electron energy and number density are high enough to generate visible light by excitation collisions. The glow discharge is characterized by currents from 10^{-4} to 10^{-1} A.

If the current increases, the electrodes become sufficiently hot that the cathode emits electrons thermionically and with a constant-voltage power supply the discharge will undergo a glow-to-arc transition. The *arc discharge* is represented by higher currents over 10^{-1} A in a plasma (cf. figure 2.3).

2.1.3 Electric characteristics of discharges

The electric current density $\mathbf{j}$ is induced by the electric field. It is given by the flow of electrons $\mathbf{j}_e$ and ions $\mathbf{j}_i$. Since it was already mentioned above on page 12 that ion flow is considerably small and can be therefore neglected in the sum of the whole flow, it is possible to write

$$\mathbf{j} = \mathbf{j}_e + \mathbf{j}_i \simeq \mathbf{j}_e. \tag{2.3}$$

The relation between $\mathbf{E}$ and $\mathbf{j}$ is defined partially by Ohm's Law

$$\mathbf{j} = \sigma_e \mathbf{E}, \tag{2.4}$$

where σ_e is the *electrical conductance* of the plasma. It may be represented by a scalar value, because lighting discharges are generally nonmagnetic.

The electrical conductance is defined as

$$\sigma_e = n_e e \mu_e, \tag{2.5}$$

where n_e is the electron density, e is the electron charge and μ_e is the electron mobility [Wha00a].

The electron density n_e in plasma strongly depends on input power. The electrical conductance σ_e is not constant, but it changes. This is the difference between plasma and wire conductors, where is the n_e fixed. The electric field increases the current increases, the number of electrons increases (also conductance) the resistance ϱ_e decreases, because

$$\sigma_e = \frac{1}{\varrho_e}. \tag{2.6}$$

However, if ϱ_e is further decreased with a constant voltage source, the current will increase without bound until something melts or the fuse blows. This is the result of the negative part of the voltage-current characteristic of a plasma (see in figure 2.4). For the discharge stabilisation is necessary to control (limit) the current. An extra circuit element is included in series to the discharge – this is called *ballast* (*control gear*) (more in section 2.5).

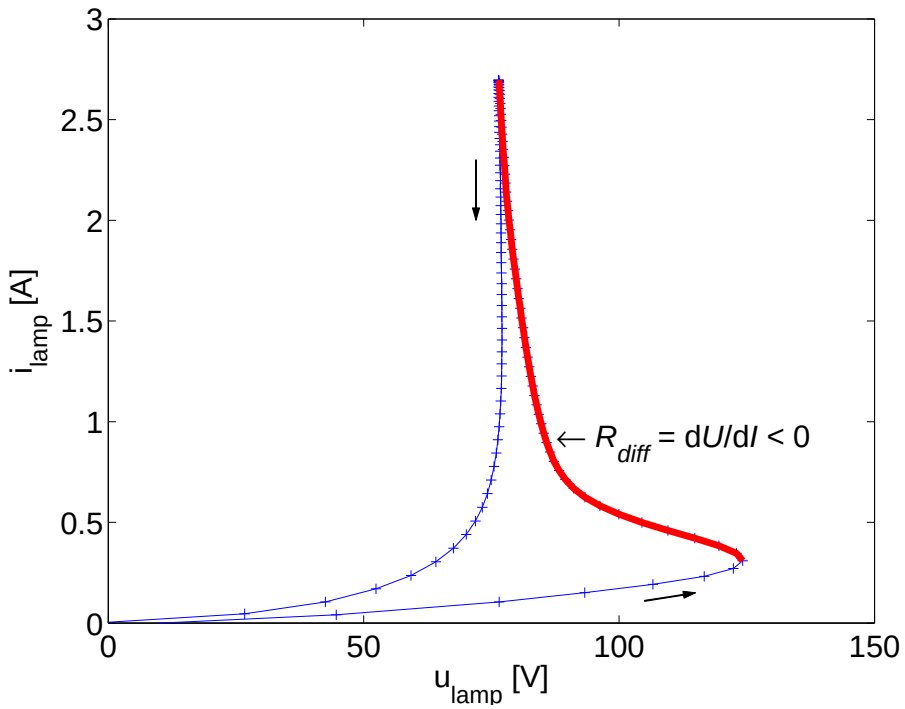

Figure 2.4: Part of the dynamic voltage-current characteristic of HID lamp powered by 50 Hz voltage with magnetic ballast. The part with negative differential resistance ($R_{diff} < 0$) is red lined. Two arrows show the counter-clockwise direction of the characteristic evolution.

2.2 Specification of discharge lamps

Such a complex phenomena like a discharge can be classified from different points of view and so can be classified also discharge lamps:

- physical (*e.g.* pressure, temperature);
- chemical (*e.g.* filling);
- electrical (*e.g.* current, frequency, power) ... *etc.*

Let us mention some certain examples. The specification by *current* ranges is often used. It was already remarked above (page 14 and fig. 2.3).

The classification into two groups based on *pressure* is most widely used for discharge lamps:

- low pressure;
- high pressure.

The energy transformation in excitation, ionization, dissociation of gas atoms and molecules, and heat of a plasma, are different in these two groups of discharge lamps. In figure 2.5 is relation of electron (T_e) and heavy particle (T_g) temperature in a plasma on pressure[9] p. The different temperature of T_e and T_g is typical for low pressure discharge lamps. When is the pressure high over approximately 10^4 Pa the particle temperature is in equilibrium what is typical for high pressure discharge lamps.

Another characterization is by the *frequency* into low frequency ($\sim$ Hz) and high frequency discharges ($\sim$ kHz and higher). The influence of the higher frequency comes out in higher efficiency, because the recombination of electrons and ions is reduced. With high frequencies ($\sim$ MHz) is possible to make an electrodeless discharge [Gro67, Wha00a].

The light colour as well as some other properties is given by the *filling* of the tube. There are lamps filled by sodium, mercury, sulphur ... *etc.*

2.3 Low pressure discharge lamps

Low pressure discharge lamps are generally characterized by current densities $\sim 10^{-2}\,\mathrm{A\,cm^{-2}}$ and pressures 10^{-1} to 10^{2} Pa. They have different temperatures of plasma particles, wich arises from figure 2.5.

[9] The scale of the pressure is in $1.33\,\mathrm{Pa} = 10^{-2}$ torr.

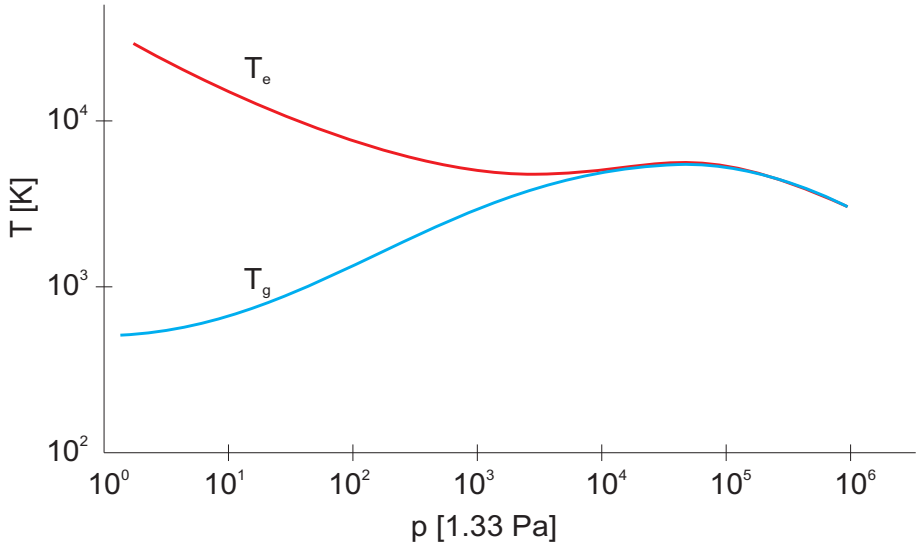

Figure 2.5: Pressure dependance of gas temperature T_g and electron temperature T_e in electric discharge [Miš79].

LP lamps use luminescence of gas filling and after of solids on a tube wall – *low pressure mercury lamps* or luminescence of gas filling directly – *low pressure sodium lamps* [Miš79].

The following text is focused on low pressure mercury vapour discharge lamps (*fluorescent lamps)*, because measurements were taken on them. That is why LP sodium lamps are not discussed.

2.3.1 Fluorescent lamps

There are variety of FLs in the market. They are produced in wide range of powers (6 up to 80 W), shapes, dimensions, colours ... *etc.* FLs can be divided into five groups [PHIa]:

- tubular;
- bent;
- integrated;
- non-integrated;
- electrodeless (induction) lamps.

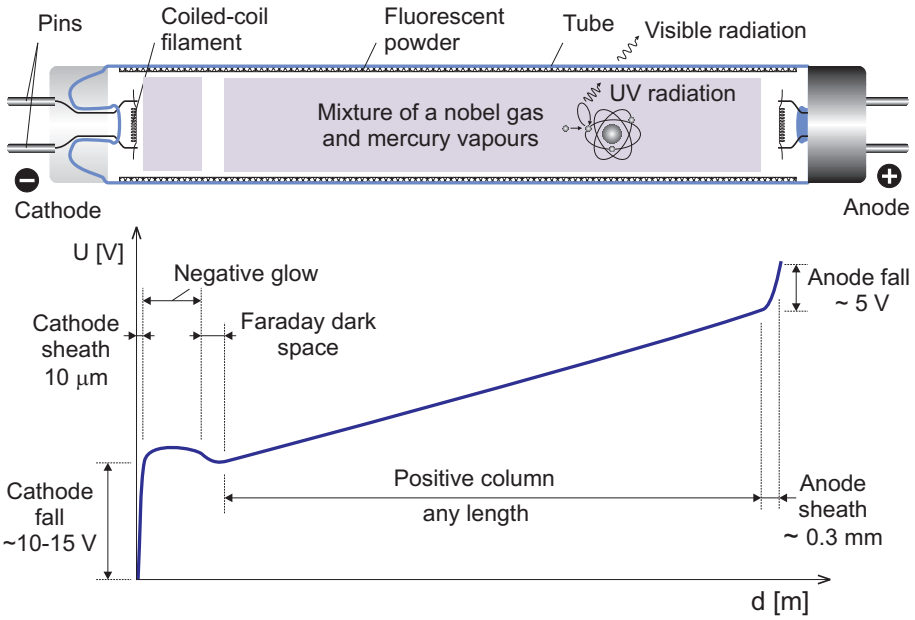

Figure 2.6: Structure of a LP rare-gas discharge lamp in DC mode [Wha00a, Way71].

Widely used are *tubular (linear) FLs*. Their construction is described in figure 2.6. The discharge tube has two electrodes (coiled-coil filaments) sealed into the ends and is filled by a noble gas (Ar, Kr, Ne or their combination) at the pressure ~ 1 torr and rare mercury vapours at 10^{-3} torr. Work temperature of a gas mixture is 300–700 K and electrons c. 12000 K. About 60–80 % of input electric energy change into UV radiation (two spectral lines 185 nm and 253.7 nm) due to mercury atoms. This invisible light is then transformed with some losses into visible spectrum in the mixture of fluorescent powder coating on the tube wall. The fluorescent mixture properties have great impact on CRI (over 80) and colour temperature CCT of the light source. The efficiency of transformation from the electric energy to visible light is 20–30 % [Miš79, Ric01].

The discharge regions of the lamp and voltage characteristic for a DC mode[10] are sketched in figure 2.6. This figure is for a better understanding of physical processes inside the tube. Electrons are accelerated from the cathode through the *cathode fall* to the *negative glow* region. This is compensated by a region of low ionization *Faraday dark space*. The following space with

[10]For a AC mode changes polarity each half cycle.

the constant electric field is the *positive column*[11]. The *anode fall* is space charge region which ensures that the correct number of electrons fall on the anode to satisfy the requirements of current continuity.

These lamps are produced in a wide range of diameters ∅ 38, 26, 16, 7 mm or T12, T8, T5, T2[12]; different lengths 136–1500 mm; and powers 4–65 W [Hab95, OSR, PHIb].

Bent FLs look like tubular, but they are shaped in space into U or O (more in [Miš79]).

Integrated and a *non-integrated lamps* try to substitute classical incandescent lamps. The difference between them is in ballast placing inside or outside of the case. These lamps are more compact than tubular FLs. They can have a number of one or several times bent tubes.

Named FLs can be connected to the power net by two common types of ballasts, by a high frequency[13] electronic ballast or by an electromagnetic ballast with starter (see in sec. 2.5).

Electrodeless fluorescent lamps are based on the induction principle, where the discharge represents single turn secondary around the primary coil of a transformer. The working frequency varies with lamp design, but popular examples use 13.6 MHz, 2.65 MHz and 250 kHz [Hab95, Wha00a, PHIa].

2.4 High pressure discharge lamps

High pressure or high intensity discharge lamps are characterized in general by compact gas discharges (1–100 mm), current densities $\sim 1\,\mathrm{A\,cm^{-2}}$ and pressures 10^4–10^6 Pa. The temperature of plasma particles is $T_e = T_g =$ 1000 K up to 8000 K (see in figure 2.5) [Way91].

There are three general types of HID lamp distinguished by their plasma forming species:

- high pressure mercury lamp;
- high pressure sodium lamp;
- metal halide lamp.

[11] PC is the major source of UV radiation in FL.

[12] Philips marking: T – tubular and 12...2 multiplied by 1/8 inch is the tube diameter, *e.g.* T12 → 12 · 1/8 inch = ∅ 38 mm.

[13] The working frequency over 20 kHz.

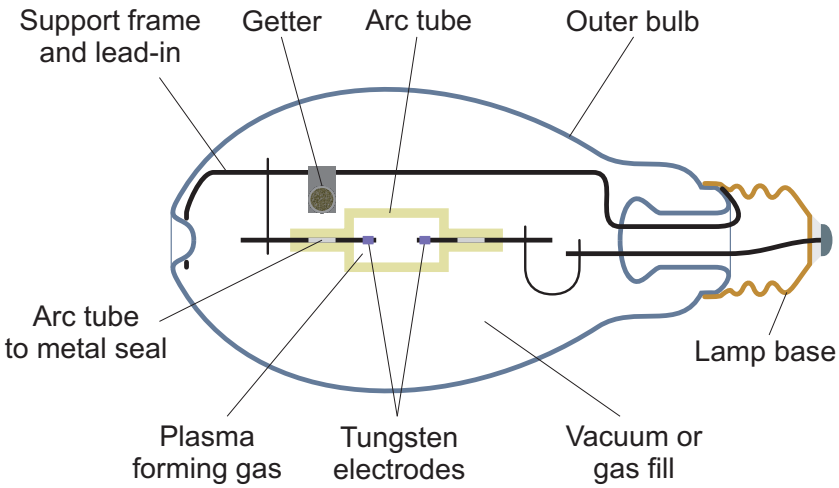

Figure 2.7: The general construction of a high pressure discharge lamp.

Typical high pressure discharge lamp (fig. 2.7) is assembled from *inner discharge tube (arc tube)*. An arc tube can have different shapes (cylinder or sphere) and can be made of different materials (glass or ceramic). The arc tube with electrodes contains plasma forming gas and is fixed by *support frame* and hermetically sealed in *outer bulb*. The outer bulb protects the inner tube and inner tube seals from oxidation, stabilizes the work conditions around the arc tube, absorbs emitted UV radiation and can be covered by fluorescent powder for the same reason as in fluorescent lamps. On the frame inside the outer bulb can be mounted a *getter* [BC04] which absorbs impurities (oxides, water vapour *etc.*) remained after the fabrication processes.

A sketch of an arc tube with two main electrodes and one *starting electrode* inside is in figure 2.8. These electrodes are sealed into the arc tube.

The electrical potential between main electrodes drawn below the arc tube represents voltage drops regions – cathode fall voltage, anode fall voltage and the voltage drop across the plasma column [Ruf05, Fle06]. This characteristic describes a DC operate mode, which changes every half cycle in an AC mode.

2.4.1 High pressure mercury lamp

High pressure mercury lamp is the prototype of the family of HID lamps. The plasma forming gas is mercury vapour and a small admixture of a noble gas (Ar) in the arc tube made of transparent *fused silica* (known as quartz, see example in figure 2.8). This mixture produce under pressure 10^5–10^6 Pa strong spectral lines in the visible part of the electromagnetic spectrum at

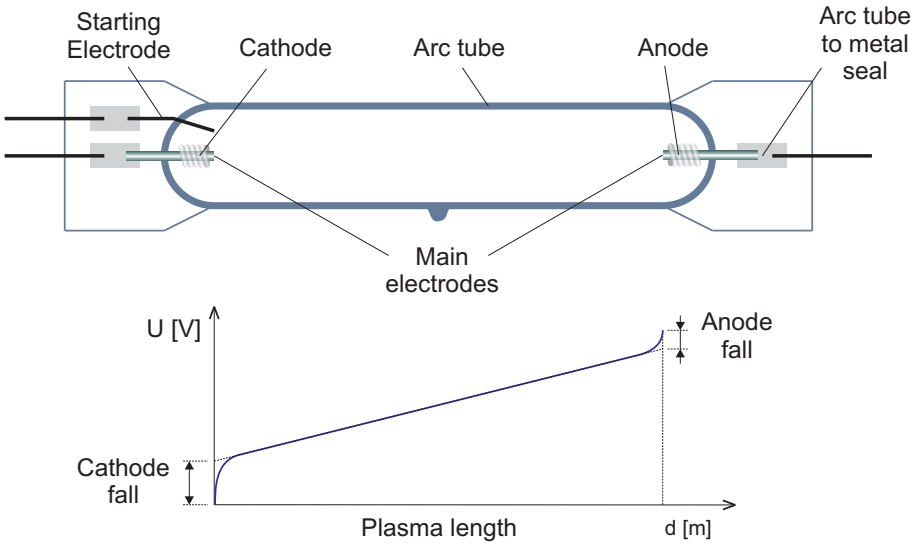

Figure 2.8: An arc tube of a high pressure discharge lamp with the characteristics of the electric potential in the plasma.

405, 436, 546, 577, and 579 nm with temperature typically 6000 K. Beside two main electrodes is sealed in the quartz one start electrode connected over 40 to 70 kΩ resistor to the lead-in. Outer bulb is filled by the mixture of Ar and N under pressure 4.5 to 5.2 10^5 Pa; on the wall can be a phosphor for UV light conversion to visible spectrum.

In the case of 400 W lamp the input energy dissipates as follows: 12% loss on the electrodes; 38% loss as heat conduction plus wall absorption; and 40% is radiated by the arc. Only 16% of this radiation is visible. The lamp luminous efficacy is maximally 60 lm/W [Hab95, Miš79, Way91, LLLG04].

2.4.2 High pressure sodium lamp

In high pressure sodium lamps is the arc tube made of ceramic – translucent polycrystalline alumina because the plasma forming material sodium is in a liquid or vaporized form very aggressive and quartz would be destroyed very quickly. In the arc tube are two electrodes only (no start electrode). It is filled by amalgam of sodium metal and a noble gas (Xe or Ar) under pressure 3 to 6.5 10^4 Pa. The visible light spectrum is more continuous than by HPML. It is very strong around 600 nm. Typical temperatures of the plasma column are 3300 to 4000 K. In the outer bulb is typically high vacuum. The construction can be similar to figure 2.7 single ended or double ended to special sockets.

In the case of 400 W lamp the input energy dissipates as follows: 6% loss at the electrodes; 38% loss as heat conduction plus wall absorption; and 56% is radiated by the arc in IR and visible light spectrum. 31 % of this radiation is visible. The lamp luminous efficacy can be up to 150 lm/W [Hab95, LLLG04].

2.4.3 Metal halide lamp

High pressure metal halide lamps are similar to HPML in the principle of the plasma forming gas is mercury vapours. However, in MH lamps are to the Hg vapours added other one or more metal halides (iodides of Na/Sc/In/Tl/Ho ... *etc.*). These metals have improving impact to the light emission and of course efficacy, because they have very strong resonance lines in the visible part of the spectrum. The arc tube can be the same as by HPML *quartz*[14] or as by HPSL *PCA*[15]. The utilization of ceramic material PCA is a modern trend for MH lamps. Such lamps are called *ceramic metal halide* lamps. This material allows higher pressures and temperature operation (quartz 1200 K, PCA 1500 K) of metal vapours which leads to efficacy and colour improvements. The temperature of the plasma column reaches 4000 to 6000 K.

In the case of 400 W MH lamp, presented by Lister [LLLG04], the input energy dissipates as follows: 12% loss at the electrodes; 25% loss as heat conduction plus wall absorption; and 57% is radiated by the arc in IR and visible spectrum. A visible radiation is 21%.

Mentioned high pressure lamps are produced in wide ranges of wattage (summarized in the table 2.1); shapes and construction layouts [GE, OSR, PHIb].

Table 2.1: HID lamps wattage ranges

	HPML	HPSL	MHL
P [W]	40 – 1000	35 – 1000	20 – 2000

Significant influence on the power balance of HIDs has operational position of the lamp. The horizontally burning lamp is about 1 to 10% more inefficient than the vertically burning lamp [KVR06, LLLG04]. A correction

[14] Example of the tube is in fig. 2.8.
[15] The cylindric shape *e.g.* in figure 2.7.

can be done by magnetic field or by operation at high frequencies. Unfortunately high frequency above 1 kHz brings problems with acoustic resonances[16] [BAC04, Mel, Hu01].

2.5 Electric circuits for electric discharge lamps

Electric discharge lamps need some electric circuits for their correct operation as was mentioned above (page 15). It is realized through ballasts, which can be constructed from classical passive components only (resistive/reactive ballasts) or from semiconductors and passive components R, L, C (electronic ballasts).

Majority of discharge lamps are powered by *AC circuits*. Such circuits have to ensure three general functions:

- start of a discharge lamp;
- a lamp relighting each half cycle;
- control of current through a discharge lamp.

Starting of a discharge was described in sec. 2.1.2. The circuit must provide open circuit voltage to ionize the gas in a discharge lamp. Its value depends generally on the type of the discharge lamp (LPLs need ∼1 kV and HPLs ∼10 kV). A method of a discharge lamp starting has great impact on its life time. Many different techniques are used. Some of them utilizes components which are internal part of a discharge lamp circuit and it is not possible to separate them. In another cases the external components are used. The working time of such circuits can be various. They can work during starting periods or continuously during operational time of the lamp.

A typical example of such internal component is *starting electrode* inside the discharge tube (fig. 2.8 by HPML and quartz MHL) that helps for thermionic emission of electrons and start voltage decreasing. After ignition sequence work main electrodes only.

The connection of an external *starter* (ignitor) in combination *e.g.* with inductive ballast is another approach. The starter can be *glow-switch starter*[17]

[16] In some frequency ranges can occur the standing pressure wave in discharge tube. This phenomenon depends on the lamp geometry, gas temperature and pressure inside the discharge tube.

[17] Two bimetallic electrodes enclosed in a glass container filled with noble gas more *e.g.* in [Way71, Miš79].

or *electronic starter*[18]. They have no impact on the lamp when is the discharge ignited. It can be demonstrated by their taking out of the circuit.

The current flows every half period through zero in AC mode. The circuit must provide the higher voltage across the lamp in the beginning of each half period than in the rest of the half period.

The control of a current through a discharge means its limitation and stabilization in operation point. This can be realized by *resistor* or *inductive* or *capacitive impedance*. Most circuits use *inductive ballasts* (also known as magnetic ballasts) because for mains frequency 50 Hz (60 Hz) are better. For higher frequencies 10^2 to 10^3 Hz the capacitive ballasts are used. The value of their impedance (id. size, efficacy, ... *etc.*) depends on frequency. It is the reason (not only this indeed) to use electronic ballast, where the frequencies are much more higher than mains frequency. Advantages and disadvantages of MB and EB are summarized in table 2.2.

Table 2.2: Influence of voltage frequency on induction ballasts [Wha00a].

at mains frequency	
+ high voltage at relight	− weight ($L \sim$ H)
+ low cost	− inefficient
+ reliable	− flicker
	− low lamp efficiency (FL)
at high frequency (>20 kHz)	
+ increased lamp efficiency (FL)	− cost
+ no flicker	− acoustic oscillations (HPL)
+ increased ballast efficiency	
+ low weight ($L \sim$mH)	
+ simple implementation (half bridge)	
+ plenty of voltage for starting	
+ features (dimming, power control)	

In figure 2.9 is the typical electric circuit with discharge lamp. The mains voltage $u(t)$ is connected in parallel to the capacitor. In series are inductive (magnetic) ballast and parallel combination of lamp and starter. During the steady operation state the current $i(t)$ induces fall voltage on ballast

[18]Bimetallic switching is replaced by triac.

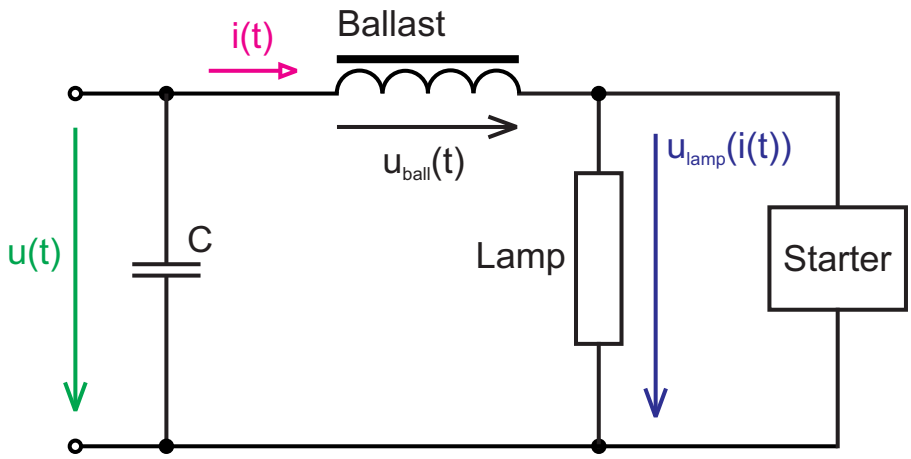

Figure 2.9: Typical electric circuit for discharge lamp with inductive ballast, starter and compensating capacitor.

$u_{ball}(t)$ and lamp $u_{lamp}(i(t))$. Through the opened starter does not flow any current. Under this condition is possible to write equation 2.7, where ballast is represented by ideal resistance R and inductance L.

$$\begin{aligned} u_{lamp} &= u - u_{ball}, \\ u_{ball} &= iR + L\frac{\mathrm{d}i}{\mathrm{d}t} \end{aligned} \tag{2.7}$$

The functional relationship between u_{lamp} and i is not in accordance with Ohm's law (eq. 2.4) as was noted above. It is highly nonlinear. Waymouth presents dependence of the lamp voltage on logarithmic derivative of current and current itself:

$$u_{lamp}\left(i, \frac{1}{i}\frac{\mathrm{d}i}{\mathrm{d}t}\right)$$

A quantitative solution for the equation 2.7 is not in [Way71] offered and has not been successfully proposed until now.

Chapter 3

Discharge lamps modelling

The mathematical modelling is used for the better understanding of real physical systems. The description of the system is realized by the number of mathematical equations. They try to characterize the objective reality more or less complex.

The creation of a model is based on these general steps:

- a task analysis and formulation;
- a mathematical model construction;
- an identification of model parameters;
- a mathematical model solving;
- a verification of the model;
- results interpretation.

The modelling of discharge lamps is the typical example of the physical systems modelling.

Mathematical equations are not able to describe all the behaviours of the system and have not in many cases analytical solution. Thus, the simplification is needed and the numerical approach of the solution is applied.

The searching of the optimal simplification and solution of the model is not trivial task. It demands deep knowledge of the physical system and experiences with its simulation.

The briefly summarized current state of art is in the section 1.1. As it was mentioned earlier, the problem of the discharge lamp modelling is solved by two general branches. *Models based on plasma equations* can represent physical or thermochemical modelling [LLLG04].

- Physical modelling:
  - Modelling of plasma properties:
    - radiation transport;
    - gas heating and thermal losses/balance;
    - electrical characteristics;
  - Thermal modelling (wall temperature distributions).
- Thermochemical modelling:
  - chemical equilibria;
  - chemical transport;
  - thermal conductivity and viscosity.

On the other side *global* (*general*) models represent semiphysical or black-box modelling which produce electrical properties of a discharge lamp. These models are more suitable for simpler tasks like electric circuits simulation, where the aim is the description of a discharge lamp as a circuit component *e.g.* impedance $\mathbf{Z}(t, u)$. There exit two main groups of such models as was mentioned in the preface. They are based on:

- nonlinear voltage-current characteristics;
- equivalent conductivity/resistance.

3.1 Models of nonlinear discharge characteristics

These models are mostly based on the description of the current voltage characteristics of the discharge at *frequencies higher than 20 kHz* . At so high frequencies is the voltage-current characteristic almost linear and can be approximated by a resistor characteristic and its modification.

This phenomenon is used in works from M. Cervi *et al.* [CFS+01], Ribarich [RR98] and S. Ben-Yaakov *et al.* [BYSL02], A. Nachbaur and C. Ganahl [NG01], and others.

They try to find some function that describe relation between voltage and current and power

$$u_{lamp} = f(i_{lamp}, P_{lamp}). \tag{3.1}$$

Cervi *et al.* choose tangential approximation

$$u_{lamp}(i_{lamp}, P_{lamp}) = A_p(P_{lamp}) \cdot \tan\left(\frac{i_{lamp}}{B_p(P_{lamp})}\right), \tag{3.2}$$

where $A_p(P_{lamp})$ and $B_p(P_{lamp})$ are power functions that represent the steady state lamp behavior. They are defined as polynomial functions where coefficients are determined from experimental data.

Ribarichs use cubic approximation

$$u_{lamp} = A\ i_{lamp} + B\ i_{lamp}^3, \tag{3.3}$$

where A, B are constants. Because the problems with its use they propose simpler parabolic model

$$u_{lamp} = k\ i_{lamp}^2, \tag{3.4}$$

where k is a constant.

They obtain graphs in figure 3.1 for the FL T8/32 W at 50 kHz. From the mathematical theory is evident, that *the parabolic model described by eq. 3.4 can not be odd function*, but *they present it so and get succesful results in first and third quadrant* (cf. 'parabolic Ribarich' curve in figure 3.1). Perhaps the article [RR98] is not exhaustive and something is missing, because the right term of their parabolic model should be

$$u_{lamp} = k\ i_{lamp}^2\ \mathrm{sgn}(i_{lamp}). \tag{3.5}$$

The right curve of parabolic function (described by eq. 3.4) is shown as 'parabolic Koprnicky' in figure 3.1.

Ben-Yaakov *et al.* suggested resistive approximation with three deviations from the linear model:

- the dependence of the voltage-current characteristic on the lamp's power level;
- the nonlinearity of the voltage-current curve at given operating condition;
- and the time domain response of the lamp to a change in excitation.

For a small power range is proposed equivalent resistance

$$R_{eq} = \frac{U_s}{I_{rms}} - R_s, \tag{3.6}$$

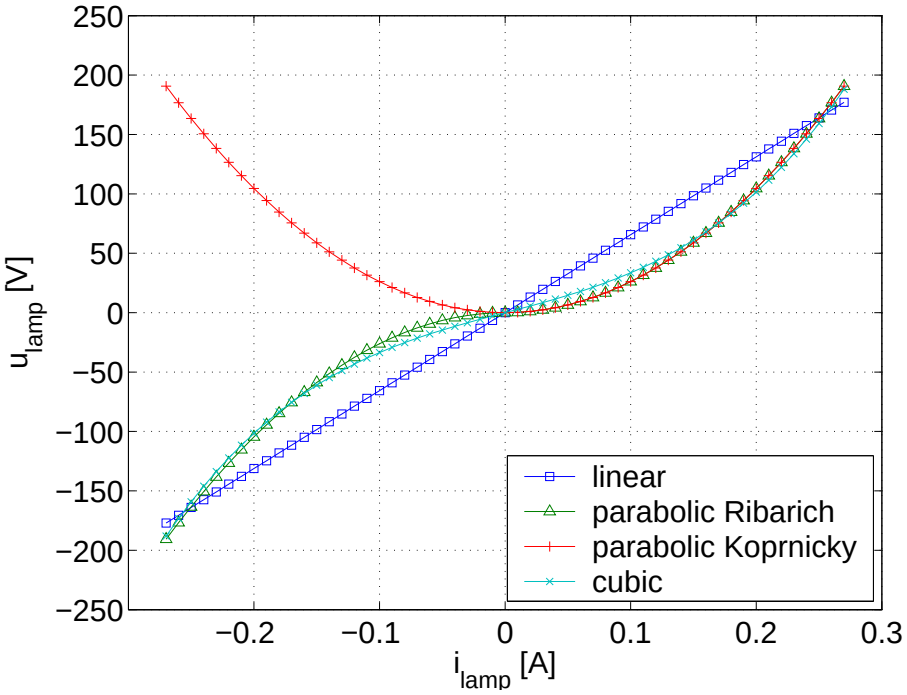

Figure 3.1: Nonlinear lamp resistance at high frequency and fitted models for T8/32 W lamp type running at 50 kHz ($P_{lamp} = 30\,\mathrm{W}, R = 656\,\Omega, k = 2615, A = 278, B = 5740$ [RR98]). The two expressions of a parabolic function are sketched.

where U_s and R_s are lamp's constant obtained from experimental data and I_{rms} is the rms current through the lamp. If the power range is wider the extension of the eq. 3.6 is applied by second (or higher order) polynomial to the form

$$R_{eq} = \frac{K_1}{I_{rms}} + K_2 I_{rms} + K_3, \tag{3.7}$$

where $K_1 - K_3$ are constants of the lamp.

3.2 Models of equivalent conductivity or resistance

These general models of discharge lamps describe the lamp behaviour at low and high frequencies under different power conditions.

They follow two general ways which are based on

- *Francis' postulates* [Fra48],
- *and thermodynamic and energy balance of a discharge.*

The first approach is used in works of P. R. Herrick [Her80], Antón *et al.* [ABF+02a, ABF+02b], Loo *et al.* [LSTD05] and others.

The second approach is applied in works of M. Stambouli [Sta84], Zissis *et al.* [ZAS+92, ZD02], Rossat-Mignod *et al.* [RMRJZ02], M. Shavartsas and S. Ben-Yaakov [SBY99], W. Yan and S. Y. R. Hui [YH05], Tapia *et al.* [TPP+04] and others.

Whereas this work uses mainly the model of Zissis *et al.* [ZD02], this will be explored especially in more detail in section 3.3.

3.2.1 Models based on Francis' postulates

Francis' equation

Francis described the dynamic characteristic of any discharge tube by differential equation (3.8). This equation employs three lamp variables: average electron density, lamp voltage and lamp current and is based on three postulates.

1. The rate of electron production in the discharge column is proportional to the current, and to the voltage gradient.
2. The rate of loss of electrons is proportional to their density n_e.
3. The instantaneous resistance of the discharge $\frac{v_L}{i_L}$ is inversely proportional to the electron density n_e.

$$\left.\begin{aligned} \frac{\mathrm{d}n_e}{\mathrm{d}t} &= \alpha i_L v_L - \beta n_e \\ \frac{v_L}{i_L} &= \frac{F}{n_e} \end{aligned}\right\}, \tag{3.8}$$

where α, β, F are constants which depend on dimensions of the tube and the gas filling; i_L is the current through the discharge; v_L is the voltage between electrodes; and $\frac{v_L}{i_L}$ is the discharge resistivity.

The postulate (3.8) with the relation for the discharge conductance $\sigma_e = \frac{i_L}{v_L}$ can be written to this form:

$$\frac{\mathrm{d}\sigma_e}{\mathrm{d}t} = \Big(\frac{\alpha}{F}\, v_L^2 - \beta\Big)\sigma_e. \tag{3.9}$$

Mathematical model of HPLs from Herrick

Herrick determined mathematical model of high pressure mercury and sodium lamps [Her80]. He devised lamp models from the Francis' equation (3.8). But his approach was mostly empirical. He considered then the lamp as a black box. The proposed model was shaped to final form by best duplicate of experimental characteristics.

He obtained these types of polynomial equations

$$\frac{\mathrm{d}y}{\mathrm{d}t} = A_4 i^4 + A_3 i^3 + A_2 i^2 + A_1 i - B_4 y^4 - B_3 y^3 - B_2 y^2 - B_1 y, \tag{3.10}$$

where y is conductivity; i is current though the lamp and A_k, B_k are parameters.

He modified the statement by another variable x (3.11) that solves the problem with not uniform conductivity in space.

$$\frac{\mathrm{d}y}{\mathrm{d}t} = A_4 i^4 + A_3 i^3 + A_2 i^2 + A_1 i - B_4 y^4 - B_3 y^3 - B_2 y^2 - B_1 (y - x), \tag{3.11}$$

where

$$\frac{\mathrm{d}x}{\mathrm{d}t} = C_4 y^4 + C_3 y^3 + C_2 y^2 + C_1 (y - x) + Dx.$$

For the HPML (400 W) is the equation with this coefficients

$$\frac{\mathrm{d}y}{\mathrm{d}t} = 0.4 i^4 + 9.15 i - 2.37 \cdot 10^7 y^4 - 1160 y, \tag{3.12}$$

and for HPSL (400 W) has this form

$$\begin{aligned} \frac{\mathrm{d}y}{\mathrm{d}t} &= 27.9 i^2 - 262 y^2 - 885 (y - x), \\ \frac{\mathrm{d}x}{\mathrm{d}t} &= 56.5 (y - x) + 925 x. \end{aligned} \tag{3.13}$$

Approach of University of Oviedo

In another articles of Antón *et al.* [ABF+02a, ABF+02b, ABV+04] is used extension of postulates proposed by Francis and applied to simulate HID lamps. They proposed recombination losses by *exponential* (3.14) and *quadratic* (3.15) factors as show following equations:

$$\frac{\mathrm{d}G}{\mathrm{d}t} = A\frac{i^2}{G} - BG - Ce^{DG}, \tag{3.14}$$

$$\frac{\mathrm{d}G}{\mathrm{d}t} = A\frac{i^2}{G} - BG - CG^2, \tag{3.15}$$

where A, B constants correspond to equation (3.8) $A = \frac{\alpha}{F}$, $B = \beta$; and C, D are added only. All constants depend on lamp type. They can be estimated by nonlinear adjusting methods using the experimental lamp data.

There were some mathematical efforts to avoid conductivity division in [BV04, BVAF+07]:

$$G' = A\frac{i^2}{G} - BG - Ce^{DG} \rightarrow y' = 2Ai^2 - 2By - 2\sqrt{y}Ce^{D\sqrt{y}}, \tag{3.16}$$

where y is substitution $y = G^2$.

Approach of University of Sheffield

In the work of Loo *et al.* [LSTD05] the plasma ionization balance equation (3.8) from Francis is used. It is utilized to simulate low pressure lamps. They rearrange it and found functional relation for the parameters α, β, and F (3.17).

$$\frac{\mathrm{d}\sigma_e}{\mathrm{d}t} = \left(\frac{\alpha}{F}\, v_L^2 - \beta\right)\sigma_e \rightarrow \frac{\mathrm{d}\sigma_e}{\mathrm{d}t} = (\psi_{ion} - \psi_{dif})\sigma_e, \tag{3.17}$$

where ψ_{ion} is the ionization function and ψ_{dif} is the diffusion function:

$$\psi_{ion} = f(v_L, T_{CS}) \tag{3.18}$$

$$\psi_{dif} = f(T_e, T_g, p_{Ar}, r), \tag{3.19}$$

where ionization function depends on the lamp voltage v_L and the cold-spot temperature T_{CS}. The diffusion function relys on the electron temperature T_e, the gas temperature T_g, the pressure of the argon p_{Ar}, and the lamp radius r.

This approach is performed for fluorescent lamp at low and high frequencies. The technological data of the lamp are required.

3.2.2 Modelling of energy balance equation

Works from Sharvatsas *et al.*, Tapia *et al.* and W. Yan and S. Y. R. Hui deal with HID lamp models based on the simplified physical laws of plasma discharge summarized in several equations.

For instance Yan and her colleague use following equations:

$$v(t) = L\frac{\mathrm{d}i}{\mathrm{d}t} + i(R+\mathcal{R}) + V_{ele} \tag{3.20}$$

$$V_{ele} = Ae^{-Bt}\sin(2C\pi ft) + Dt \tag{3.21}$$

$$\frac{\mathrm{d}T}{\mathrm{d}t} = a_1(P_{in} - P_{con} - P_{rad}) \tag{3.22}$$

$$P_{in} = i^2\mathcal{R} \tag{3.23}$$

$$P_{rad} = a_2 \exp\left(\frac{-ea_3}{kT}\right) \tag{3.24}$$

$$P_{con} = a_4(T - T_0) \tag{3.25}$$

$$\mathcal{R} = \frac{1}{G} = \frac{l}{\int \sigma_e(T)\mathrm{d}S} = a_5 T^{-\frac{3}{4}} \exp\frac{ea_6}{2kT}. \tag{3.26}$$

First equation describes ballast circuit (see in fig. 2.9 without starter and capacitor). The eq. (3.20) is essentially the same as eq. (2.7) with addition of the total electrode voltage drop V_{ele}. The ballast is represented by L, R, and lamp by its discharge resistance $\mathcal{R}$.

Model constants A, B, C, D in (3.21) depend on mains frequency f. They are obtained by a numerical method.

The equation (3.22) is the energy balance equation with terms of the input power (3.23), the thermal conduction (3.24) and the radiation loss (3.25), where a_{1-4} are adjustable model constants, e is the charge of electron, k is Boltzmann's constant, T is the gas temperature and T_0 is the arc tube wall temperature.

The last equation (3.26) is based on Saha eq., where l is the length of an arc, S is the cross-sectional area of the arc, $\sigma_e(T)$ is the electric conductivity of the arc, and a_5 and a_6 are adjustable model constants.

While constants of eq. 3.21 are obtained by simple linear regression, other model constants a_{1-6} are solved as an optimum problem by genetic algorithm.

This last mentioned approach of the solution is very similar to the objective of this work, which is not focused on deep physical analysis of the problem, but on the general solution of the optimum problem and application in electric circuit analysis.

3.3 G-model of a discharge lamp

In works of Stambouli [Sta84], Zissis *et al.* [ZAS+92, ZD02], Rossat-Mignod *et al.* [RMRJZ02] are used the same models that were obtained under some conditions. They describe a discharge lamp conductance by a differential equation of the first-order. Let us name it 'G-model':

$$\frac{\mathrm{d}G}{\mathrm{d}t} = a_2 i^2 - \sum_{k=1}^{n} b_k G^k, \tag{3.27}$$

where coefficients a, b_i can be *determined experimentally* from the voltage-current characteristics or from physical evaluation. The *physical evaluation* is possible when n is 2 or 3. In this case have coefficients physical meaning. It will be presented below in the section 3.3.1. Such model was presented for low and high pressure discharge lamps.

3.3.1 Calculation of the G-model

The Laboratory CPAT of UPS of Toulouse, namely prof. J.-J. Damelincourt, had presented on the COST Work group meeting 2004 in Liberec the approach of discharge conductivity calculation [DZ04]. The short description is presented below.

In figure 3.2 is model of the discharge channel in direct current mode. The discharge tube is divided into two zones. First *central hot zone* is described by $2\xi r$ and temperature T_c. $2\xi r$ is assumed that is constant along the L length. Second *cold zone* with temperature T_p surrounds the central one and is bounded by wall tube with $2r$ dimension. It is supposed the constant thermic flux in cold T_p zone.

An electric conductivity of the discharge can be calculated from

$$I = \frac{U}{\mathcal{R}} = GU \tag{3.28}$$

where I is current through discharge, U is discharge voltage, $\mathcal{R}$ is resistivity and G is the electric conductivity of the discharge.

With the conductivity times length of the discharge positive column g_s is possible to write

$$I = g_s E \tag{3.29}$$

where E is intensity of electric field, and g_s is

$$g_s = \sigma(T_c) S,$$

the $\sigma(T_c)$ is electric conductance per cross-section and S – the cross-section of the hot zone

$$S = \pi\xi^2 r^2.$$

The equation (3.29) is then

$$I = \sigma(T_c)\pi\xi^2 r^2 E. \tag{3.30}$$

The electric conductivity of the discharge could be defined under some conditions and simplifications:

$$G = \frac{I}{U_l}, \tag{3.31}$$

where U_l represents the voltage drop and I current through the plasma. The U_l is described by this equation with approximation term:

$$U_l = \Delta U_{electrodes} + hE \approx LE,$$

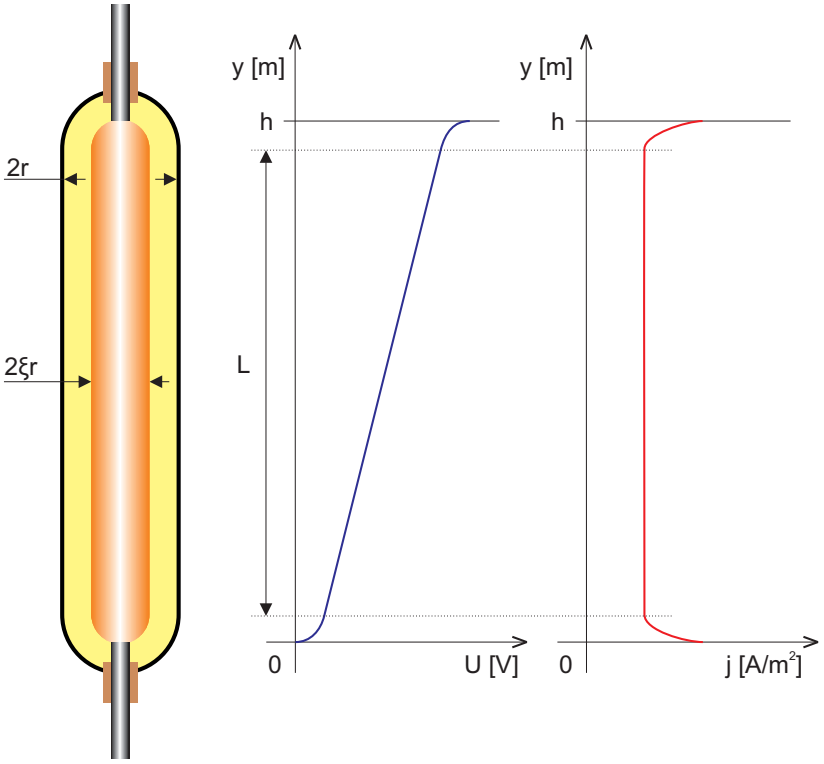

Figure 3.2: Model of the discharge channel.

where h is the discharge length, and L the length of the homogenous discharge (see in figure 3.2). With the mathematical reformulation

$$\frac{L}{h} = \frac{LE}{hE} = \frac{U_l}{hE} = \frac{1}{h}\frac{\frac{U_l}{I}}{\frac{E}{I}} = \frac{1}{h}\frac{\frac{1}{G}}{\frac{1}{g_s}} = \frac{1}{h}\frac{g_s}{G}$$

is given

$$G = \frac{g_s}{L} = \frac{\sigma(T_c)\pi\xi^2 r^2}{L}\,. \tag{3.32}$$

The term $\sigma(T_c)$ is substituted in the next step and with the knowledge of plasma physics is the whole equation calculated (see [DZ04]). The result for the stationary mode is as follows:

$$\frac{\mathrm{d}G}{\mathrm{d}t} = a_2 I^2 - \left[b_1 G + b_2 G^2\right], \tag{3.33}$$

where a_2, b_1, b_2 are quasi constant:

- $\dfrac{1}{a_2}$ means **input energy to the plasma** [J];
- b_2 means **radiation losses** $\left[\dfrac{\mathrm{V}^2}{\mathrm{A}^2\,\mathrm{s}}\right]$;
- b_1 means **thermal losses and the number of elastic collisions** [Hz].

This model is valid for the AC stationary mode too, where $I = i(t) = i$.

With the statements above can be equation (3.33) generalized to the polynomic form:

$$\frac{\mathrm{d}G}{\mathrm{d}t} = a_2 i^2 - \sum_{k=1}^{n} b_k\, G^k. \tag{3.34}$$

The physical meaning of coefficients b_k, where $k > 2$, is problematic.

3.3.2 Analytical solution of the G-model

Let us suppose the differential equation (3.34) with the $k = 2$. The equation is then

$$\frac{\mathrm{d}G}{\mathrm{d}t} = a_2 i^2 - b_2\, G^2 - b_1\, G. \tag{3.35}$$

This shape of nonlinear differential equation is similar to *Ricatti's equation*

$$\frac{\mathrm{d}y}{\mathrm{d}x} = a(x)y^2 + b(x)y + c(x), \tag{3.36}$$

where a, b, c are functions of x.

The Ricatti's equation has not analytical solution neither the G-model equation. The numerical solution is needed.

3.4 Identification of model parameters

Almost all mentioned models used coefficients (parameters) in their mathematical equations. Such parameters were identified either from

- *mathematical-physical analysis*

or

- *experimentally.*

The approach used for parameters' identification in works mentioned above was not discussed so clearly although it is the essential problem of models. Only in works of Loo [LSTD05], Yan [YH05], and Nachbaur [NG01] was this theme investigated more deeply. The optimum problem was taken into account and the identification algorithm was chosen.

The structure of the identification process under the condition of the zero mean value of a noise signal is sketched in figure 3.3.

Actuating signal $u(t)$ drive identified system and model. Their output signals $y(t)$ and $y_M(t)$ are toted up. On the difference Δy is applied the criterion $J(\mathbf{x})$. Strategy of parameters estimation is solved as the free extreme searching of the function with many variables $\mathbf{x}$. A number of searching methods exists.

The most used algorithms for nonlinear signals processing are iteration methods, where the solution (parameters) of the actual cycle are the improvement of the previous evaluation and the input for the next step in the cycle. The estimation of start parameters plays important role for convergency and stability of the method. For the extreme searching can be used for instance these two methods *Gaussian* or *Simplex* [Mod04].

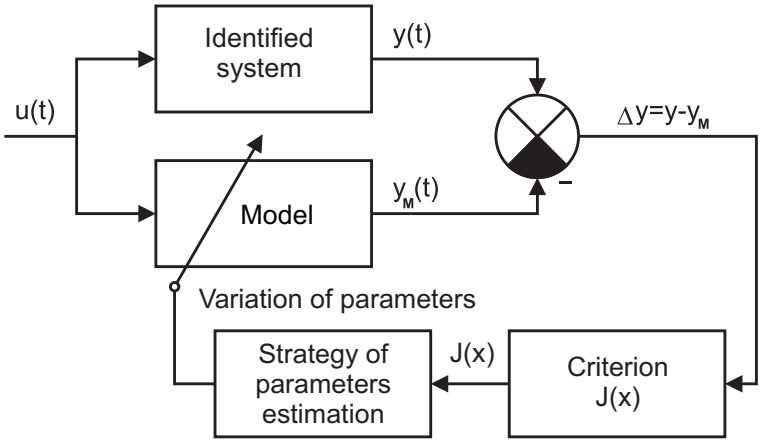

Figure 3.3: Parameter identification structure [Mod04].

3.4.1 Solution of the optimum problem

The mathematical model of discharge lamps has several parameters which should be determined. This task can be expressed as an optimum problem

$$min(J(\mathbf{x})), \tag{3.37}$$

where $J(\mathbf{x})$ is the function with variables (parameters) represented by a vector $\mathbf{x}$. In this case the quadratic criterion is used:

$$J(\mathbf{x}) = \int_0^{\tau} [y(t) - y_M(t)]^2 dt \simeq \sum_{i=1}^{N} [y_i - y_{Mi}]^2, \tag{3.38}$$

where $y(t)$ is the output from real system; $y_M(t)$ is the output from the model in continuous form. Outputs y_i, y_{Mi} are in discrete form and N is the number of measured samples.

3.5 The determination and implementation of numerical model

A mathematical model of a lamp with its circuit is given by differential and algebraic equations.

As a software tool for such mathematical and electrical analysis can be used number of professional programs separately. For equations solving is

possible to use *f.i.* MATLAB, MathCad, Mathematica, Octave *etc.* For electric simulation are here *e.g.* PSpice, Electronics Workbench, MATLAB Simulink with its Power system blockset *etc.*

For implementation of proposed algorithm, data processing and electric circuit simulation were chosen MATLAB the language of technical computing with its *Optimization Toolbox* and Simulink package.

Chapter 4

Experiments – data mining for modelling

This chapter describes experiments on different types of discharge lamps powered by commercially produced ballasts. It presents electric characteristics such as voltage, current, voltage-current, conductivity and electric parameters of circuits' parts. All of the characteristics were obtained in stable working state under the laboratory conditions. The transient phenomena (starting periods) were not observed.

Measurements were realized on the devices at both the department of electrical engineering at FM TUL and partner institution CPAT at UPS in Toulouse.

The aim of experiments was the observation of different discharge lamps behaviour and acquirement of their electrical data for the offline identification and verification of lamp models.

4.1 Measurement devices

For majority of all measurements were used a multichannel recorder EMU-2 of TU of Liberec[1] designed for measurements on three-phase transformers. This device is therefore able to acquire simultaneously analog signals from 18 channels (9× low voltage BNC inputs, 9× high voltage inputs) with the sample frequency up to 12.8 kSa/s. Each channel has its own signal path with 16 bits A/D Σ-Δ converter AD73360, with a S/N of around 70 dB. The system has ethernet interface for data transfer to external computer. All parameters are summarized in table A.2.

[1] designed by J. Václavík and M. Novák

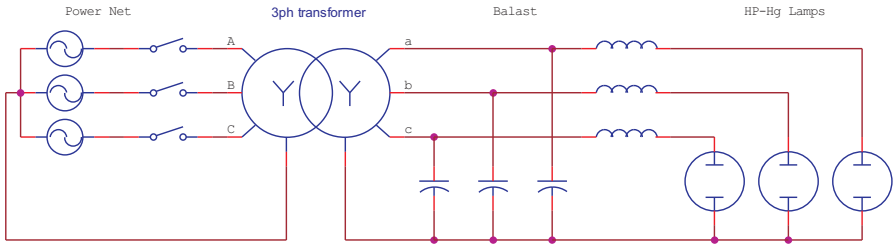

Figure 4.1: The layout of the mini-lighting network in configuration with HPMLs [NVR02].

Mini-lighting network in lab of CPAT is the experimental device for investigation of different phenomena on power net loaded by various lamps. It is constructed as rack of high pressure lamps (HPMLs and HPSLs). Each rack can contain nine lamps, three for each phase, and their appropriate ballasts. Various combinations and numbers of active lamps are possible. The set of lamps is supplied over the 10 kVA three-phase transformer from a power net (see in fig. 4.1). Although the system has necessary measurement electronics (Fasttrack AD card, high-voltage differential and current probes) the EMU-2 system for data acquisition was used.

The measurements on the MLN are in parts presented in technical reports of M. Novák and Václavík, and mine [NV01, NVR02, VK03, NV04].

Some presented measurements were provided by multifunction analyzer PULSE LabShop v.10.1.0.15 of Bruel-Kjaer of the department of measurement KAM at TUL. This commercial capture analyzer was used for comparative measurements. The sample frequency is 65536 kHz.

For some experiments the one phase AC power source KIKUSUI PCR 2000A was used. This source can simulate mains voltage of different shapes, frequency with the high quality and high stability (tab. 4.1). The using of such source allows to avoid negative influence of deformed mains voltage[2] on a lamp load. It can be seen in waveform *eg.* in figure 4.7. The voltage has not sine shape but almost trapezoidal. In figure 4.11 is supply voltage deformed evidently.

[2] A deformation caused by other electric loads in net.

4.2 Data processing

All taken data were captured and saved as multicolumn matrixes to *.mat files. Where every column means separate quantity for time, voltage and current.

Data in one row was all taken in one time. Several programs (*.m files) were developed to work with these data. They can filter data or split them to separate vectors due to its meaning. The set of programs contain preliminary release of power electronics Matlab toolbox developed in our laboratory KEL. All *.m files contain standard Matlab help, which can be used by typing *help name.m* to Matlab command window. Most of them have comment too, but some less important in Czech only. Names of the function remain in Czech because of compatibility. For instance the m-file for the rms value evaluation *efektiv.m* or average value *stredni.m etc.* were developed (see in appendix A.1).

4.2.1 Conductivity computation

It is impossible to measure the electric conductivity directly. It is computed as the fraction of measured current $i_{lamp}(t)$ and voltage $u_{lamp}(t)$:

$$g(t) = \frac{i_{lamp}(t)}{u_{lamp}(t)}. \tag{4.1}$$

Both the current and the voltage signal may contain some offset which appears as a parasitic term in the determination of $g(t)$. It is discussed in sec. 4.2.2.

The ratio (4.1) becomes problematic when the voltage u_{lamp} cross zero. The conductivity waveform get almost unbounded peaks (fig. 4.2).

Their values and directions are different in each period. They depend on sampled values of voltage and current.

The approaches how to avoid problems with conductivity computation:

Table 4.1: Parameters of KIKUSUI AC power source PCR 2000A [Kik].

Output rating, AC mode (AC rms value)	
Voltage	1 to 150 V/2 to 300 V
Current	20 A/10 A
Power capacity	2 kW
Frequency	1 Hz to 999.9 Hz

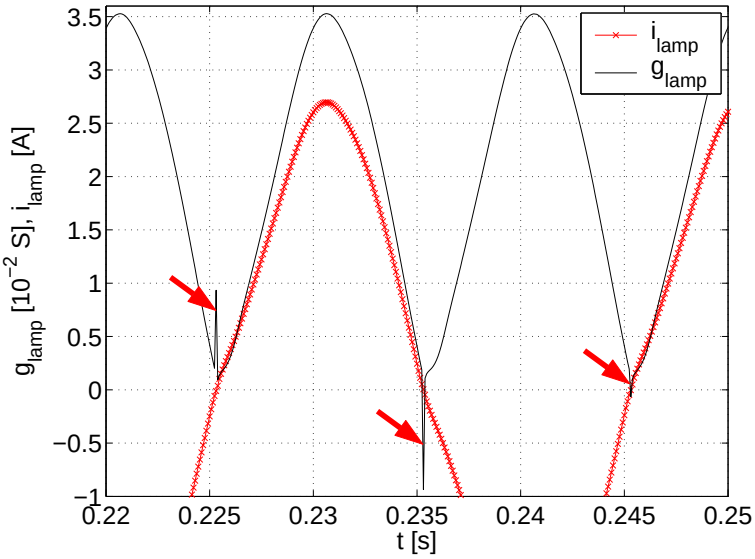

Figure 4.2: Peaks in conductivity waveforms after *cutdc* correction obtained on metal halide lamp in circuit with magnetic ballast (sec. 4.6).

- remove problematic samples of voltage and current [RKM04, Kob04];
- limit conductivity in specific range and filter [Kop05a];
- redefine the conductivity ratio computation *eg.* use of time-varying phasors [Dup05, DKD+06].

4.2.2 Offset in measured signals

Offsets in curent and voltage were observed in all measurements. There exist two possible causes:

- an offset of measuring probes;
- an unsymmetry of a lamp behaviour in AC mode.

The offset of measuring probes is known and calibration of used measuring channels is required. Unfortunately the offset can shift during measuring and a recalibration is therefore needed after each measurement. Another approach can be a correction of measured signals (oscilograms) by software way.

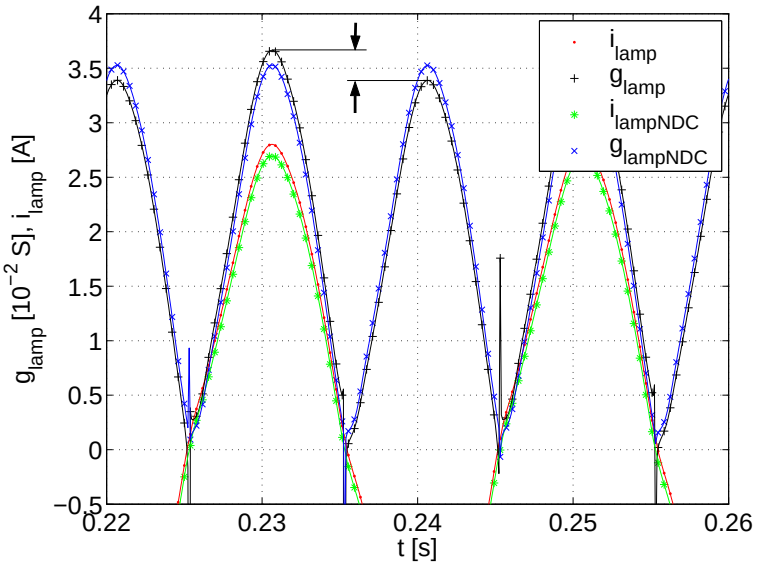

Figure 4.3: Waveforms of lamp current and conductivity of metal halide lamp in circuit with magnetic ballast (sec. 4.6). Difference between waveforms of conductivity g_{lamp} calculated from current with DC part i_{lamp}, and conductivity $g_{lampNDC}$ calculated from current without DC part $i_{lampNDC}$.

An impact of *unsymmetrical behaviour of a lamp conductivity in AC mode* of the power supply and *in different operation position of the lamp* (sec. 4.6.3) was needed to explore.

The impact of influence of DC value in current is shown in figure 4.3. In this case g-unsymmetry represents the difference between maximal values circa 3 mS ($\sim$10 % of maximal value).

The questions above had to be answered before the data processing in identification procedures. The special measuring on MH lamp (sec. 4.6) was also provided. The purpose of this measurement was information acquisition of unsymmetrical behaviour of a lamp conductivity and the eventual impact of DC values on voltage and current.

Probes and channels were calibrated at first. An oscillogram of DC current from the current source was measured and saved. The value of the DC current was measured by the precise amperemeter too. Then the measurement of oscilograms of u_{lamp} and i_{lamp} was realised. After this the DC current was measured again. The measured values from the amperemeter and from EMU-2 were compared and appropriate enclosures were deduced.

According to this experiment it was observed that the unsymmetry is greatly influenced more the current probes offset than by the offsets of EMU-2 high voltage channels. The lamp offset was noticed also, but its value was negligible compared to measurement errors.

On the basis mentioned above it was possible to simplify the measurements and use function *cutdc.m*[3] for data processing. This function is for removing of DC part (average value) from measured signal, that has to be in vector form. In principle it realizes this function

$$i_{lampNDC}(t) = i_{lamp}(t) - \frac{1}{T}\int_0^T i_{lamp}(t)\,\mathrm{d}t. \tag{4.2}$$

It is also possible to assume this effect of symmetrical behaviour of the lamp from its construction 4.7. Both electrodes have the same shape and are made of the same material. Of course the impurities and technological defects can appear but in this case they are not taken into account.

4.2.3 Parts of electric circuits

The magnetic ballasts were used for number of measured lamps. The linear model mentioned in sec. 2.5 was chosen for MB description in sec. 6.1.2. The impedance of lossless ferromagnetic coil is given

$$\mathbf{Z}_{ball} = R_{ball} + jX_{ball}, \tag{4.3}$$

where ballast reactance X_{ball} is defined as follows

$$X_{ball} = \omega L_{ball}. \tag{4.4}$$

The ballast reactance depends on ballast inductance L_{ball} and angular frequency (speed) ω that can be defined via period T of supply voltage or its frequency f

$$\omega = \frac{2\pi}{T} = 2\pi f. \tag{4.5}$$

For simulation purpose was important to get alternative parameters of such coil, the ballast inductance L_{ball} and resistance R_{ball}.

Measurement of L_{ball} and R_{ball} by RLC meter was not successful. The obtained values were not realistic, because the driving frequency and signal of the measurement system. The frequency was too high over the net frequency, and the signal was too low and could not saturate the coil core.

[3] A function from PEM Toolbox of KEL TUL see in appendix A.1

The method based on powers was applied to evaluate ballast parameters. The circuit equation (2.7) was used to get voltage drop on the ballast

$$u_{ball} = u - u_{lamp}. \tag{4.6}$$

Powers (real power P, reactive power Q, and complex power S) are solved as follows:

$$P_{ball} = \frac{1}{T}\int_0^T u_{ball} \cdot i_{lamp}\,\mathrm{d}t \tag{4.7}$$

$$S_{ball} = U_{ball} \cdot I_{ball}, \tag{4.8}$$

$$Q_{ball} = \sqrt{S_{ball}^2 - P_{ball}^2}, \tag{4.9}$$

U_{ball} and I_{ball} are rms values of oscilograms u_{ball}, i_{ball}, defined as

$$U = U_{ef} = U_{rms} = \sqrt{\frac{1}{T}\int_0^T u^2(t)\,\mathrm{d}t}. \tag{4.10}$$

Ballast parameters are calculated as fraction of real/reactive power and rms value of the current through the ballast:

$$R_{ball} = \frac{P_{ball}}{I_{ball}^2}, \tag{4.11}$$

$$L_{ball} = \frac{Q_{ball}}{I_{ball}^2\,\omega}. \tag{4.12}$$

Alternative ballast parameters are given from the statement for reactive power (4.9), which neglects the impact of nonlinearities to net currents. In such deformed currents can occur DC values, that cause this unequality

$$S^2 \geq P^2 + Q^2. \tag{4.13}$$

The difference between left and right side is in deformation power:

$$P_{def}^2 = S^2 - P^2 - Q_1^2, \tag{4.14}$$

where the Q_1 is a reactive power of the first harmonic (more in [RRK98]).

Thanks to the simplification in ballast alternative parameters evaluation presented above, the errors have to be taken into account.

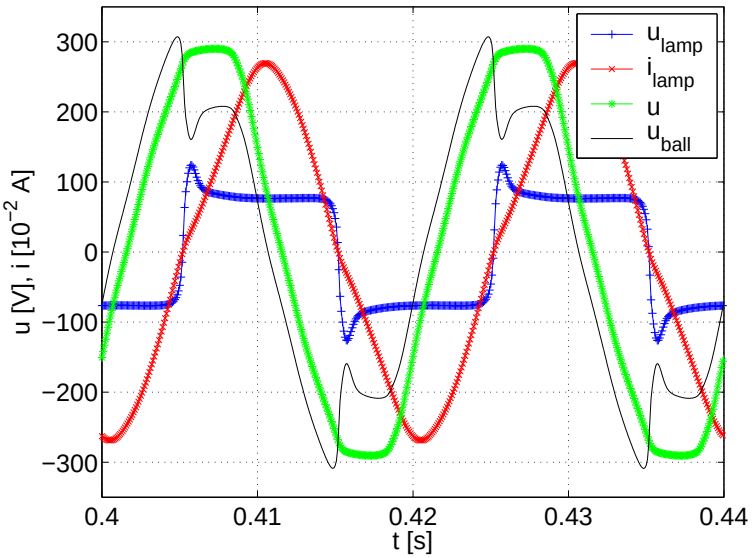

Figure 4.4: Wavefoms of voltages and current in circuit of metal halide lamp with magnetic ballast (sec. 4.6).

4.2.4 Phasor diagrams

A discharge lamp is without any doubts a non linear load which causes deformation in both current and voltage. In time domain in figure 4.4 are visible phase shifts. The voltage on ballast leads supply voltage and lamp voltage/current. The lamp voltage seems to be in phase with the lamp current.

In publications of Waymouth [Way71] and Miškařík [Miš79] phasor diagrams for discharge lamps with magnetic ballasts where the lamp current lags the lamp voltage are presented.

How is it possible? It is the result of non linear behaviour of the discharge lamp.

Waymouth says the lamp has a virtual *power factor* defined [RRK98] as follows

$$\lambda = \frac{P}{S} = \frac{\frac{1}{T}\int_0^T u(t)\cdot i(t)dt}{\sqrt{U_{rms}^2 I_1^2 + U_{rms}^2 (I_{avg}^2 + \sum_{n=2}^{\infty} I_n^2)}}, \tag{4.15}$$

that is in general inductive, because the voltage is higher between 0° and 90° of the current half cycle than between 90° and 180°. Their presented phase diagrams show vectors of first harmonics only, what is not so clearly mentioned.

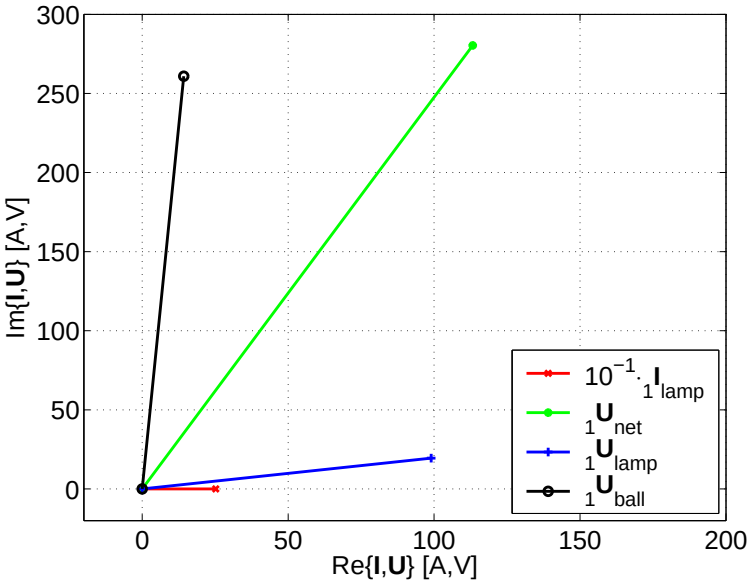

Figure 4.5: Phasor diagram of rms values of voltages and current first harmonics in circuit of metal halide lamp with magnetic ballast. (sec. 4.6).

The lamp current lags the lamp voltage due to ionisation effects explains Miškařík. There is no further specification of what harmonics of voltage are used in phasor diagrams.

In figure 4.5 is phasor diagram of MH lamp voltages and current. Vectors of first harmonics illustrate phase shifts among all electric quantities. The phasor of $\mathbf{U}_{lamp}$ leads $\mathbf{I}_{lamp}$, but first harmonics only. This description acknowledges arguments above (the inductive character of the discharge lamp) but does not describe other harmonics.

For the description of nonlinearities caused by lamp or any nonlinear electric load is used *total harmonic distortion THD*. For instance THD of voltage is defined as follows

$$\text{THD V} = \frac{\sqrt{\sum_{n=2}^{50} U_n^2}}{U_1} = \frac{\sqrt{U_{rms}^2 - U_1^2}}{U_1}, \tag{4.16}$$

where U_{rms} is rms value of voltage and U_1 is rms value of the first harmonic of voltage [RRK98].

4.3 Low pressure mercury lamps

There are many types of low pressure mercury lamps (sec. 2.3.1).

Following measurements were provided with standard[4] linear lamps of different wattage in circuits with magnetic ballasts with no compensation capacitors.

In figure 4.6 is typical circuit connection of fluorescent lamp, magnetic ballast, and glow starter. Their specifications are summarized in tables for each measurement setup. A supply voltage $u(t)$ was obtained from the power network or from the voltage power source. The supply voltage, the lamp voltage $u_{lamp}(t)$ and the lamp current $i_{lamp}(t)$ were measured. Because the transient phenomenon, starting phase of lamps, were not studied the current $i_s(t)$ passing through the starter was supposed as *zero*. Hence the lamp current corresponds to the current from net:

$$i(t) = i_{lamp}(t). \tag{4.17}$$

The ballast voltage $u_{ball}(t)$ indicates losses in the coil and magnetic material. This voltage drop was not measured. It was calculated from Kirchoff's voltage law by eq. (4.6).

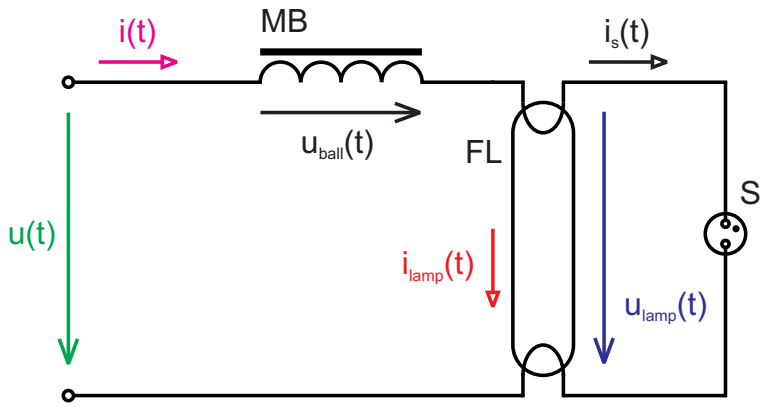

Figure 4.6: Electric circuit of fluorescent lamp powered by magnetic ballast. MB – magnetic ballast; FL – fluorescent lamp; S – glow starter.

Besides the specification of circuit components there are also rms values of circuit quantities and alternative parameters of magnetic ballasts in the table. Figures with measured or computed waveforms of voltage, current, conductivity and volt-current are included.

[4]commercial products

4.3.1 Linear fluorescent lamp 58 W

The experiment was provided on standard commercial luminary set with fluorescent lamp in circuit with magnetic ballast (figure 4.6). The specification of used components are in table 4.2.

Table 4.2: Parameters of the circuit with 58 W FL

FL	Sylvania standard F 58 W/154				
MB	Layrton ARC 65/23, 65 W, 230 V, 50 Hz, 0.67 A				
U_{net}	=	221 V	U_{lamp}	=	126 V
I_{lamp}	=	0.52 A	G_{lamp}	=	5 mS
P_{net}	=	61 W	P_{lamp}	=	51 W
Q_{net}	=	98 VAr	Q_{lamp}	=	41 VAr
S_{net}	=	115 VA	S_{lamp}	=	65 VA
R_{ball}	=	37 Ω	L_{ball}	=	970 mH
THD_{lamp} V	=	57.43 %	THD_{net} V	=	7.74 %
THD_{lamp} A	=	15.32 %	λ_{lamp}	=	0.778

In figure 4.7 are waveforms u, u_{lamp}, i and i_{lamp}. The deformation of the supply voltage is not so great. The lamp voltage has peaks over 200 V with one overshoot and than falls down to stable part at c. ±120 V, it corresponds with rms value 126 V. In the current curve the influence of the ballast inductance is visible. The shape of the conductivity curve copy the current. The conductivity maximum rises up to 8 mS. Peaks in conductivity are preset at the characteristic.

The voltage-current characteristic in figure A.1(a) clearly encloses the working ranges.

The measurement was taken by multichannel recorder EMU-2 with hall probes PR30 (range 20 A, 100 mV/A) under the laboratory condition at KEL FM. As a power supply was used network voltage.

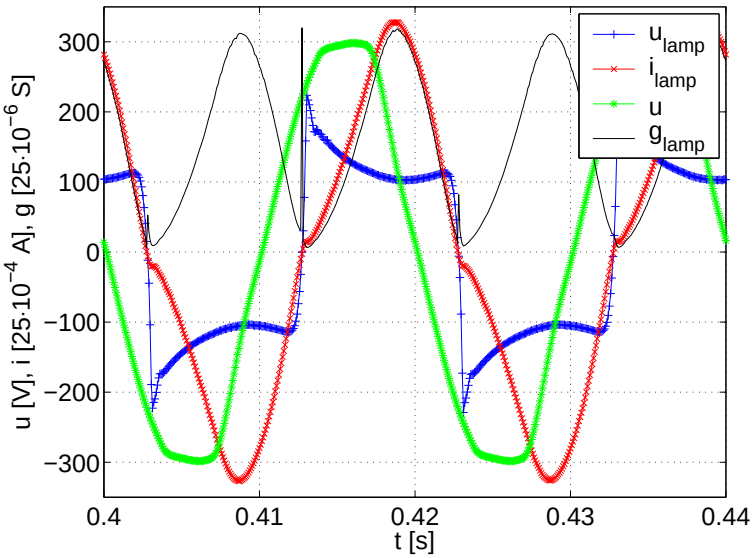

Figure 4.7: Measured electric characteristics of 58 W linear fluorescent lamp and waveform of computed conductivity.

4.3.2 Linear fluorescent lamp 36 W

Conditions of measurement setup with 36 W linear fluorescent lamp was the same as in previous case (figure 4.6). The change was in luminary setup only (tab. 4.3).

Table 4.3: Parameters of the circuit with 36 W FL

FL	Philips master LTD 36 W/840				
MB	Elektrokovina DFT 5338 50 Hz				
U_{net}	=	226 V	U_{lamp}	=	104 V
I_{lamp}	=	0.41 A	G_{lamp}	=	5 mS
P_{net}	=	43 W	P_{lamp}	=	34 W
Q_{net}	=	82 VAr	Q_{lamp}	=	26 VAr
S_{net}	=	93 VA	S_{lamp}	=	43 VA
R_{ball}	=	54 Ω	L_{ball}	=	1.380 H
THD_{lamp} V	=	59.94 %	THD_{net} V	=	4.62 %
THD_{lamp} A	=	10.49 %	λ_{lamp}	=	0.794

In figures 4.8, and A.1(b) are all measured and computed characteristics. Almost no difference between previous measurement and this. The lamp

voltage peak is the same as previous, but the stable region is lower than by 58 W FL around ±100 V (see the rms value 104 V). The influence of a noise or oscillation of the plasma in this region are shown. The conductivity value is approximately the same also.

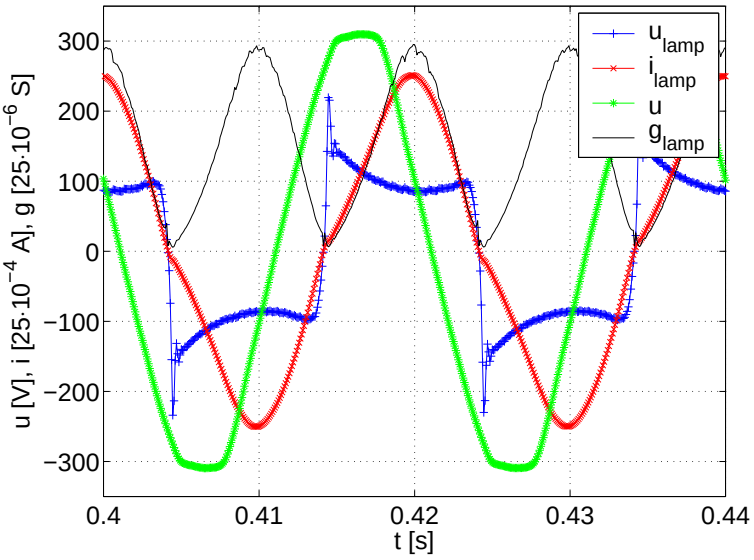

Figure 4.8: Measured electric characteristics of 36 W linear fluorescent lamp and waveform of computed conductivity.

4.3.3 Linear fluorescent lamp 18 W

The experiment with standard 18 W linear fluorescent tube brought other information on low pressure mercury lamps. With its size approaches to compact fluorescent lamps and behaviour too. Unfortunately characteristics of CFLs were not studied for appropriate comparison.

The circuit consisted of commercially produced components. The circuit of the lamp, magnetic ballast and starter was connected the same way as in figure 4.6. The specification of components and other electrical parameters are summarized in table 4.4.

The supply voltage is pure sine wave see in fig. 4.9 and in THD_{net} V in table 4.4. In figure 4.9 are all measured electric characteristics. The voltage peak reaches ±140 V and then stabilizes its value at rms value 57 V with high frequency oscillations c. 15 kHz. These oscillations impact, of course, the lamp conductivity waveform.

Analogous to previous was generated voltage-current characteristics of the lamp (in figure A.1(c)) which shows the work ranges of the lamp.

Table 4.4: Parameters of the circuit with 18 W FL

FL	Osram Cool White 18 W/20				
MB	Brilux model PC – Z118, 20 W, 230 V, 50 Hz, 0.37 A				
U_{net}	=	233 V	U_{lamp}	=	57 V
I_{lamp}	=	0.37 A	G_{lamp}	=	8 mS
P_{net}	=	49 W	P_{lamp}	=	17 W
Q_{net}	=	71 VAr	Q_{lamp}	=	12 VAr
S_{net}	=	86 VA	S_{lamp}	=	21 VA
R_{ball}	=	234 Ω	L_{ball}	=	1.560 H
THD_{lamp} V	=	58.59 %	THD_{net} V	=	0 %
THD_{lamp} A	=	7.61 %	λ_{lamp}	=	0.824

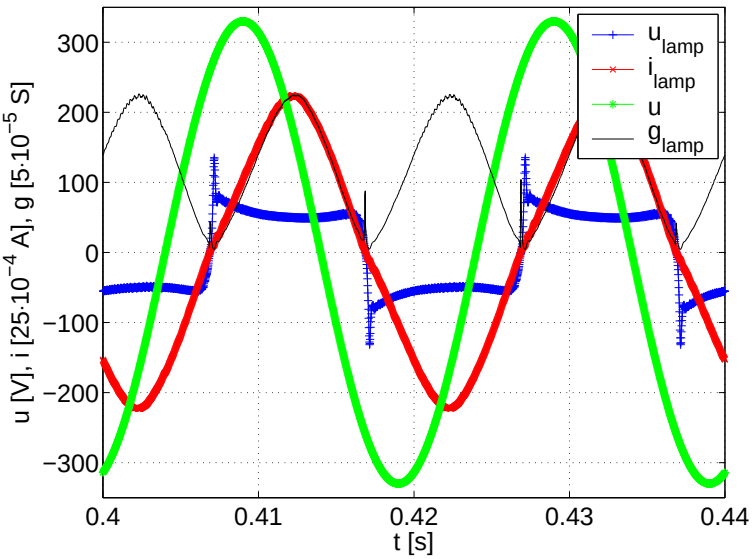

Figure 4.9: Measured electric characteristics of 18 W linear fluorescent lamp and waveform of computed conductivity.

4.4 High pressure mercury lamps

The general information about high pressure mercury lamps is in section 2.4.1. These experiments were realized with measurement setup of minilighting network system in Toulouse (fig. 4.1) where were used the same nine high pressure mercury lamps.

The electric circuit of one lamp and ballast only in figure 4.10.

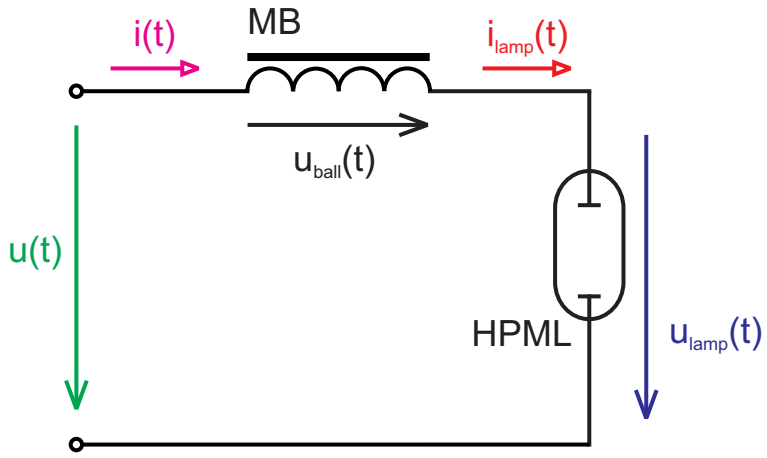

Figure 4.10: Electric circuit of HPM lamp powered by magnetic ballast. MB – magnetic ballast; HPML – high pressure mercury lamp.

The HPML does not need external starter due to its start electrode. The specification of one circuit shown in figure 4.10 is in table 4.5.

Table 4.5: Parameters of the circuit with 400 W HP mercury lamp

HPML	Philips HPL – N 400 W				
MB	Philips HID – HeavyDuty BHL 400 L32 240 V 50 Hz				
U_{net}	=	226 V	U_{lamp}	=	140 V
I_{lamp}	=	2.9 A	G_{lamp}	=	21 mS
P_{net}	=	373 W	P_{lamp}	=	365 W
Q_{net}	=	537 VAr	Q_{lamp}	=	177 VAr
S_{net}	=	654 VA	S_{lamp}	=	405 VA
R_{ball}	=	1.0 Ω	L_{ball}	=	170 mH
THD_{lamp} V	=	37 %	THD_{net} V	=	7.12 %
THD_{lamp} A	=	10.45 %	λ_{lamp}	=	0.899

In the MLN are in each phase three standard HPM lamps operating in horizontal burning position with appropriate magnetic ballasts (more in company catalogue [PHIb]).

All the electric characteristics are summarized in figure 4.11. The MLN use its own three phase power transformer, so the power supply is quite deformed. The lamp voltage has not oscillation waves after each ignition like LP lamps. The stabilisation in voltage is for this 400 W lamp c. 140 V. The lamp current has almost harmonic shape with rms value 2.9 A. The sizable difference against LP mercury lamps is in conductivity which is five times greater.

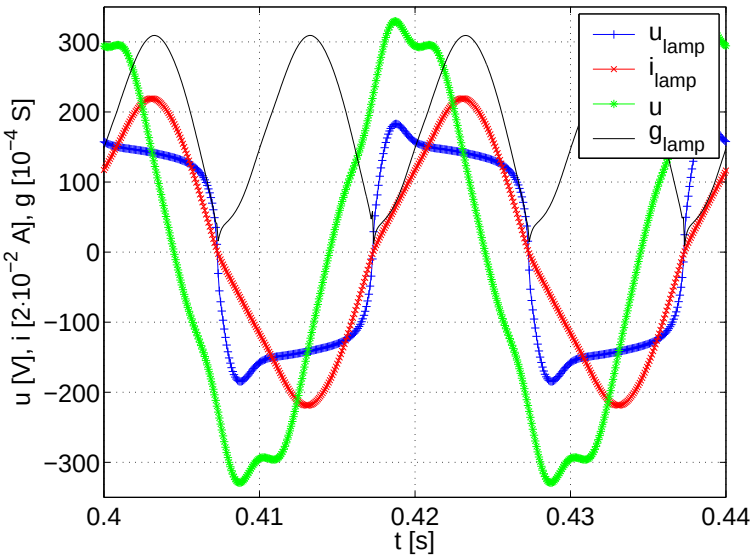

Figure 4.11: The electric characteristics of 400 W HP mercury lamp in circuit with magnetic ballast.

4.5 High pressure sodium lamps

High pressure sodium lamps were mentioned in section 2.4.2. They were measured in the MLN setup. They operated in horizontal burning position. In figure 4.12 is general electric circuit[5] for one of nine lamps connected to magnetics ballast and starters. These lamps and accessories are standard

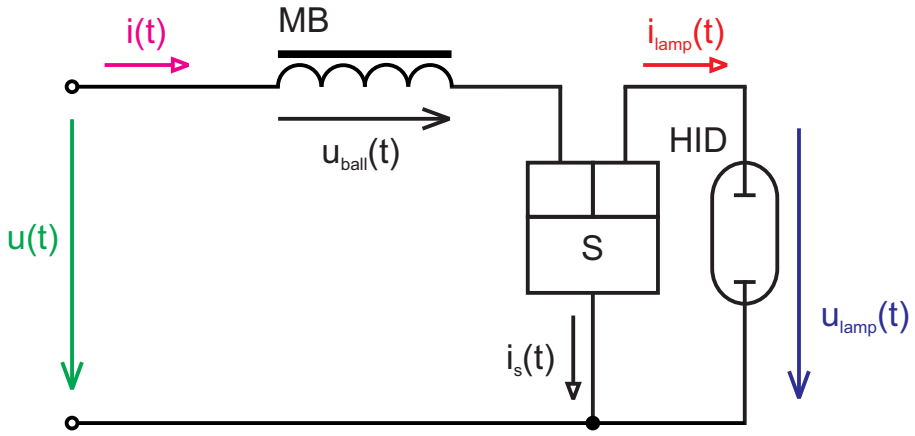

Figure 4.12: Electric circuit of HID lamp powered by magnetic ballast. MB – magnetic ballast; HID – high intensity discharge lamp; S – starter (ignitor).

products of Philips company [PHIb]. Their specification is in table 4.6.

Table 4.6: Parameters of the circuit with 400 W HP sodium lamp

HID	Philips SON – T 400 W				
MB	Philips HID – HeavyDuty BSN 50 L34 240 V 50 Hz				
S	SN 58 220 – 240 V 50/60 Hz				
U_{net}	=	219 V	U_{lamp}	=	73 V
I_{lamp}	=	3.81 A	G_{lamp}	=	54 mS
P_{net}	=	305 W	P_{lamp}	=	244 W
Q_{net}	=	777 VAr	Q_{lamp}	=	134 VAr
S_{net}	=	835 VA	S_{lamp}	=	279 VA
R_{ball}	=	4 Ω	L_{ball}	=	160 mH
THD_{lamp} V	=	63.16 %	THD_{net} V	=	33.36 %
THD_{lamp} A	=	37.42 %	λ_{lamp}	=	0.876

[5]The same circuit is for the MHL.

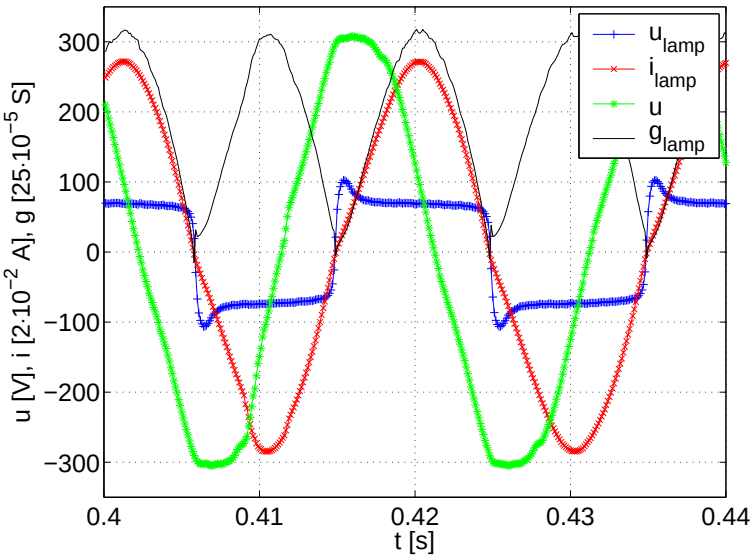

Figure 4.13: Measured electric characteristics of 400 W HP sodium lamp and computed conductivity.

The mains supply for lamp electric circuit in figure 4.12 is not directly from the network, but from the three phase transformer of MLN. The supply voltage is not so deformed as in measurements with HPMLs.

4.6 High pressure metal halide lamp

The metal halide lamp with ceramic discharge tube (see the construction in sec. 2.4.3) was the light source for all follow experiments. The lamp was standard type Osram Powestar HCI – T 150 W NDL that can work in any position, and operate with magnetic or electronic ballast. More information about this lamp is in company catalogue [OSR].

4.6.1 Lamp with magnetic ballast

The measurement setup consists of the circuit illustrated in fig. 4.12. Values of the components and electric characteristics are in table 4.7. The lamp was operating in vertical position. Some results of measurements on this electric load powered with mains real voltage was presented in ECMS03 conference [KN03].

In presented figures and tables was used measurement with KIKUSUI power supply. That is why the total harmonic distortion of the supply voltage is equal to zero.

Table 4.7: Parameters of the circuit (fig. 4.12) with 150 W MH lamp and MB

HID	Osram Powerstar HCI – T 150 W/NDL
MB	OMBIS 150 A604W 220 – 240 V 50 Hz
	– connection to the tap 230 V
S	ZRM 2,5 – WS/B

U_{net}	=	230 V	U_{lamp}	=	95 V
I_{lamp}	=	1.81 A	G_{lamp}	=	21 mS
P_{net}	=	164 W	P_{lamp}	=	142 W
Q_{net}	=	382 VAr	Q_{lamp}	=	97 VAr
S_{net}	=	416 VA	S_{lamp}	=	172 VA
R_{ball}	=	7 Ω	L_{ball}	=	350 mH
THD_{lamp} V	=	59.35 %	THD_{net} V	=	0 %
THD_{lamp} A	=	8.17 %	λ_{lamp}	=	0.825

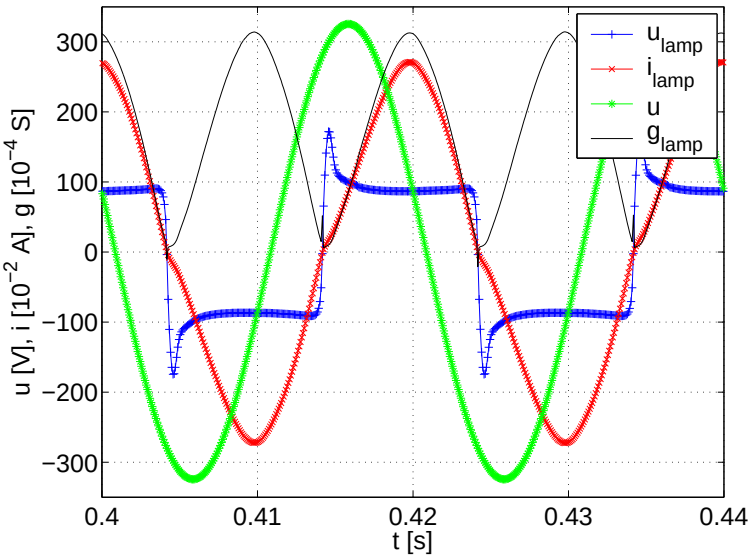

Figure 4.14: Measured voltages, current and computed conductivity of 150 W MH lamp in circuit with MB.

4.6.2 Lamp with electronic ballast

In figure 4.15 is schematic connection of metal halide lamp supply by electronic ballast. The specification of the ballast is in table 4.8. It is standard digital electronic nondimmable ballast (see more in product catalogue [Tri]).

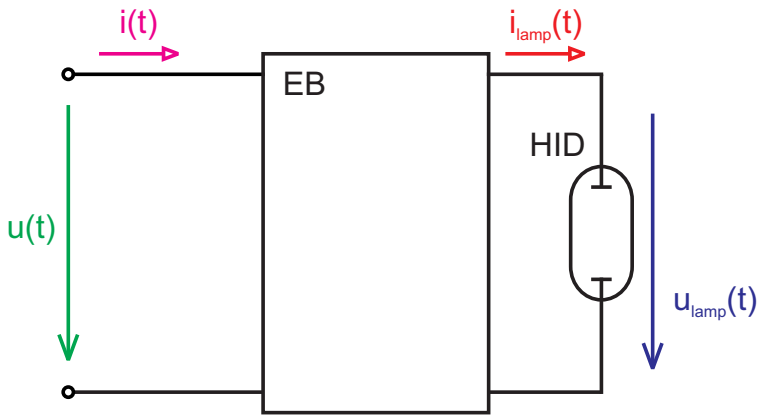

Figure 4.15: Electric circuit of HID lamp powered by electronic ballast.

In figure 4.16 are all input and output characteristics with the waveform of conductivity.

Table 4.8: Parameters of the circuit with 150 W MH lamp powered by EB

HID	Osram Powerstar HCI – T 150 W/NDL				
EB	Tridonic PCI 0150 A001				
U_{net}	=	233 V	I_{lamp}	=	1.65 A
U_{lamp}	=	89 V	I_{net}	=	0.73 A
G_{lamp}	=	19 mS			
P_{net}	=	166 W	P_{lamp}	=	147 W
Q_{net}	=	35 VAr	Q_{lamp}	=	8 VAr
S_{net}	=	169 VA	S_{lamp}	=	147 VA
THD_{lamp} V	=	50.34 %	THD_{net} V	=	5.21 %
THD_{lamp} A	=	48.17 %	THD_{net} A	=	11.35 %
λ_{lamp}	=	0.998	λ_{net}	=	0.979

Input of the electronic ballast is connected to the power net. The values of power factor and currents agree with catalogue's. The electronic ballast is supposed as a black box. Because there is no simulation efforts, the structure of the electronic power source were not studied.

The output of the electronic ballast is the square signal of 89 V and 1.65 A

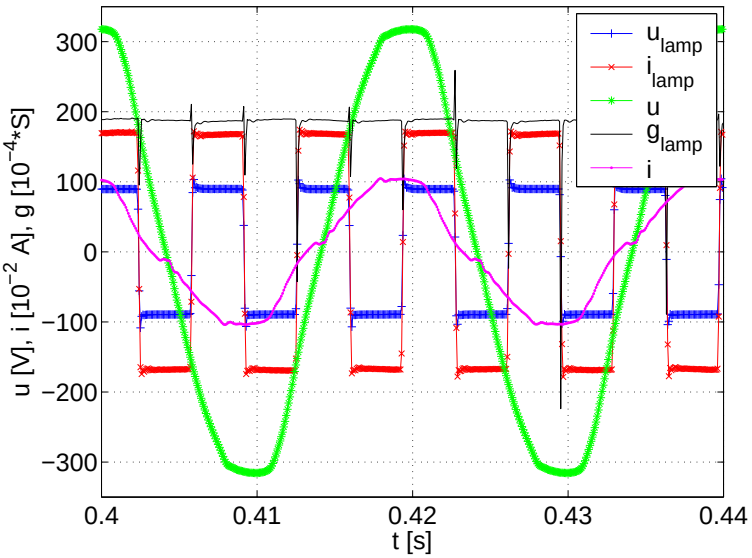

Figure 4.16: Voltages, current and conductivity of 150 W MH lamp powered by electronic ballast.

of the frequency 145 Hz. The conductivity changes in transient regions of the voltage/current in peaks form. There is not so visible impact of nonlinearity of the lamp, because the voltage and current are in phase (cf. the power factor in table 4.8).

4.6.3 Experiments with lamp operation positions

Since this type of the lamp can operate in any burning position some experiments were realized. It was observed the impact on electric characteristics *e.g.* unsymmetry change, conductivity change ... *etc.*

The lamp was powered through magnetic ballast with the same parameters as are mentioned in table 4.7. The power supply KIKUSUI supplied the circuit. The EMU-2 with PR30 current probe were used as the data acquisition device.

The two voltage-current characteristics of the same discharge lamp but in different operation position are in figure 4.17. The lamp in horizontal operation position has less conductivity than in vertical. The difference is caused by physical process inside the arc tube ([Way71, Fle06]).

The topic of operation position influence on lamp behaviour was presented

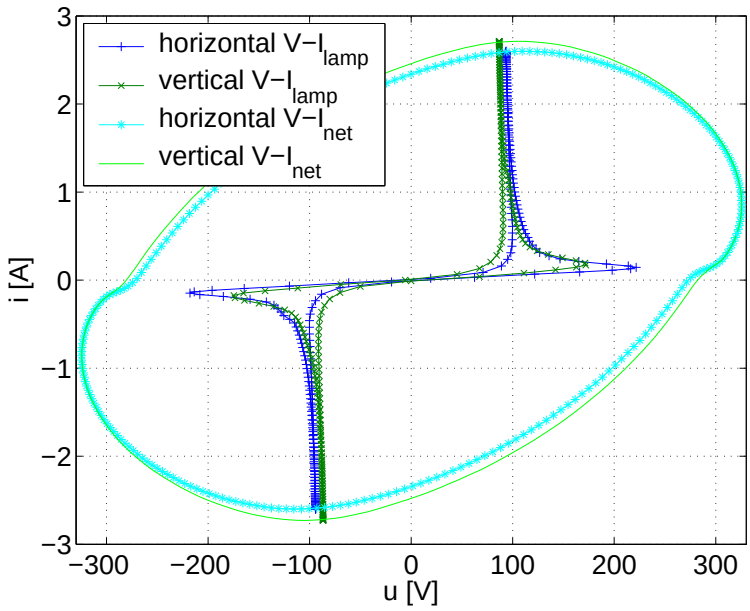

Figure 4.17: Voltage-current characteristics of 150 W MH lamp in horizontal and vertical operation position.

on COST MC meeting in Mierlo NL [KVR06].

Table 4.9: Parameters of operation position of 150 W MH lamp.

Horizontal position					
U_{net}	=	230 V	U_{lamp}	=	106 V
I_{lamp}	=	1.73 A	G_{lamp}	=	18 mS
P_{net}	=	166 W	P_{lamp}	=	146 W
Q_{net}	=	361 VAr	Q_{lamp}	=	111 VAr
S_{net}	=	397 VA	S_{lamp}	=	183 VA
R_{ball}	=	7 Ω	L_{ball}	=	350 mH
THD_{lamp} V	=	64.55 %	THD_{net} V	=	0 %
THD_{lamp} A	=	8.86 %	λ_{lamp}	=	0.797
Vertical position					
U_{net}	=	230 V	U_{lamp}	=	95 V
I_{lamp}	=	1.81 A	G_{lamp}	=	21 mS
P_{net}	=	164 W	P_{lamp}	=	142 W
Q_{net}	=	382 VAr	Q_{lamp}	=	97 VAr
S_{net}	=	416 VA	S_{lamp}	=	172 VA
R_{ball}	=	7 Ω	L_{ball}	=	350 mH
THD_{lamp} V	=	59.35 %	THD_{net} V	=	0 %
THD_{lamp} A	=	8.17 %	λ_{lamp}	=	0.825

4.6.4 Experiments with lamp operation frequency

Although the measured metal halide lamp was designed for the mains frequencies 50/60 Hz there was an interest to know the behaviour of the lamp powered by sine voltage of different frequencies from the KIKUSUI power supply. The EMU-2 with the PR30 current probe were used to acquire data. Unfortunately EMU-2 system is designed for mains frequencies especially. The acquisition frequency 12.8 kHz is low for voltage of higher frequencies so the number of samples per period is low *eg.* 12.8 samples for 1 kHz signal.

The MH lamp was operated in vertical position in circuit fig. 4.18. For the starting the lamp works the circuit as in figure 4.12. The switches S1 and S2 were on. After the ignition of the lamp is the circuit switched by the switch S1 to the mode with resistive ballast $R = 110\,\Omega$. The switch S2 was off just to be sure that there flows no current.

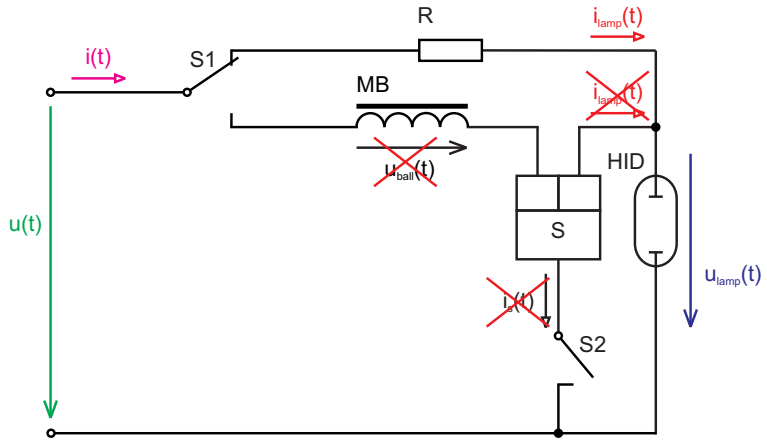

Figure 4.18: Modification of electric circuit for frequency change of supply voltage.

The frequency was changed in 40 Hz to 1 kHz range. The characteristics in figure 4.19 are for operation frequency 50 Hz. The waveform of the current is similar to any waveform of a current in a circuit with thyristor.

In another figure 4.20 are two samples of voltage-current characteristics for 50 Hz and 1 kHz. There is visible the trend of linearization behaviour of the lamp.

For low frequencies behaves the lamp unsymmetrical. For instance for 40 Hz voltage frequency reach the lamp voltage in one direction more than 25 V than in the other one. The characteristics of the frequency dependance of voltages and currents, and other voltage-current characteristics are pre-

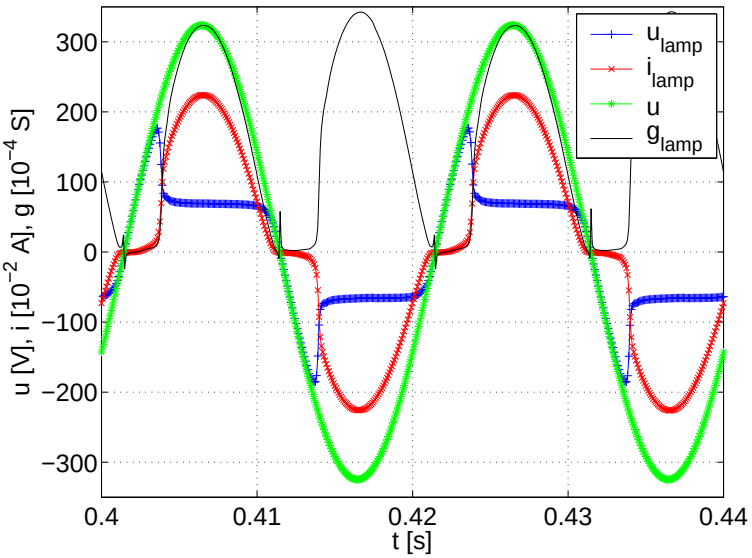

Figure 4.19: Measured voltages, current and computed conductivity of 150 W MH lamp in circuit with resistive ballast and operation frequency 50 Hz.

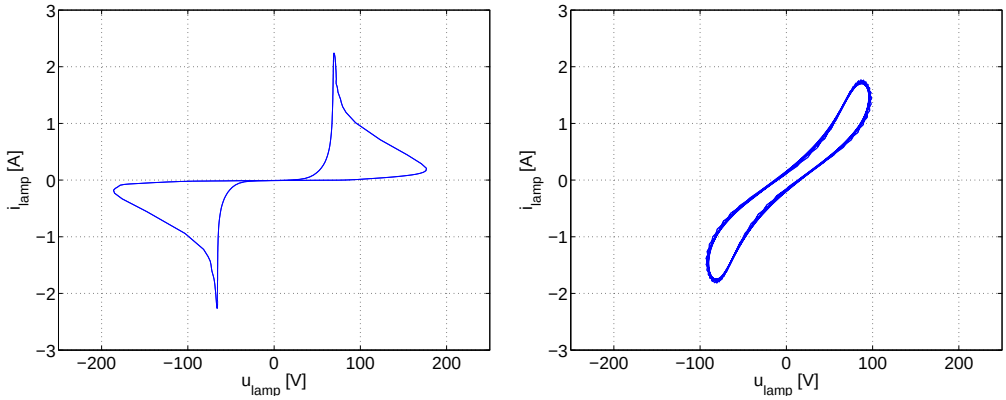

(a) 50 Hz (b) 1000 Hz

Figure 4.20: Voltage-current characteristics for two frequencies of power supply.

sented in appendix A.4 in figures A.2, A.3, A.4. The tables with electrical parameters for all frequencies are there also included.

4.6.5 Experiments with changes of supply voltage

The lamp was operated in vertical position in circuit with magnetic ballast figure 4.12. The change of voltage was realized in the first case by switching of taps on magnetic ballast – the voltage values were changed; and in second case was changed the voltage shape from the power generator KIKUSUI.

The change of supply voltage value

The operation of the MH lamp is optimized for nominal values of current and voltage[6]. If they are exceeded the life time of the lamp shortens. In distribution network can the value of voltage change due to distances from the source, transformers, loads ... *etc.* Hence the magnetic ballast (tab. 4.7) has three taps for voltage connection (220, 230 and 240 V) for optimizing the operation of the lamp. Influence of switching between taps under constant net voltage is described in figure 4.21 by voltage-current characteristics. The taps are in principle transformer taps, the change of voltage is evident [KN03].

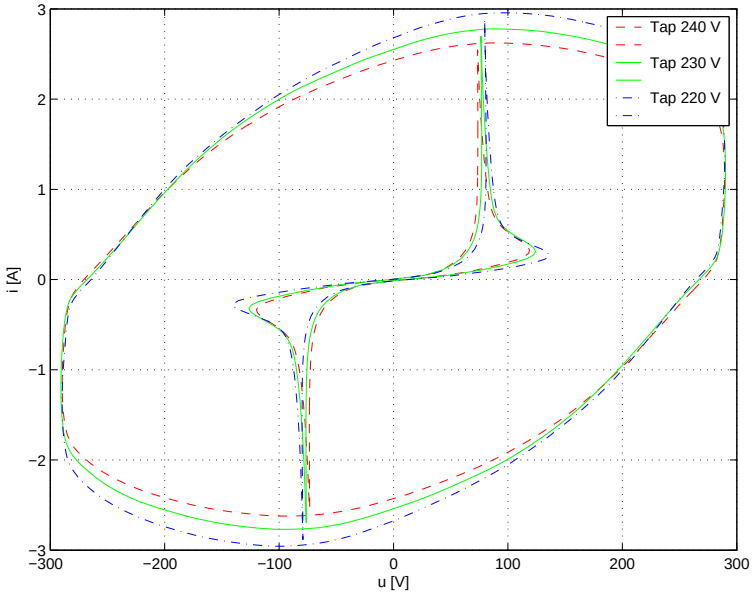

Figure 4.21: Voltage-current characteristics of 150 W MHL with MB with ballast taps switching.

[6] Of course not MH lamps only.

Change of supply voltage shape

For this experiment the circuit with magnetic ballast was used as shown in figure 4.12, powered by triangle supply voltage of 50 Hz and amplitude 330 V. The characteristics on lamp are in 4.22 and other electric parameters in table 4.10.

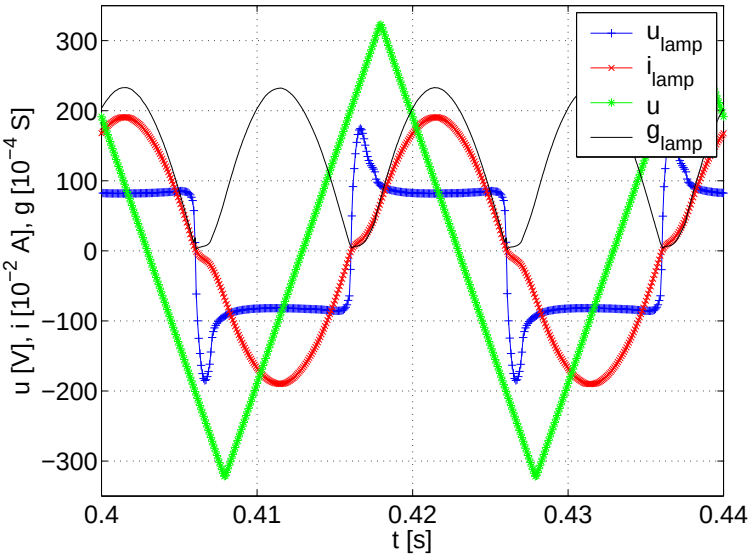

Figure 4.22: Characteristics of 150 W MHL supplied by triangle voltage.

Table 4.10: Electric parameters of MHL in circuit with MB powered by 50 Hz tiangle supply voltage.

U_{net}	=	188 V	U_{lamp}	=	94 V
I_{lamp}	=	1.3 A	G_{lamp}	=	16 mS
P_{net}	=	108 W	P_{lamp}	=	97 W
Q_{net}	=	219 VAr	Q_{lamp}	=	76 VAr
S_{net}	=	245 VA	S_{lamp}	=	123 VA
R_{ball}	=	7 Ω	L_{ball}	=	370 mH
THD_{lamp} V	=	65.31 %	THD_{net} V	=	11.95 %
THD_{lamp} A	=	7.75 %	λ_{lamp}	=	0.785

Chapter 5

Identification of lamp models

The approach of offline experimental identification of lamp model parameters (fig. 5.1) is described in this chapter. The optimal lamp model structure for high and low pressure lamps is proposed, the behaviour of the model under frequency, voltage value and shape change is studied also.

The data processing and computation routines were programmed in Matlab language[1] [Mat]. Some of them are compatible with the free alternative programming language – Octave [Eea].

5.1 Computation structure

The identification procedure is the part in the computation structure. Some steps (*f.i.* data preprocessing) have to be done before identification. The whole technique can be summarized as follows:

1. data loading;
2. data preprocessing:
    - data filtration (removing of bad samples of EMU-2, data allocation);
    - data analysis (signal period, values ...);
    - creating of whole periods of signals;
    - conductivity computation from $\mathbf{u}_{lamp}, \mathbf{i}_{lamp}$ vectors;
    - display of analyzed waveforms of voltage, current and conductivity;

[1] Optimized for Matlab version 6.5 Release 13.

- data adjustment for identification:
  - remove of DC component from signals u_{lamp}, i_{lamp},
  - remove of critical samples near zero,
  - conductivity limitation in specific range,
  - reformulating the conductivity computation process;
- data visualisation after correction;

3. identification:
   - optimum criterion;
   - identification methods:
     - iterative method [RKM04, Kob04, Kop05a],
     - non-itearative method [Dup05, DKD+06];
4. simulation.

Step 1 and part of step 2 were discussed in the previous chapter already. The problems with signal offset and its influence on conductivity computation was mentioned. This phenomenon is included in the identification structure and its influence on model parameters is observed. This will be explained further.

The item 3 is the main topic of this chapter. The last point 4 in proposed structure is simulation which is the subject of the next chapter.

In figure 5.1 is modified general structure of identification in figure 3.3. The structure was adapted for experimental offline discrete identification based on lamp conductivity models.

The *lamp system* is characterized by vectors of lamp voltage $\mathbf{u}_{lamp}$ and current $\mathbf{i}_{lamp}$. The output is computed vector of the lamp conductivity $\mathbf{g}$.

The input of the *lamp model* is vector of measured current $\mathbf{i}_{lamp}$. The parameters of mathematical description can vary in dependence on *strategy of parameters estimation*. The output of the model is a vector of the lamp model conductivity $\mathbf{g}_M$.

The vectors $\mathbf{g}$ and $\mathbf{g}_M$ are subtracted. On the output $\Delta\mathbf{g}$ is then applied the *optimum criterion* $J(\mathbf{x})$.

5.2 Lamp system

Lamp system as the real system of different lamps is described by general voltage $u_{lamp}(t)$ and current $i_{lamp}(t)$. They are saved in discrete forms in

vectors $\mathbf{u}_{lamp}$, $\mathbf{i}_{lamp}$. The technique of their acquisition was mentioned in previous chapter.

5.3 Lamp model

For the purpose of this thesis the number of lamp models were used. They came out of different hypothesis (see section 3.3 and 3.2.1), but they describe the equivalent lamp conductivity and are basically the same. Let us summarize them:

- Zissis *et al.*

$$\frac{\mathrm{d}G(t)}{\mathrm{d}t} = a_2 i^2(t) - \sum_{i=1}^{3} b_i \, G^i(t); \tag{5.1}$$

- Antón *et al.*

$$\frac{\mathrm{d}G(t)}{\mathrm{d}t} = A\frac{i^2(t)}{G(t)} - BG(t) - Ce^{DG(t)}; \tag{5.2}$$

$$\frac{\mathrm{d}G(t)}{\mathrm{d}t} = A\frac{i^2(t)}{G} - BG(t) - CG^2(t). \tag{5.3}$$

The structures of models for identification purposes can be defined more complete with the modification of the current term $a_2(i + a_1)^2$. That allows

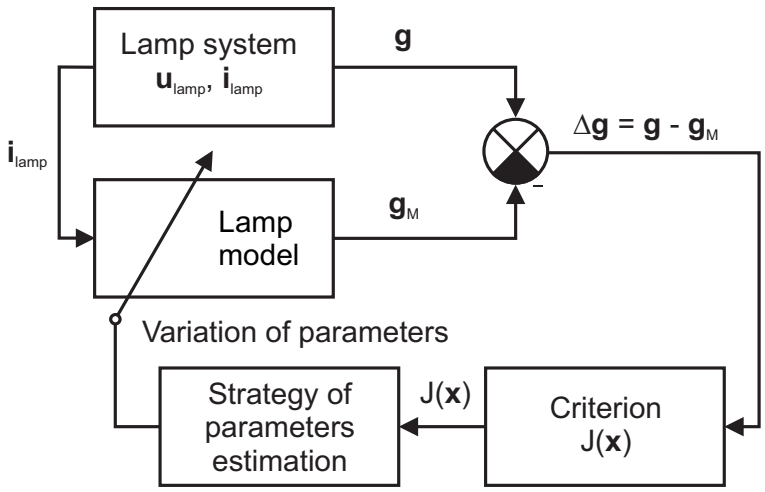

Figure 5.1: Structure of experimental offline identification of a lamp model.

some offset of the current, taking only the variations around some operating point. The formulations are as follows:

$$\frac{\mathrm{d}G(t)}{\mathrm{d}t} = a_2(i(t)+a_1)^2 - [b_3\ G^3(t) + b_2\ G^2(t) + b_1\ G(t) + b_0]; \tag{5.4}$$

$$\frac{\mathrm{d}G(t)}{\mathrm{d}t} = \frac{a_2}{G(t)}(i(t)+a_1)^2 - [b_2\ e^{b_3 G(t)} + b_1\ G(t) + b_0]; \tag{5.5}$$

$$\frac{\mathrm{d}G(t)}{\mathrm{d}t} = \frac{a_2}{G(t)}(i(t)+a_1)^2 - [b_3\ G^3(t) + b_2\ G^2(t) + b_1\ G(t) + b_0]. \tag{5.6}$$

Of course the reformulation above and using of the same name of parameters is mathematical operation. Their physical units are not the same. The physical meaning is defined in section 3.2 of models of equivalent conductivity/resistance.

5.4 Iterative computation method

For the strategy of parameters estimation the `fminsearch` function of Matlab Optimization Toolbox [Mat] was used. `fminsearch` finds a minimum of a scalar function of several variables

$$\min_x f(\mathbf{x}), \tag{5.7}$$

starting at an initial estimate. This is generally referred to as *unconstrained nonlinear optimization*. This function uses *simplex search method* [Mod04].

In program is used this call of `fminsearch`:

```
x = fminsearch(fun, x0, OPTIONS)
```

where

- `fun` defines a function;
- `x0` is a vector of start parameters for `fun`;
- `OPTIONS` is the structure with optimization parameters;
- `x` is a vector of model parameters for local minimum of function described in `fun`.

As the `fun` function was written `gk_minprezg` which realizes computation of conductance with new parameters

$$G(t) = \int \left[a_2\big(i+a_1\big)^2 - \sum_{i=1}^{3} b_i\ G^i(t)\right]\mathrm{d}t, \tag{5.8}$$

where the integration is performed numerically as explicit one-step Euler method; and realizes criterion (5.9)

$$J(\mathbf{x}) = \sum_{i=1}^{N} [g_i - g_{Mi}]^2. \tag{5.9}$$

Optimization parameters are set by

```
OPTIONS = optimset('MaxIter', valueMI);
```

where

- `MaxIter` is the allowance of maximum number of iterations;
- `valueMI` is a value of the parameter `MaxIter`.

5.4.1 Graphical user interface for the lamp model identification

For friendly application and visualisation of proposed identification algorithm (see page 69) a graphical user interface was designed. The application window developed in Matlab GUIDE environment [Mat] is shown in figure 5.2. The graphical interface `IdenVyboj.m` function is started by calling in `A_startGUIG_model.m` routine, where are all global variables.

It enables the work with lamp data saved in **m** matrix in *.mat file. The structure is optimized for data from EMU-2, but if the format of **m** matrix (table 5.1) is kept the use for other data from different data acquisition device is possible. **m** matrix can have up to 19 columns where the first column is time vector. The rest of columns can be various.

Table 5.1: Format of **m** matrix; vectors of sampled $\mathbf{t}$, $\mathbf{u}_{lamp}$, $\mathbf{i}_{lamp}$, $\mathbf{u}_{net}$.

	1	2	3	4	5	...	19
	$\mathbf{t}$	$\mathbf{u}_{lamp}$	$\mathbf{i}_{lamp}$	$\mathbf{u}_{net}$		...	
1	⋮	⋮	⋮	⋮		⋮	
2	⋮	⋮	⋮	⋮		⋮	
⋮	⋮	⋮	⋮	⋮		⋮	

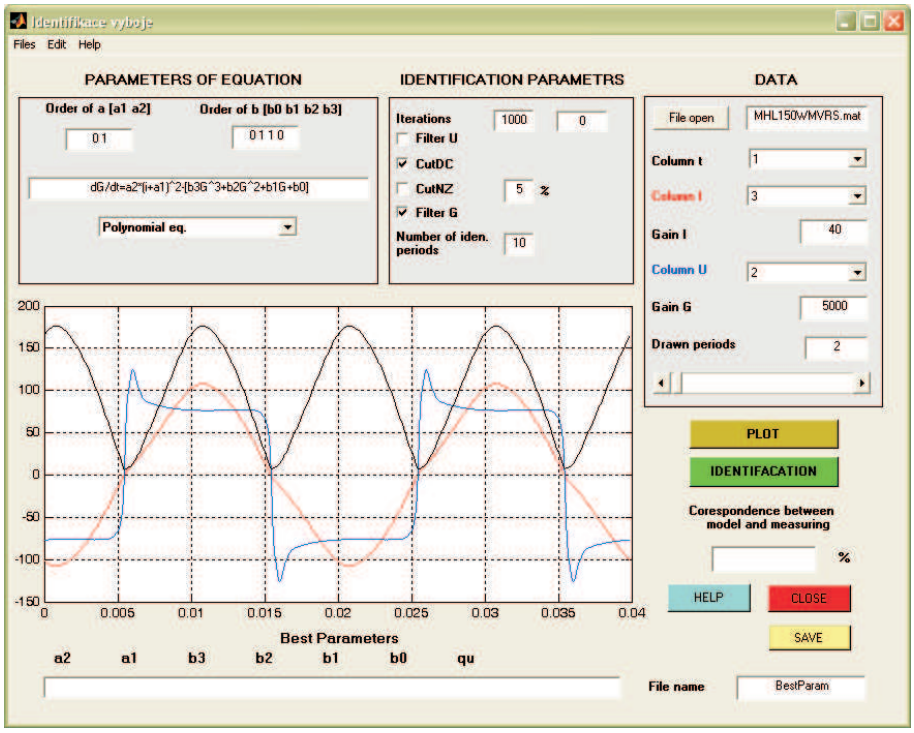

Figure 5.2: The application window of the graphical user interface for the lamp model identification.

'Data' frame

In this frame there are functions for data visualisation and preparation for next steps.

The lamp data are loaded from *.mat file with use of standard I/O dialog. The name of the file is shown in edit box in the right corner. Other edit boxes – Column t, Column I, and Column U are for vectors allocation and zooming of conductivity Gain G and current Gain I signals in figure. It is possible to visualize number of periods Drawn periods by slide moving or edit box above it.

'Identification parameters' frame

Functions of this frame prepare data for iterative identification computation and set parameters for `fminsearch` function. Each change in checkboxes shows in figure after Plot button clicking.

In the left-handed edit box Iterations is set the maximal number of allowed

iterations `MaxIter`. The right-handed edit box shows actual iteration step number.

Filter U executes averaging filter on voltage vector; for data from EMU-2 is this function redundant.

CutDC realizes the *cutdc.m* function which removes DC part from the signal according to eq. (4.2) of PEM toolbox A.1.

CutNZ removes samples of voltage near zero and than the same samples in other vectors.

Filter G uses for conductivity waveform an averaging filter and limitation in specific range (0 – 80 mS).

Number of iden. periods tells the number of analyzed (identified) periods of signal.

'Parameters of equation' frame

Order of a [a1 a2] provides the order of parameters in current term. The same as previous makes Order of b [b0 b1 b2 b3], but with parameters in conductivity term.

In editbox is shown solved one of the conductivity equation mentioned on page 72

- Polynomial eq. (5.4);
- Quadratic eq. (5.6);
- Exponential eq. (5.5).

Control buttons

Control buttons are placed in lower right-hand corner of the application window.

Plot button updates the waveforms in figure at actual settings in mentioned frames.

Identification button starts the identification procedure that is visualized in figure.

Help button invokes help for this application.

The application of Close button finishes the application and close the window without any savings.

Save button saves best parameters in *.txt format to the file whose name is in edit box below the button.

Corespondence between model and measuring is shown in percents and is computed as follows

$$100 - \frac{|\sum_{i=1}^{N} g_i - g_{Mi}|}{|\sum_{i=1}^{N} g_i|} \cdot 100 \ [\%], \tag{5.10}$$

where

- N is the number of samples;
- g_i is sample of measured conductivity;
- g_{Mi} is sample of simulated conductivity.

Figure is a display for data preparation and visualisation tool for identification convergence and online solution.

Best Parameters is the vector of best parameters **a** and **b**. To the vector is added the criterion number $qu = J(\mathbf{x})$. The values are updated during the identification process. With the vector operates simulation model of the lamp with or without magnetic ballast built in Simulink (see more in chapter 6).

5.4.2 Results of identifications

The number of discharge lamps were measured and data for the identification were acquired. The results for certain setting of identification process are summarized in following sections:

- results of the identification of MHL;
- results of identifications of FLs;
- results of identifications of HPM and HPS lamps.

There exist many options for identification as was mentioned above. The identification of 150 W metal halide lamp was chosen as a demonstration example. Some considerations about model settings are discussed in the following text. Note, that it is not exhaustive description.

The results of the identification of other lamps is set briefly in table forms.

5.4.3 Results of the identification of 150 W metal halide lamp

The result of the identification is illustrated on measured data of 150 W metal halide lamp in vertical operation position, powered by real power supply (50 Hz), in circuit with magnetic ballast (see in section 4.6).

The analysis of the influence of

- the type of a lamp model,
- the variation of analyzed periods of measured signal,
- the variation of the number of allowed iterations,

is described.

The settings of the identification is summarized in table 5.2.

Table 5.2: Identification settings for 150 W MH lamp.

Analyzed data	MHL150WMVRS.mat
Used model	*varying*
Number of iterations	*varying*
Filter U	no
CutDC	yes
CutNZ	no
Filter G	yes
Number of iden. periods	*varying*

Example The result of the identification of *polynomial model* (G-model), with the *number of allowed iterations* 1000, and the *number of identified periods* 10 is as follows.

The parameters of the lamp model are in the vector,

$$[a_2, a_1, b_3, b_2, b_1, b_0] = [53, 0, 0, 293050, 670, 0].$$

The comparison of experimental and simulation curves of discharge lamp conductivity can be then visualized as in figure 5.3.

Type of the lamp model

The three types of models (5.4), (5.6), (5.5) for discharge lamps description were proposed.

The discussion about parameters from the identification of different models is based on statistical computation of parameters. The statistical data were obtained with the same settings as they are in table 5.2. The number of analyzed periods were changed in the range from 10 to 30 periods of the signal and the number of analyzed periods was 1000.

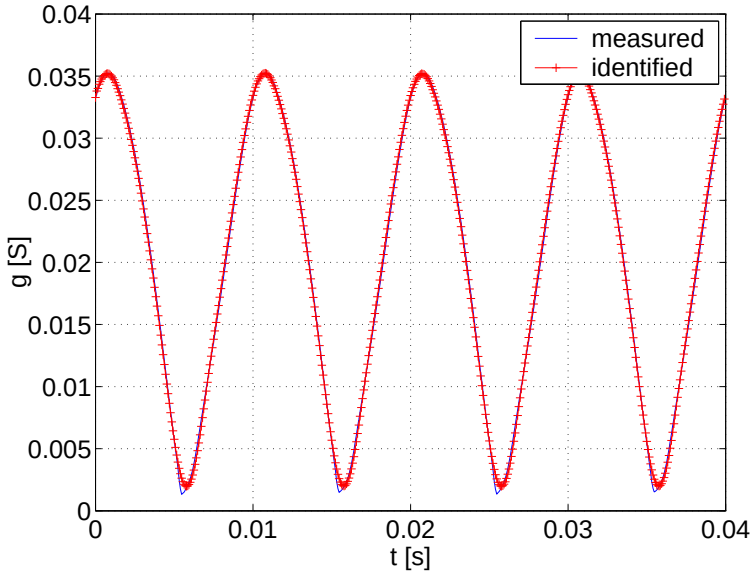

Figure 5.3: Comparison of measured and simulated (lamp model with Best Parameters) conductivity waveforms.

For values in the following tables the definitions for standard deviation σ (5.11) and mean value 5.12 $\bar{x}$ are used:

$$\sigma = \left(\frac{1}{n-1} \sum_{i=1}^{n} (x_i - \bar{x})^2 \right)^{\frac{1}{2}}, \tag{5.11}$$

where the sample average is

$$\bar{x} = \frac{1}{n} \sum_{i=1}^{n} x_i. \tag{5.12}$$

In Matlab are there standard functions `STD` and `mean` [Mat].

Polynomial model

The polynomial model (5.4) with the different number of parameters was used. Their comparison is in tables 5.3 – 5.7.

If the tables 5.3 and 5.4 are compared, the minimal influence of b_3 coefficient to other parameters is evident. Thus, this parameter can be neglected.

The model of the first order in tab. 5.5 with parameter b_1 does not fit the conductivity very well and is useless to use such model.

Table 5.3: Parameters of polynomial model (5.4) with conductivity polynomial of third order.

	a_2	a_1	b_3	b_2	b_1	b_0	qu
$\bar{x}$	53.0733	0	-0.99523	292231.1192	664.1696	0	0.00067621
σ	0.080683	0	0.36509	392.2836	2.5194	0	0.00020511

Table 5.4: Parameters of polynomial model (5.4) with conductivity polynomial of second order.

	a_2	a_1	b_3	b_2	b_1	b_0	qu
$\bar{x}$	53.0733	0	0	292231.0785	664.1699	0	0.00067621
σ	0.080683	0	0	392.2835	2.5194	0	0.00020511

Table 5.5: Parameters of polynomial model (5.4) with conductivity polynomial of first order.

	a_2	a_1	b_3	b_2	b_1	b_0	qu
$\bar{x}$	30.7061	0	0	0	5529.3149	0	0.10956
σ	0.017128	0	0	0	3.5016	0	0.033169

Table 5.6: Parameters of polynomial model (5.4) without b_0.

	a_2	a_1	b_3	b_2	b_1	b_0
$\bar{x}$	53.0727	-0.0011891	-0.88844	292226.1933	664.2204	0
σ	0.080713	2.8725e-005	0.24925	392.5559	2.5181	0

qu
0.000675
0.00020477

The parameter a_1 helps to accelerate the identification for the unsymmetrical current. On the other hand, in the case of symmetrical current is this coefficient redundant and slows down the identification.

The optimal structure of polynomial model for identification purpose re-

Table 5.7: Parameters of polynomial model (5.4) with b_0.

	a_2	a_1	b_3	b_2	b_1
$\bar{x}$	52.591	-0.0012095	-0.55964	283731.3011	859.1231
σ	0.17102	2.7988e-005	1.3925	2705.5535	60.4965
	b_0	qu			
	-0.94741	0.00066053			
	0.29803	0.00019856			

sults from presented tables and it is as follows:

$$\frac{\mathrm{d}G(t)}{\mathrm{d}t} = a_2(i(t) + a_1)^2 - [b_2\ G^2(t) + b_1\ G(t)]. \tag{5.13}$$

This model structure is used for identification of parameters of different conditions of metal halide lamp operation. The values of identified parameters of polynomial model are all summarized in appendix in table A.9.

Quadratic model

The quadratic model (5.6) was used with different numbers of parameters (see tables 5.8 and 5.9) the same way as was described in previous section.

Table 5.8: Parameters of quadratic model (5.6) with conductivity polynomial of second order.

	a_2	a_1	b_3	b_2	b_1	b_0	qu
$\bar{x}$	0.57676	0	0	-16282.355	3926.8843	0	0.00079857
σ	0.0005239	0	0	32.538	4.1365	0	0.00024578

The extension parameters b_3 and a_1 slow down the identification and there is no significant benefit of their using if the current is symmetrical. Optimal structure is the same as (5.3) was proposed by authors

$$\frac{\mathrm{d}G(t)}{\mathrm{d}t} = \frac{a_2}{G(t)}\ i^2(t) - [b_2\ G^2(t) + b_1\ G(t)].$$

Although this model was used for high pressure lamp characterisation in work of Antón *et al.* [ABF+02a], the low pressure lamp description is more suitable as presents Loo *et al.* [LSTD05].

Table 5.9: Parameters of quadratic model (5.6) with conductivity polynomial of second order with a_1 parameter.

	a_2	a_1	b_3	b_2	b_1	b_0
$\bar{x}$	0.57676	-0.0013928	0.10437	-16285.9788	3926.9748	0
σ	0.00052697	2.826e-005	0.12669	32.4615	4.1521	0
	qu					
	0.00079688					
	0.00024529					

The same identification approach for measured fluorescent lamps was chosen. The results are in section next 5.4.4 in table 5.12.

Exponential model

The exponential model (5.5) was also tested as quadratic. The results are in table 5.10.

Table 5.10: Paramters of exponential model (5.5).

	a_2	a_1	b_3	b_2	b_1	b_0	qu
$\bar{x}$	0.54988	0	-0.0005417	4.6229	3117.1778	0	0.0008657
σ	0.0002815	0	0.00012673	0.010647	1.4052	0	0.00026738

From table 5.10 follows that the coefficient b_3 tends to zero

$$b_3 \rightarrow 0 \Rightarrow e^{b_3\ G(t)} \simeq 1, \tag{5.14}$$

then can be supposed the eq. (5.5) as follows

$$\frac{\mathrm{d}G(t)}{\mathrm{d}t} = \frac{a_2}{G(t)}(i(t)+a_1)^2 - [b_2\ 1 + b_1\ G(t) + b_0] \tag{5.15}$$

$$\frac{\mathrm{d}G(t)}{\mathrm{d}t} = \frac{a_2}{G(t)}(i(t)+a_1)^2 - [b_1\ G(t) + \underbrace{(b_2+b_0)}_{new\ b_0}] \tag{5.16}$$

The equation (5.16) is the same as the quadratic model (5.6) of first order with coefficient b_0.

The exponential model does not bring anything new in the lamp description. It is different way of the lamp losses description, but the quadratic model can describe them too and more general.

Variation of analyzed periods of measured signal

Settings of the identification for this study is in table 5.2. The number of iterations is 1000 and the polynomial lamp model 5.4 is used. The number of analyzed periods changes in the range from 1 period to 30 periods (cf. figure 5.4).

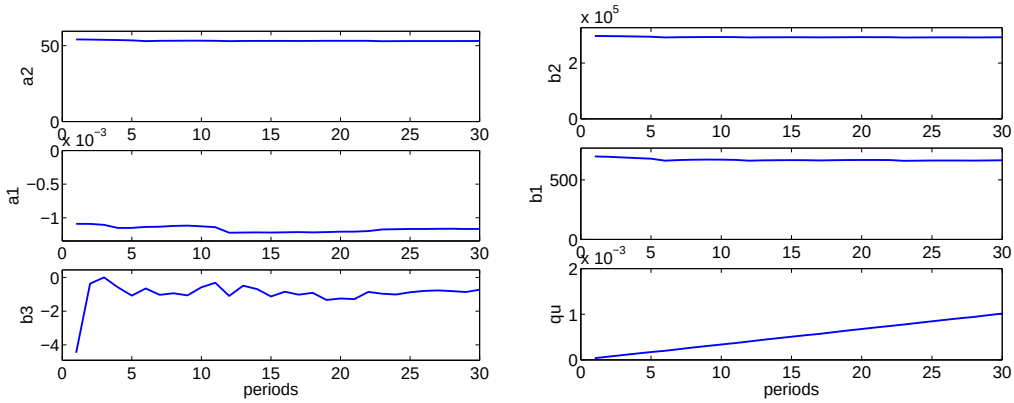

Figure 5.4: Parameters of polynomial lamp model dependence on the variation of the number of analyzed periods of measured signal.

It is evident the values of parameters do not depend on the number of analyzed periods of measured signal. The number of periods 10 is sufficient value for identification. The increasing value of qu is obvious and expected.

Variation of the number of iterations

The optimization options parameters can be used by `fminsearch`. The influence of parameter `MaxIter` on values of identified parameters was observed (cf. figure 5.5).

Settings of the identification for this study is in table 5.2, where the polynomial model and 10 periods of analyzed signal are set.

The influence of maximum number of iterations affects values of parameters up to c. 500. From this value are all values stationary. The setting of the number of iterations on to 1000 is high enough above the border value. Of course, this value could be decreased for accelerating of the identification process.

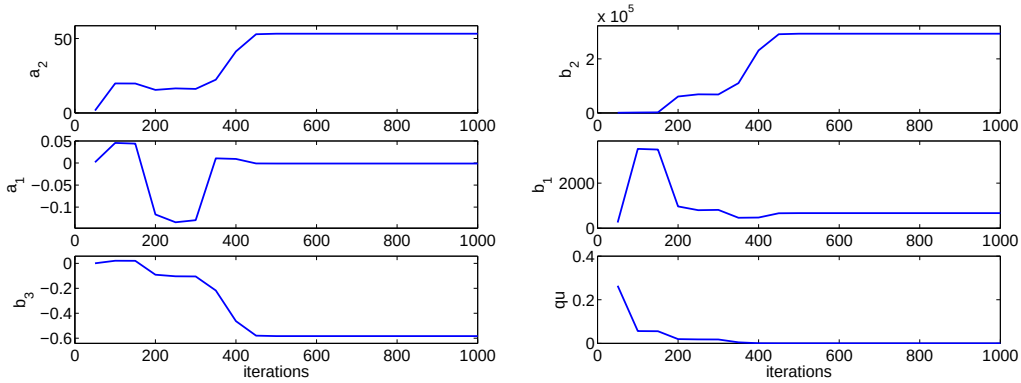

Figure 5.5: Parameters of polynomial lamp model dependence on the variation of the number of iterations.

5.4.4 Results of the identification of fluorescent lamps

The parameters of quadratic model in table 5.12 were obtained with options of identification as it is shown in table 5.11 and appropriate experimental data (sec. 4.3).

Table 5.11: Identification settings for models of fluorescent lamps.

Analyzed data	LPFL*xx*W.mat
Used model	quadratic model (5.6)
Number of iterations	1000
Filter U	no
CutDC	yes
CutNZ	no
Filter G	yes
Number of iden. periods	10

Table 5.12: Parameters of quadratic model (5.6) of fluorescent lamps.

	a_2	a_1	b_3	b_2	b_1	b_0	qu
FL18W	1.12	0	0	1074	3778	0	0.00402
FL36W	0.30	0	0	-208009	3727	0	0.00004
FL58W	0.20	0	0	-169190	3525	0	0.00026

The qu value gives the information about quantitative difference between simulated and experimental curves of conductivity. How do the models with these parameters qualitatively fit the experimental curves? This question tries to be answered further in sections about simulations.

In work of Rossat-Mignod *et al.* [RMRJZ02] the polynomial model for fluorescent lamp description is used. Unfortunately there is no specification of wattage of used FL. The polynomial model to 58 W FL[2] is also applied for confrontation (cf. tab. 5.13). There is no similarity in values in table 5.13.

Table 5.13: Confrontation of parameters of polynomial models applied to 58 W fluorescent lamps.

	a_2	a_1	b_3	b_2	b_1
Koprnický	68	-	-	$6.3\,10^5$	1022
Rossat-Mignod	$21\,10^3$	-	-	15	80

The parameters of Rossat-Mignod seem to be too high (a_2) and too small (b_i). Their values induce too high conductivity in simulation. The magnitude reaches approximately 100 S what is not realistic compare to the measured value 8 mS in table 4.2.

5.4.5 Results of identifications of 400 W HPM and HPS lamps

Options of identifications are summarized in table 5.14. The adjustable model parameters in table 5.15 for 400 W HPML and 400 W HPSL (sec. 4.4 and 4.5) follows.

In this case the comparison of parameters with other works is possible, *e.g.*, Herrick proposed similar model structure 3.13 for 400 W HPSL:

$$\frac{\mathrm{d}y}{\mathrm{d}t} = 27.9i^2 - 262y^2 - 885(y - x),$$

$$\frac{\mathrm{d}x}{\mathrm{d}t} = 56.5(y - x) + 925x.$$

Stambouli [Sta84] proposes model for 400 W HPML with the same structure as it is polynomial (5.4) and reaches these comparable parameters (cf. table 5.15).

[2]The similar values of parameters of magnetic ballast are mentioned $R_{ball} = 39\,\Omega, L_{ball} = 955\,\mathrm{mH}$ (cf. table 4.2).

Table 5.14: Identification settings for models of high pressure lamps.

Analyzed data	HPxL400W.mat
Used model	polynomial model (5.4)
Number of iterations	1000
Filter U	no
CutDC	yes
CutNZ	no
Filter G	yes
Number of iden. periods	10

Table 5.15: Parameters of polynomial model (5.4) with conductivity polynome of second order.

	a_2	a_1	b_3	b_2	b_1	b_0	qu
HPML400W	5.4	0	0	104230	85	0	0.00227
HPSL400W	21	0	0	100171	299	0	0.01049
HPML400W Stambouli	2.8	–	753000	40300	141.2	–	–

With regarding to presented values in table 5.15 is possible to say that parameters are quantitively in the same order.

5.5 Non-iterative computation method

In cooperation with Pascal Dupuis modified identification procedure as an one-step process was proposed [Dup05]. This procedure was used for model structure as given in (5.4), but with little change in current term

$$\frac{\mathrm{d}G}{\mathrm{d}t} = a_2 i^2 + a_1 i + a_0 - [b_3\, G^3 + b_2\, G^2 + b_1\, G]. \tag{5.17}$$

This implies that the a_1 coefficient of eq. (5.4) is not the same as a_1 coefficient of eq. (5.17).

The procedure is based on the time-varying phasors of voltage and current

defined as follows:

$$\bar{U}(t) = \frac{u(t)}{s(t)}, \tag{5.18}$$

$$\bar{I}(t) = \frac{i(t)}{s(t)}, \tag{5.19}$$

where $s(t)$ is a base sine with the period of the input signals phase-adjusted to have exactly the same zero-crossings.

The conductivity computation is then defined

$$\bar{G}(t) = \frac{\bar{I}(t)}{\bar{U}(t)} \text{ outside zero-crossings} \tag{5.20}$$

$$\bar{G}(t) = \frac{\dot{I}(t)}{\dot{U}(t)} \text{ at zero-crossings.} \tag{5.21}$$

To obtain an analytic signal from a time-varying vector the Hilbert transformation is needed,

$$u(t) = \mathrm{R}e\left(\bar{U}e^{j\omega t}\right). \tag{5.22}$$

It is in ideal state, where the rotational speed is constant [Dup05].

As both the current and the voltage are supposed to be in-phase, the conductance is a pure real number.

In real signals the rotational speed varies. The analytic signal is given from a multifrequency phasor [DKD+06]

$$u(t) = \mathrm{R}e\left(\sum_{k=0}^{nh} \bar{U}_k e^{jk\omega t}\right), \tag{5.23}$$

where nh is the total number of harmonics; ω is the basis frequency; and $\bar{U}_k$ is the complex phasor associated with the k^{th} harmonic.

As the model is linear in respect with all the unknowns, a regression matrix $\mathbf{A}$ is constructed as

$$\mathbf{A} = \left[\bar{I}^2(t), \bar{I}(t), 1, -\bar{G}^3, -\bar{G}^2, -\bar{G}, \mathrm{d}\bar{G}\right]. \tag{5.24}$$

The solution is obtained by Singular Values Decomposition as

$$\mathbf{A} \cdot [a_2, a_1, a_0, b_3, b_2, b_1, -1]' \simeq 0. \tag{5.25}$$

A performance criterion is defined as the norm of the residuals between the values predicted by the linear combination of the powers of i and G , and the

observed dG. By searching upon the different models structure, it appeared that dropping the G^3 term leads to the smallest error.

As the minimization expression was used

$$\chi^2 = \sum_{j=1}^{S} \sum_{k=1}^{n_j} \frac{(x_j(k) - \hat{x}_j(k))^2}{\sigma_j^2} \tag{5.26}$$

where

- S is the number of sequences;
- n_j is the length of the j^{th} sequence;
- $\hat{x}_j$ is the best approximation of the time-varying signal, as computed from (5.22);
- the σ_j^2 is the variance for each sequence.

5.5.1 Results of the identification of 150 W metal halide lamp

This identification approach was tested on data of metal halide lamp in circuit with magnetic ballast presented in section 4.6, but powered by real network supply voltage and lamp current two times less than reality[3].

The data preprocessing routines and identification algorithm were developed and are compatible for Matlab either Octave.

The solutions of various optimization approaches: LS, TLS, QR and Iter. Method are summarized in table[4] 5.16.

The whole description of the methodology of this computation approach, results as well, are presented in the article [DKD+06]. The main part is the work of Pascal Dupuis and I would not to present it here.

[3]It was caused by mistake in measured data processing. The current probe measured value/2 and it was not taken into account.

[4]Note that the coefficients from LS, TLS, QR methods are for the equation (5.17). The coefficients from Iter. method (cf. sec. 5.4) are for eq. (5.13).

Table 5.16: Comparison of lamp model coefficients (5.17) for different identification approaches.

	LS	TLS	QR	Iter. method
a_2	91.3	98.3	91.3	107
a_1	-0.59	-0.63	-0.59	–
a_0	0	0	0	–
b_3	$8\,10^5$	$39.1\,10^5$	$-3.2\,10^5$	0
b_2	$-53.5\,10^4$	$-72.7\,10^4$	$-47.9\,10^4$	$-58.2\,10^4$
b_1	$-8.75\,10^2$	$7.53\,10^2$	$-14.9\,10^2$	-788

Chapter 6

Simulation models

Simulation of lamp models and electric circuits were implemented in MATLAB Simulink[1].

6.1 Simulation model of a discharge lamp with a ballast

Simulation diagram (cf. figure 6.1) represents electric circuit with discharge lamp in connection with magnetic ballast as describes equation

$$u(t) = R_{ball}\ i(t) + L_{ball}\frac{\mathrm{d}i(t)}{\mathrm{d}t} + u_{lamp}(t). \tag{6.1}$$

The same equation was already mentioned in section 2.5 Electric circuits for discharge lamps.

6.1.1 Simulation model of a discharge lamp

Simulation scheme in figure 6.2 is universal lamp model. It simulates this equation

$$u_{lamp}(t) = \frac{i_{lamp}(t)}{G(t)}. \tag{6.2}$$

The time dependant conductivity is given by differential equation (6.3). It includes three types of models:

- polynomial (5.4);

[1] Optimized for Simulink version 5.0 Release 13.

- exponential (5.5);
- quadratic (5.6).

$$\begin{aligned}\frac{\mathrm{d}G(t)}{\mathrm{d}t} &= \frac{a_2}{G(t)^{\texttt{fraG}}}\,(i(t)+a_1)^2 \\ &\quad - \Big[\big(b_2\; e^{b_3 G(t)}\texttt{eqE}\big) \\ &\quad + \big(b_3\; G^3(t) + b_2\; G^2(t)\big)\texttt{eqE} \\ &\quad + b_1\; G(t) + b_0\Big],\end{aligned} \tag{6.3}$$

where

- N is a number of lamps (default is 1);
- $a_2, a_1, b_3, b_2, b_1, b_0$ are model parameters;
- `fraG` is the first universal constant:
  - if is 0 then the polynomial model is chosen,
  - if is 1 then the conductivity is in fraction (quadratic and exponential model);
- `eqE` is the second universal constant:

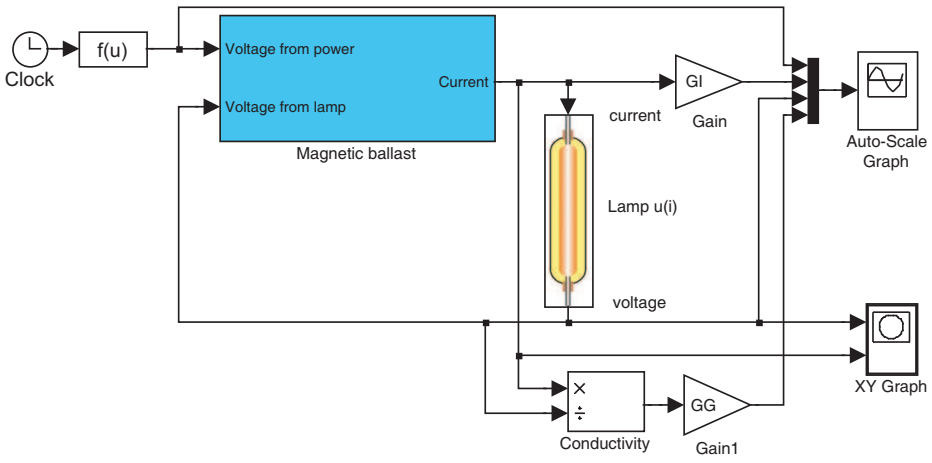

Figure 6.1: Simulation model of an electric circuit with a lamp load.

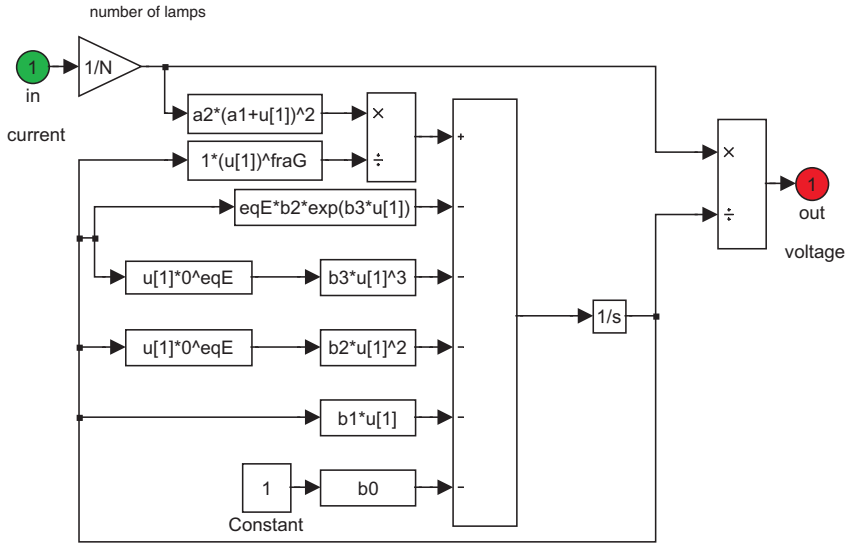

Figure 6.2: Universal simulation scheme of a discharge lamp.

– if is 0 then the polynomial or quadratic model are chosen,
– if is 1 then the exponential model is chosen.

The initial value of the integrator in output of the *Sum block* is set to 10^{-3} ($G(t=0) = 1\,\mathrm{mS}$).

The parameters are given into the model in vector form as follows:

```
[N a2 a1 b3 b2 b1 b0 fraG eqE].
```

6.1.2 Simulation model of a magnetic ballast

The magnetic ballast is described by simple linear model, with two parameters R_{ball} and L_{ball}. The model in figure 6.3 simulates equation (6.1). The initial value of the integrator in the model is 10^{-6} ($i(t=0) = 1\,\mu\mathrm{A}$).

6.1.3 Simulation model of a power supply

The power net was simulated as ideal source of sine wave signal

$$u(t) = \sqrt{2}U_{rms}\sin(\omega t), \tag{6.4}$$

where

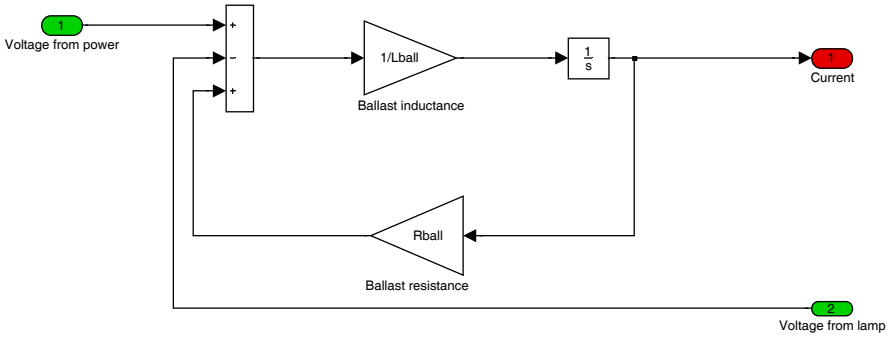

Figure 6.3: Linear model of a magnetic ballast.

- U_{rms} is rms value of supply voltage;
- ω is the angular velocity of supply voltage (4.5).

6.2 Simulation model of a discharge lamp without a ballast

The source and ballast can be replaced by blocks *Signal Generator* or *From File* or *From Workspace*, where the vectors of measured time $\mathbf{t}$, lamp current $\mathbf{i}_{lamp}$ and lamp voltage $\mathbf{u}_{lamp}$ (cf. figure 6.4) can be saved.

6.3 Visualisation of electric characteristics

The blocks for visualisation are in general diagrams in figures 6.1 and 6.4. The simulated values of u, u_{lamp}, i_{lamp} and g are displayed in *Auto-Scale Graph* and lamp voltage-current characteristic is displayed in *XY Graph*.

Parametes `GG` and `GI` scale signals for better fitting to graphs. Their values are entered into the model as model parameters.

6.4 Simulation with parameters

The model proposed in fig. 6.1 can be initiated with all parameters in dialog settings, *e.g.* in Graphical User Interface the commands are used as follows:

```
xp = [xp fraG Rball Lball eqE];
[xp,GG,GI]=sim('universsModelLampCircMB.mdl');
```

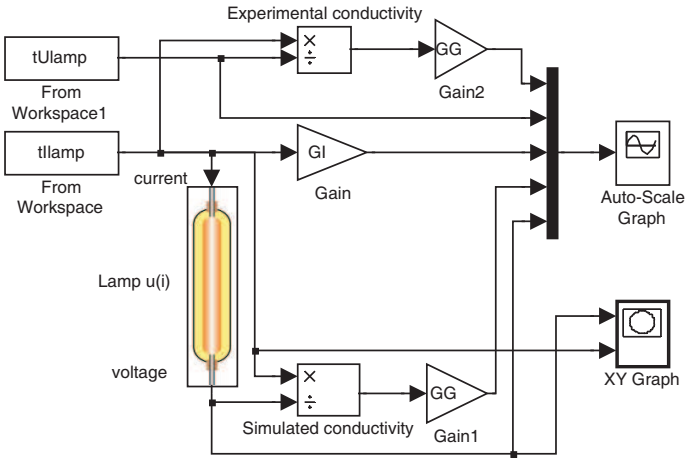

Figure 6.4: Simulation diagram of a lamp model powered from current source from Matlab workspace.

where `universModelLampCircMB.mdl` is the name of the simulation model of electric circuit with the lamp as an electric load (cf. figure 6.1).

Figure 6.5 shows application of the 'full' model (6.1). The experimental and completely simulated lamp voltage, current and lamp conductivity of 150 W HML with magnetic ballast

```
Rball = 7; Lball = 0.35;
```

are there recorded.

The lamp model without ballast (fig. 6.4) can be applied in a similar way to previous case. Of course, parameters `Rball` and `Lball` are redundant.

6.5 Experimental verification

The verification of experimental and simulated curves of lamp conductivity, lamp current, and lamp voltage was done.

The simulation models of the whole electric circuit with the discharge lamp or parts of it were partially verified. The simulation of the whole electric system is problematic due to *starting phase* (cf. figure 6.5) that can cause divergence of the simulation. Therefore the lamp model powered by current source for experimental verification is used.

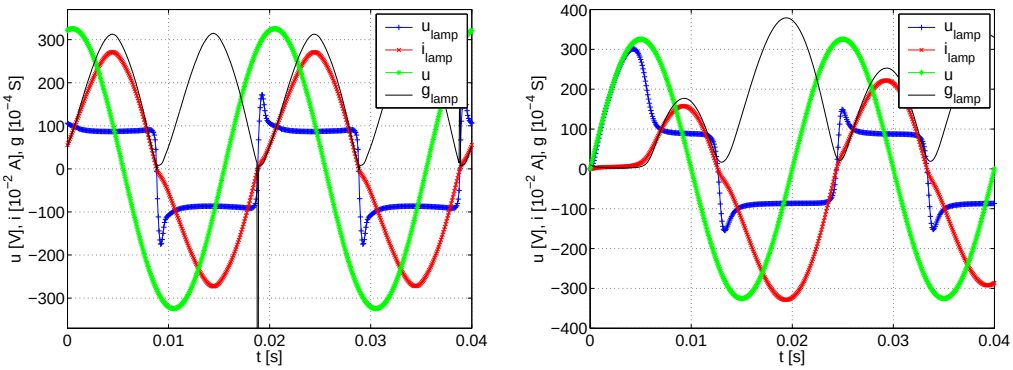

(a) experiment (b) simulation of polynomial model fig. 6.1

Figure 6.5: Comparison of experiment and simulation characteristics with the complete electric circuit model with 150 W metal halide lamp.

6.5.1 Experimental verification with 150 W MHL

Variance of lamp models at frequency 50 Hz

In experiment proposed in sec. 4.6.1 the data of metal halide lamp, in vertical operation position, in circuit with magnetic ballast, powered by ideal sine supply voltage were saved in file `MHL150WMVIS.mat`.

Three types of lamp models in simulation diagram without model of magnetic ballast fig. 6.4 are presented.

In figure 6.6 experimental and simulation curves for three types of models are compared. Settings for all simulations are shown in table 6.1.

Table 6.1: Settings of simulations with three types of lamp models of 150 W metal halide lamp.

model	`xp`							`fraG`	`eqE`
type	a_2	a_1	b_3	b_2	b_1	b_0	qu		
poly	54	0	0	$3.87\,10^5$	710	0	$1.8\,10^{-3}$	0	0
quad	0.53	0	0	$-2.4\,10^4$	$4.8\,10^3$	0	$2.3\,10^{-3}$	1	0
expon	0.52	0	0.037	4.3	$3.9\,10^3$	0	$2.5\,10^{-3}$	1	1

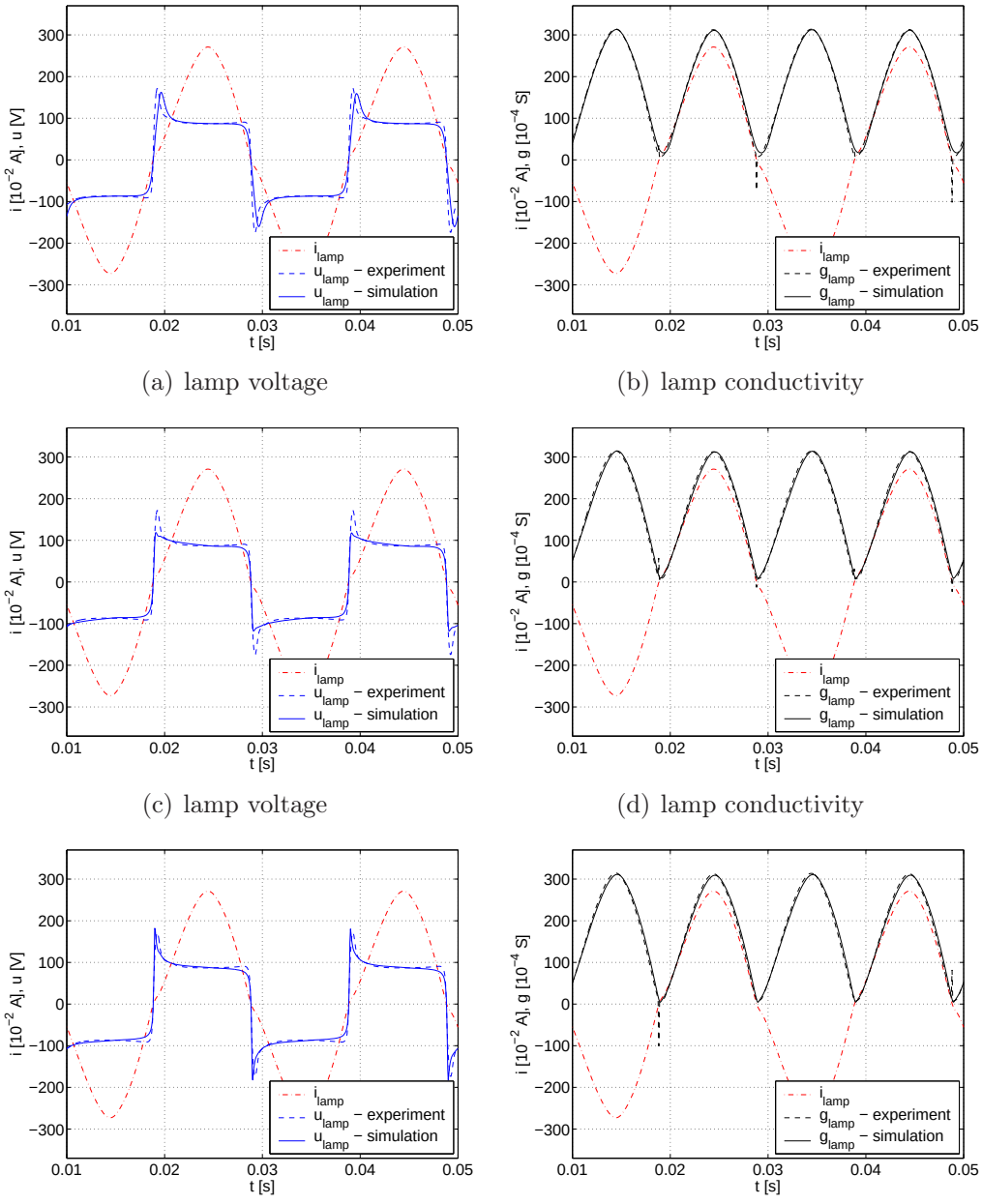

(a) lamp voltage (b) lamp conductivity

(c) lamp voltage (d) lamp conductivity

(e) lamp voltage (f) lamp conductivity

Figure 6.6: Experimental and simulated lamp voltage and conductivity of 150 W MHL with polynomial (a)–(b); quadratic (c)–(d); exponential (e)–(f) lamp model application.

Variance of frequency of supply current with polynomial lamp model

The simulation with supply current variation is observed. The data of 150 W MHL with resistive ballast (see sec. 4.6.4) are used. The simulated characteristics in figures 6.7 and 6.7 are obtained with polynomial lamp model. The settings are the same as in table 6.1 which are obtained from identification of the lamp at 50 Hz with the magnetic ballast.

The results of simulations show differences between experimental and simulated curves. It is expectable taking to account that variation of parameters values of identification is present (cf. table in appendix A.9). The dependence of model parameters on frequency and input power is then evident.

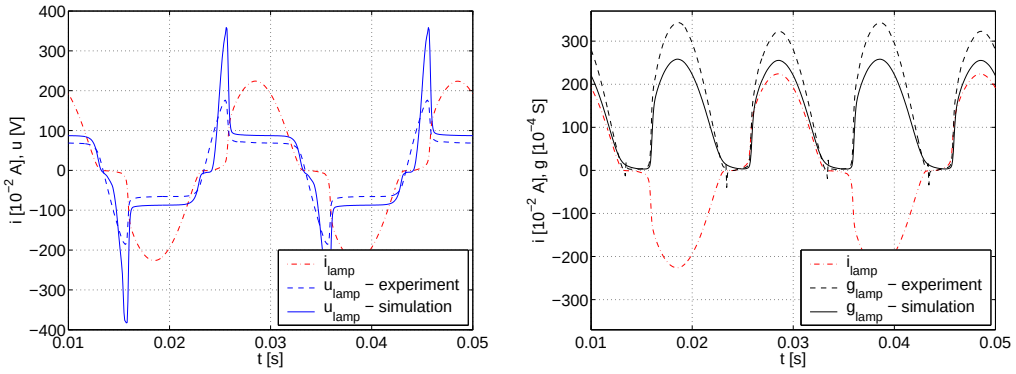

(a) lamp voltage

(b) lamp conductivity

Figure 6.7: Experimental and simulated lamp voltage and conductivity of 150 W MHL with polynomial model at frequency 50 Hz.

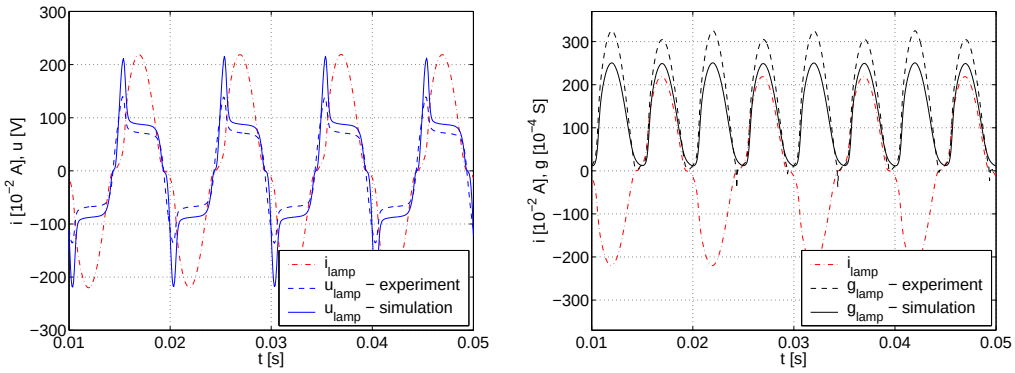

(a) lamp voltage

(b) lamp conductivity

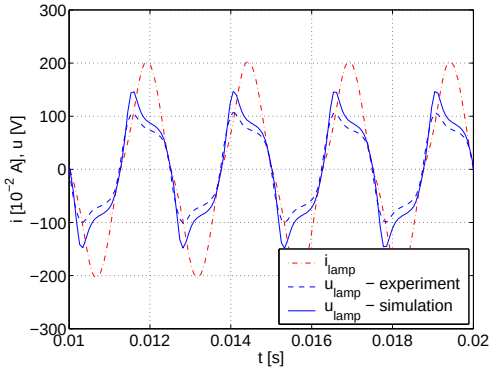

(c) lamp voltage

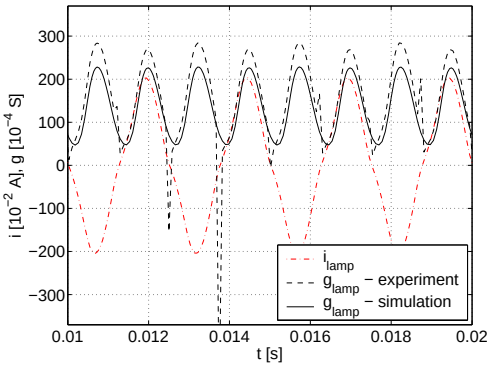

(d) lamp conductivity

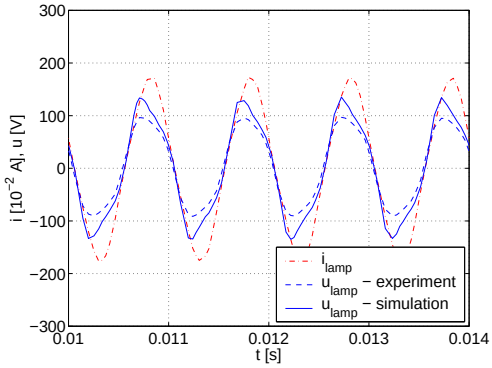

(e) lamp voltage

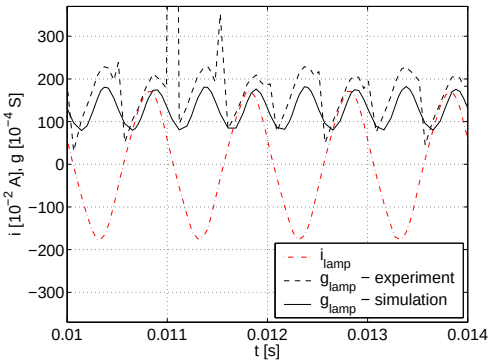

(f) lamp conductivity

Figure 6.8: Experimental and simulated lamp voltage and conductivity of 150 W MHL with polynomial model at frequency 100 Hz (a)–(b); 400 Hz (c)–(d); and 999 Hz (e)–(f).

6.5.2 Experimental verification with 58 W fluorescent lamp

The quadratic lamp model with experimental lamp current source from `LPFL58W.mat` file, and with settings in table 6.2 was used. The results of verification is shown in figure 6.9.

Table 6.2: Settings of simulations with three types of lamp models of 58 W fluorescent lamp.

model	`xp`							`fraG`	`eqE`
type	a_2	a_1	b_3	b_2	b_1	b_0	qu		
poly	67	0	0	$6.3\,10^5$	10^3	0	$2.7\,10^{-4}$	0	0
quad	0.20	0	0	$-1.7\,10^5$	$3.5\,10^3$	0	$2.6\,10^{-4}$	1	0
expon	0.18	0	0	1.7	$1.9\,10^3$	0	$3.3\,10^{-4}$	1	1

The simulation shows the conductivity is predicted well but voltage curve not. This type of model can not describe fast peaks in voltage as *f.i.* exponential model or polynomial, but stable state fits very well. It is evident that simulation of low pressure lamp at 50 Hz with this simple lamp model is problematic.

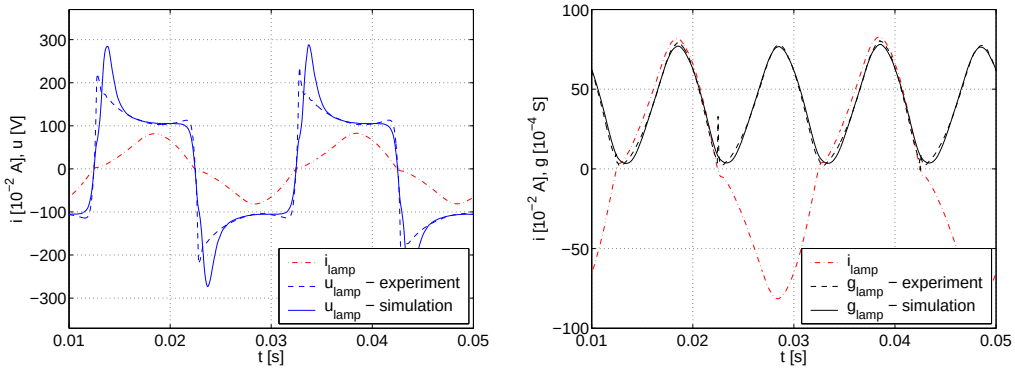

(a) lamp voltage

(b) lamp conductivity

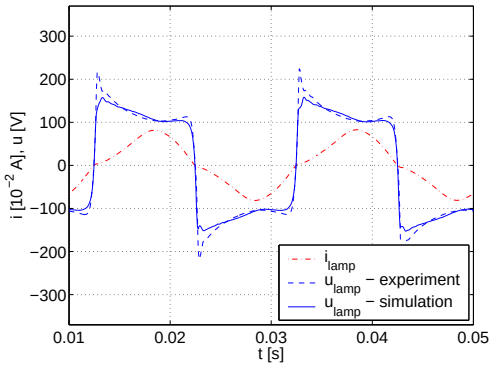

(c) lamp voltage

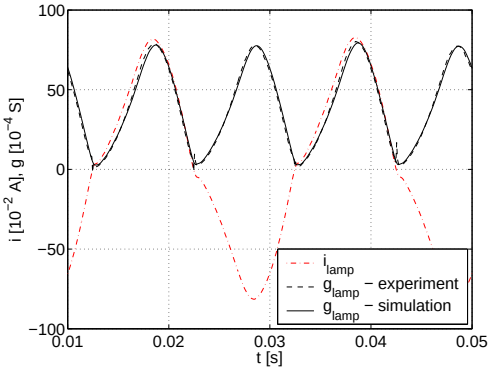

(d) lamp conductivity

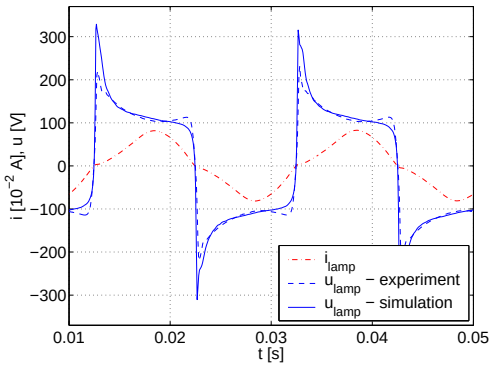

(e) lamp voltage

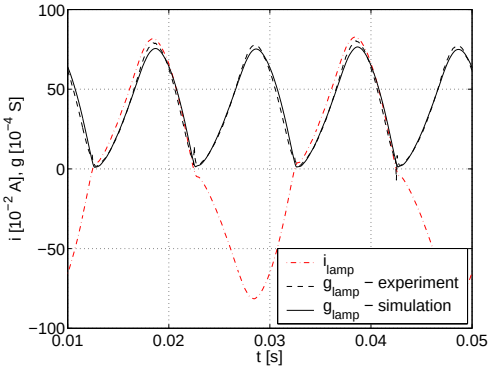

(f) lamp conductivity

Figure 6.9: Experimental and simulated lamp voltage and conductivity of 58 W fluorescent lamp with polynomial (a)–(b); quadratic (c)–(d); exponential (e)–(f) lamp model application.

6.5.3 Experimental verification with 400 W HPML

The polynomial lamp model with experimental lamp current source from `HPML400W.mat` file, with settings in table 6.3 was used. The results of verification is shown in figure 6.10.

Table 6.3: Settings of simulation with polynomial type of lamp model of 400 W HPML.

model	`xp`							`fraG`	`eqE`
type	a_2	a_1	b_3	b_2	b_1	b_0	qu		
poly	5.4	0	0	104230	85	0	0.00227	0	0

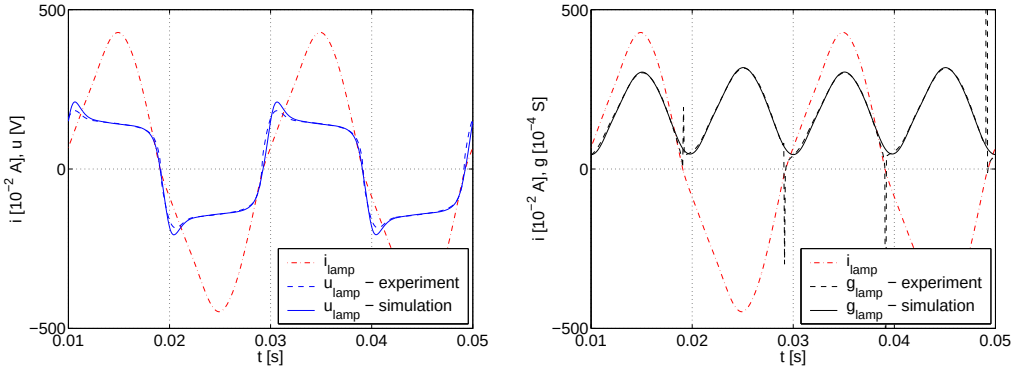

(a) lamp voltage (b) lamp conductivity

Figure 6.10: Experimental and simulated lamp voltage and conductivity of 58 W fluorescent lamp with polynomial lamp model application.

Simulation characteristics from the polynomial model describes lamp behaviour at low frequency operation compare to experiment very well. Unfortunately there are no experimental data at high frequency operation for the verification.

6.5.4 Experimental verification with 400 W HPSL

The polynomial lamp model with experimental lamp current source from `HPSL400W.mat` file, with settings in table 6.4 was used. The results of verification is shown in figure 6.11.

Table 6.4: Settings of simulation with polynomial type of lamp model of 400 W HPSL.

model	`xp`							`fraG`	`eqE`
type	a_2	a_1	b_3	b_2	b_1	b_0	qu		
poly	21	0	0	100171	299	0	0.01049	0	0

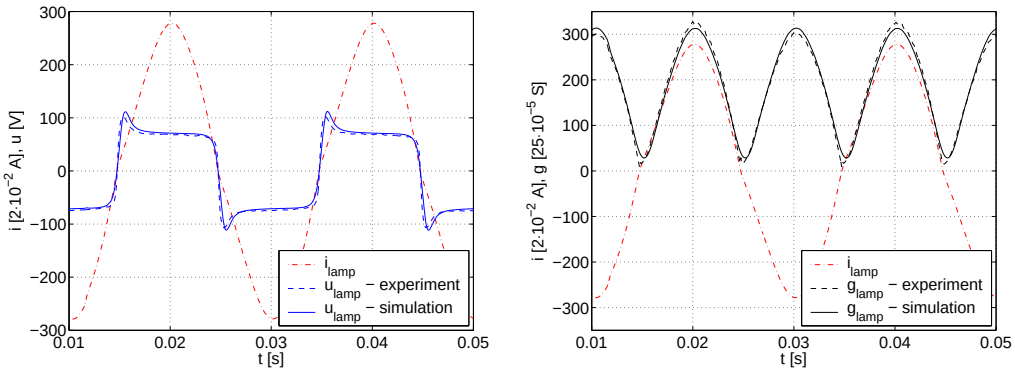

(a) lamp voltage (b) lamp conductivity

Figure 6.11: Experimental and simulated lamp voltage and conductivity of 58 W fluorescent lamp with polynomial lamp model application.

Simulation characteristics from the polynomial model describes behaviour of this lamp type at certain condition compare to experiment very well as it is mentioned in previous case for HPML.

Chapter 7

Conclusion

The modelling of discharge lamps is not a simple task, mainly due to the fact that the discharge is a complex phenomenon which involves electrical, chemical, thermal and optical characteristics.

This thesis studies low and high pressure electric discharge lamps from the electrical point of view. It is focused on stable operation behaviour of such highly nonlinear electric loads.

It presents briefly the vast field of the theory of electric discharges used partially in lighting applications and modelling used for discharge lamps description for electric circuit simulations.

Two optimal structures of lamp models for low (5.3) and high pressure (5.13) discharge lamps based on the equivalent conductivity function of the lamp current and several parameters were proposed.

The methodology of parameters searching was exposed as the offline identification where the iterative or non-iterative approaches were applied. Problems with conductivity computation from measured lamp voltage u_{lamp} and current i_{lamp} were solved. So the parameters are determined from measurements only and no manufactures' data are required. A graphical user interface for the iterative method was designed in GUIDE Matlab environment.

The simulation of models with identified parameters was verified against measured data in Matlab Simulink. The models approximate measurements for certain operation very well, but applicability in wide range of frequency or powers is discutable. Because model parameters are semi-constants and depend on input signals, the identification for other operation state is needed. The parameters' dependence can be explored in further research work.

Bibliography

[ABF+02a] J.C. Antón, C. Blanco, F. Ferrero, P. Roldán, and G. Zissis. An equivalent conductance model for high intensity discharge lamps. In *IEEE Industry Applications Conference. 37th IAS Annual Meeting*, pages 1494–1498. Pittsburgh, USA, Oct 13th–18th 2002.

[ABF+02b] J.C. Antón, C. Blanco, F. Ferrero, P. Roldán, and G. Zissis. Simulation of the dynamic behavior of HID lamps based on electrical conductance. In *IEEE IECON*. Sevillia, 2002.

[ABN00] R. M. S. Almeida, M. S. Benilov, and G. V. Naidis. Simulation of the layer of non-equilibrium ionization in a high-pressure argon plasma with multiply-charged ions. *Journal of Physics D: Applied Physics*, 33(8):960–967, 2000. ISSN 0022-3727.

[ABV+04] J. C. Alvarez, C. Blanco, J. Viera, N. Bordel, A. Martín, and G. Zissis. Electrical conductivity model for HID lamps. In *Light Sources 2004, Proceedings of the 10th International Symposium on the Science and Technology of Light Sources (LS10)* [RKM04], pages 259–260. ISBN 0-7503-1007-3.

[BAC04] S. Bhosle, M. Aubès, and M. Cristea. Acoustic resonance in HID lamps. In *Light Sources 2004, Proceedings of the 10th International Symposium on the Science and Technology of Light Sources (LS10)* [RKM04], pages 35–40. ISBN 0-7503-1007-3.

[BC04] C. Boffito and A. Corazza. Getters for Lighting Applications. In *Light Sources 2004, Proceedings of the 10th International Symposium on the Science and Technology of Light Sources (LS10)* [RKM04], pages 95–104. ISBN 0-7503-1007-3.

[BD04] D. Buso and J. J. Dammelincourt. Thermodynamic modelling of fluorescent lamp electrodes. In *Light Sources 2004, Proceedings*

of the 10^{th} *International Symposium on the Science and Technology of Light Sources (LS10)* [RKM04], pages 499–500. ISBN 0-7503-1007-3.

[Ben00] M. S. Benilov. Collision-dominated to collisionless electron-free space-charge sheath in a plasma with variable ion temperature. *Physics of Plasma*, 7(11):4403–4411, 2000. ISSN 1070-664X.

[Ben01] M. S. Benilov. Near-cathode phenomena in HID lamps. *IEEE Transactions on Industry Applications*, 37(4):986–993, Jul–Aug 2001. ISSN 0093-9994.

[BV04] C. Blanco-Viejo. COST 529 - short term mission report. Technical report, TUL, Liberec, September 17–25 2004.

[BVAF+07] C. Blanco-Viejo, J. C. Alvarez, V. Ferrero, J. C. Campo, M. González, and G. Zissis. A Discharge Lamp Model Based on Lamp Dynamic Conductance. Unpublished article, May 2007.

[BYSG02] S. Ben-Yaakov, M. Shvartsas, and S. Glozman. Statics and dynamics of fluorescent lamps operating at high frequency: Modeling and simulation. *IEEE Trans. Applicat. Ind.*, 38:1486–1492, Nov./Dec. 2002.

[BYSL02] S. Ben-Yaakov, M. Shvartsas, and J. Lester. A behavioral SPICE compatible model of an electrodeless fluorescent lamp. In *IEEE Applied Power Electronics Conference and Exposition, APEC 2002* 17^{th}. Dallas, 2002. ISBN 0-7803-7404-5.

[Cal] J. B. Calvert. Electrical discharges. http://www.du.edu/~jcalvert/phys/dischg.htm.

[CFS+01] M. Cervi, E. C. Fortes, A. R. Seidel, F. E. Bisogno, and R. N. do Prado. Fluorescent lamp model employing tangent approximation. In *Power Electronics Specialists Conference, PESC 2002. IEEE* 33^{rd} *Annual*, volume 1, pages 187–191, 2001. ISBN 0-7803-7262-X.

[COSa] COST - European Cooperation in the field of Scientific and Technical Research. http://www.cost.esf.org.

[COSb] Efficient lighting for the 21^{st} century 2001–2006, COST action no. 529. http://www.efficient-lighting.org.

[DKD+06] P. Dupuis, J. Koprnický, J. Driesen, R. Belmans, and A. Richter. High intensity discharge (HID) lamps conductance model computation. Unpublished article, May 2006.

[Dup05] P. Dupuis. COST 529 - short term mission report. Technical report, TUL, Liberec, June 2005.

[DZ04] J.-J. Damelincourt and G. Zissis. Calculation of the discharge conductance G, May 11–12 2004.

[Eea] John W. Eaton and et. al. GNU Octave high-level language. http://www.gnu.org/software/octave/.

[Fle06] P. Flesch. *Light and Light Sources. High-Intensity Discharge Lamps*. Springer, Berlin, June 2006. ISBN 3-540-32684-7.

[Fra48] V. J. Francis. *Fundamentals of discharge tube circuits*. J. Wiley & Sons Inc., New York, 1948. 39 pp.

[GE] GE. Product catalogue of GE Lighting. http://www.gelighting.com/na.

[Gen] M. F. Gendre. Electric Light Source – History in a Nutshell. http://www.lampreview.net/.

[Ger] S. Gershman. Structure of a DC Glow Discharge. http://science-education.pppl.gov/SummerInst/SGershman/Structure_of_Glow_Discharge.pdf.

[Gro67] B. Gross. *Elektrické výboje v plynech*. SNTL, Praha, 1967. ISBN 04-019-67.

[Hab95] J. Habel. *Světelná technika a osvětlení*. FCC Public, Praha, 1995. ISBN 80-901985-0-3.

[Her80] P. R. Herrick. Mathematical models for High-Intensity Discharge lamps. *IEEE Trans. Applicat. Ind.*, 16(5):648–654, Sept./Oct. 1980.

[Hu01] Y. Hu. Analysis and Design of High-Intensity-Discharge Lamp Ballast for Automotive Headlamp, 2001.

[Kik] Kikusui electronics corporation. *Multifunctional AC Power Supply PCR-LA Series*. http://www.kikusui.co.jp/common/product/pdf/pcr-la.pdf.

[KN03] J. Koprnický and M. Novák. Electric parameters of the metal halide lamp with ceramic discharge tube. In *Proceedings ECMS, 6th International Workshop on Electronic, Control, Measurement and Signals*, pages 374–378. Technical University, Liberec, June 2–4 2003. ISBN 80-7083-708-X.

[Kob04] A Kobrle. Modelování světelných výbojů. Master's thesis, FM TUL, Liberec, Czech Republic, June 2004.

[Kop05a] J. Koprnický. Conductivity model of discharge lamps for electric circuits modelling. In *Proceedings ECMS 2005, Electronique, Cotrôle, Modélisation, Mesure et Signal*. Université Paul Sabatier, Toulouse, May 17–20 2005, [CD-ROM] file://ECMS05/SplénièresECMS05etED/J-Koprnicky.pdf.

[Kop05b] J. Koprnický. Účinné osvětlení pro 21. století. *Elektroinstalatér*, XI(5):62, October 2005. ISSN 1211-2291.

[KVR06] J. Koprnický, J. Václavík, and A. Richter. Electric conductivity model of discharge lamps. In *COST Model inventory workshop*. Mierlo, NL, March/April 2006.

[LC04] B. Lafitte and J. J. Curry. Bench-top x-ray absorption imagining of Hg in ceramic metal-halide lamps. In *Light Sources 2004, Proceedings of the 10th International Symposium on the Science and Technology of Light Sources (LS10)* [RKM04], pages 333–334. ISBN 0-7503-1007-3.

[Lis92] G. G. Lister. Low-pressure gas discharge modelling. *Journal of Physics D: Applied Physics*, 25:1649–1680, December 1992.

[LLLG04] G. G. Lister, J. E. Lawler, W. P. Lapatovich, and V. A. Godyak. The physics of discharge lamps. *Reviews of modern physics*, 76: 541–598, April 2004.

[LMT+04] K. H. Loo, G. J. Moss, R. C. Tozer, D. A. Stone, M. Jinno, and R. Devonshire. A dynamic collisional-radiative model of a low-pressure mercury-argon discharge lamp: a physical approach to modeling fluorescent lamps for circuit simulations. *IEEE Trans. Power Electron.*, 19(4):1117 – 1129, July 2004.

[LSTD05] K. H. Loo, D. A. Stone, R. C. Tozer, and R. Devonshire. A dynamic conductance model of fluorescent lamp for electronic

ballast design simulation. *IEEE Trans. Power Electron.*, 20(5): 1178 – 1185, Sep 2005.

[Mat] The MathWorks. Online documentation for MATLAB. http://www.mathworks.com/access/helpdesk/help/helpdesk.html.

[Mel] J. Melis. Electronic ballasts for HID lamps. http://www.ballastdesign.com/.

[Miš79] S. Miškařík. *Moderní zdroje světla.* SNTL, Praha, 1979. ISBN 04-509-79.

[Mod04] O. Modrlák. *Úvod do identifikace.* TU of Liberec, http://www.fm.vslib.cz/~krtsub/fm/modrlak/pdf/tar1_zid.pdf edition, 2004.

[MT04a] M. A. Malkov and V. A. Terekhin. Calculation of a near-wall sheath of space charge inHg-Ar low pressure discharge. In *Light Sources 2004, Proceedings of the* 10^{th} *International Symposium on the Science and Technology of Light Sources (LS10)* [RKM04], pages 203 – 204. ISBN 0-7503-1007-3.

[MT04b] M. A. Malkov and V. A. Terekhin. Calculation of drift velocity of ions of mercury in a nonuniform electric field in a Hg-Ar low pressure discharge. In *Light Sources 2004, Proceedings of the* 10^{th} *International Symposium on the Science and Technology of Light Sources (LS10)* [RKM04], pages 205 – 206. ISBN 0-7503-1007-3.

[MT04c] M. A. Malkov and V. A. Terekhin. Radial distributions of densities of charged particles, electric field strength and potential in a positive column of the Hg-Ar discharge. In *Light Sources 2004, Proceedings of the* 10^{th} *International Symposium on the Science and Technology of Light Sources (LS10)* [RKM04], pages 201 – 202. ISBN 0-7503-1007-3.

[NG01] A. Nachbaur and C. Ganahl. Lamp-modelling, from the measurement to the simulation model. In *IEEE Industry Applications Conference,* 36^{th} *IAS Annual Meeting*, volume 2, pages 1254–1259. Chicago, USA, 2001. ISBN 0-7803-7114-3.

[Nov03] M. Novák. *Přechodový děj při zapnutí transformátoru, způsoby omezování zapínacího proudu.* PhD thesis, Technical University of Liberec, Czech Republic, 2003.

[NV01] M. Novák and J. Václavík. Model and measurement of mini-lighting network. Technical report, TUL and UPS, Toulouse, October 2001.

[NV04] M. Novák and J. Václavík. Oscillation in power net. Technical report, TUL and UPS, Toulouse, September 2004.

[NVR02] M. Novák, J. Václavík, and A. Richter. Measurement of the city lighting network. Technical report, TUL and UPS, Toulouse, May–June 2002.

[OSR] OSRAM. Product catalogue of Osram. http://catalog.myosram.com.

[PHIa] PHILIPS. *Application guide to lamp control gear 'TL', CFL, QL and halogen lamps*. http://www.ueen.feec.vutbr.cz/cz/kos/applgfluo.pdf>.

[PHIb] PHILIPS. Product catalogue of lighting of Philips. http://www.lighting.philips.com/gl_en/catalogue.

[Ric01] A. Richter. Elektrické parametry a energetická bilance zářivkového výboje. In *Sborník EPVE 2001*. VUT FEI UVEE Brno, 2001. ISBN 80-214-1987-3.

[RKM04] A. Richter, J. Koprnický, and J. Mareš. Conductance model of discharge lamps, parameter verification and identification for modelling of electric circuits in light-nets. In *Light Sources 2004, Proceedings of the* 10^{th} *International Symposium on the Science and Technology of Light Sources (LS10)*, pages 555–556. Toulouse, July 18–22 2004. ISBN 0-7503-1007-3.

[RMRJZ02] P. Rossat-Mignod, G. Rojat, Ch. Joubert, and G. Zissis. Constraints generated by fluorescents lamps on the electrical network. In *IEEE Industry Applications Conference.* 37^{th} *IAS Annual Meeting*, pages 355–362. Pittsburgh, USA, Oct 13^{th}–18^{th} 2002.

[RR98] T. J. Ribarich and J. J. Ribarich. A New High-Frequency Fluorescent Lamp Model. *IEEE Trans. Applicat. Ind.*, 3:2094–2098, October 12-16 1998.

[RRK98] A. Richter, P. Rydlo, and E. Konečná. Harmonické zkreslení jednofázové sítě. In *Sborník ze 7. semináře Kvalita energie, Dynamika systémů*, pages 29–33. KTE FEI VŠB TU Ostrava, April 22^{nd} 1998. ISBN 80-7078-554-3.

[Ruf05] J. B. Ruffet. *Modelisation des lampes a descharge aux halogenures metalliques avec enveloppe en ceramique a l'ade d'un code fluide.* PhD thesis, Université Paul Sabatier de Toulouse III, France, 2005.

[Ryb99] J. Rybička. *LaTeXpro začátečníky.* Konvoj, Brno, 1999. ISBN 80-85615-42-8.

[SBY99] Moshe Shvartsas and Sam Ben-Yaakov. A SPICE compatible model of High Intensity Discharge lamps. In *Power Electronics Specialists Conference, 1999. PESC 1999.* 30^{th} *Annual IEEE*, volume 2, pages 1037 – 1042. Charleston, SC, USA, Jun./Jul. 1999. ISBN 0-7803-5421-4.

[Sta84] M Stambouli. *Modélisation d'une Décharge de Mercure Haute Pression: Application à l'Analyse de Circuits Électriques comportant des Lampes à Décharge.* PhD thesis, ENSET, Tunis, Avril 1984.

[TPP+04] J. L. Tapia, J. Pacheco, M. Pacheco, G. Zissis, and J. J. Gonzalez. Arc discharge model as a two terminal electronic device. In *Light Sources 2004, Proceedings of the* 10^{th} *International Symposium on the Science and Technology of Light Sources (LS10)* [RKM04], pages 473–474. ISBN 0-7503-1007-3.

[Tri] Tridonic. Datasheet of digital electronic ballast PCI 150. http://www.tridonicatco.com/kms/media/uploads/products/hid_0607_291_en.pdf.

[VK03] J. Václavík and J. Koprnický. COST 529 – short term mission report. Technical report, CPAT, Toulouse, May 12–23 2003.

[VLH+98] T. Vos, F. Ligthart, M. Hendrix, T. Stommen, U. Chittka, J. v. d. Mullen, and W. v. d. Bosh. Modelling fluorescent lamps for power supply design. In *Proceedings of the* 8^{th} *International Symposium on the Science and Technology of Light Sources (LS-8)*. Greifswald, 1998.

[Way71] J. F. Waymouth. *Electric Discharge Lamps*. The M.I.T. Press, Cambridge, Massachusetts and London, England, 1971. ISBN 0-262-23048-8.

[Way91] J. F. Waymouth. LTE and Near-LTE Lighting Plasmas. *IEEE Trans. Plasma Sci.*, 19(6):1003–1012, Dec. 1991.

[Wha00a] D. Wharnby. Discharge lamps physics. In *IAS IEEE Annual Meeting*. Roma, October 8–12 2000.

[Wha00b] D. Wharnby. Electrodes for fluorescent lamps. In *IAS IEEE Annual Meeting*. Roma, October 8–12 2000.

[Wha02] D. Wharnby. Science and technology of light sources state of the artfuture challenges. In *COST meeting*. Toulouse, 2002.

[WWRN03] D. Wharnby, R. Weitzel, A. Richter, and M. Novák. Science and technology of power systems for light sources, state of the art, future challenges. In *Proceedings ECMS, 6th International Workshop on Electronic, Control, Measurement and Signals*. Technical University, Liberec, June 2–4 2003. ISBN 80-7083-708-X.

[YH05] W. Yan and S. Y. R. Hui. A universal PSpice model for HID lamps. *IEEE Trans. Applicat. Ind.*, 41(6):1594–1602, Nov./Dec. 2005.

[ZAS+92] G. Zissis, M. Aubes, N. Sewraj, M. Stambouli, N. Elleuch, and M. Annabi. Simulation d'une installation d'éclairage utilisant des lampes à décharge dans la vapeur de mercure hp, alimentée par un transformateur triphase. *Extraits de la Revue générale de l'Eletricité*, 1, Janvier 1992.

[ZD02] G. Zissis and J.-J. Damelincourt. Modelling discharge lamps for electronic circuit designers: a review of the existing methods. In *The 29th IEEE International Conference on Plasma Sciences (ICOPS2002)*, page 318. Banff, Canada, May 26–30 2002.

[Zis05] G. Zissis. Light Sources: what evolution for the future? Sources de lumière artificielle, Quel avenir? In *Proceedings ECMS 2005, Electronique, Contrôle, Modélisation, Mesure et Signal*. Université Paul Sabatier, Toulouse, Mai 17–20 2005, [CD-ROM].

Appendix A

Appendices

A.1 Functions of PEM Toolbox of KEL TUL

Table A.1: Used functions of Power Electronics Matlab Toolbox of KEL TUL.

cutdc.m	Cut off a DC part of a signal.
efektiv.m	An effective (RMS) value of a signal.
fazor.m	A generation of a phasor of a signal in complex space.
perioda.m	A period of a signal.
pf.m	An evaluation of a Power Factor λ of signals u and i.
pvykon.m	A real power evaluation.
qvykon.m	A reactive power evaluation.
stredni.m	An average value of a signal.
svykon.m	A complex power evaluation.
thd.m	A total harmonic distortion.

A.2 Parameters of the data acquisition device EMU-2

Table A.2: Parameters of EMU-2 measurement device [Nov03].

Parameter	Value	Commentary
Power supply		
Supply voltage	230 V	
Input power	36 W	
Central processing unit		
Computing power	40 MIPS	ADSP21 061
Operation in floating point	120 MFLOPS	
Memory in processor	128 kB	
Cash DRAM	up to 64 MB	SIMM72
Ethernet interface		
Physical layer	TP	RTL8019AS
Velocity	10 Mb/s	
Protocol	UDP/IP	
Analog inputs		
Resolution	16 b	AD73360
Sampling rate	0.4-12.8 kSa/s	parallel in all channels
Low voltage inputs – BNC		
Number	9 channels	
Ranges	±150 mV; ±1 V; ±5 V; ±15 V	
Input resistor	1 MΩ	
SNR	70 dB	
High voltage inputs		
Number	9 channels	
Range	±750 V	
Input resistor	10 MΩ	
SNR	70 dB	

A.3 Voltage-current characteristics of discharge lamps

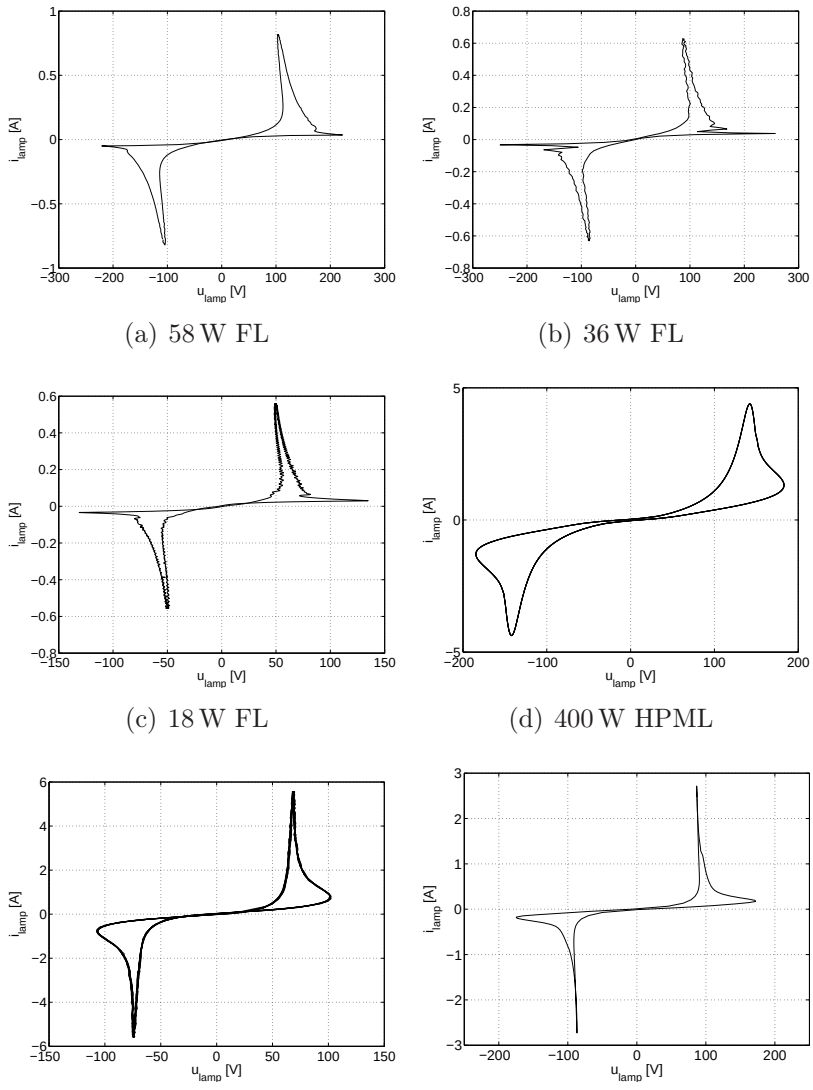

(a) 58 W FL (b) 36 W FL

(c) 18 W FL (d) 400 W HPML

(e) 400 W HPSL (f) 150 W MHL

Figure A.1: Voltage-current characteristics for measured discharge lamps.

A.4 Different frequency of the supply voltage

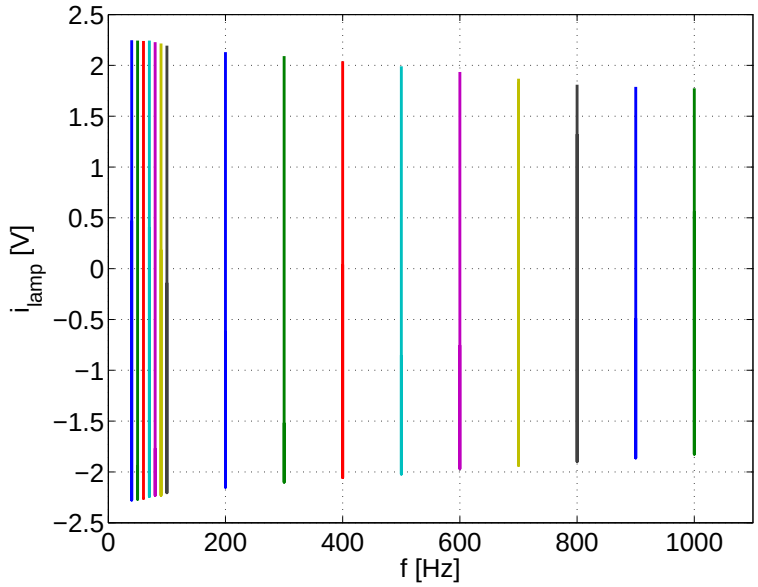

(a) $i_{lamp} = f(f)$

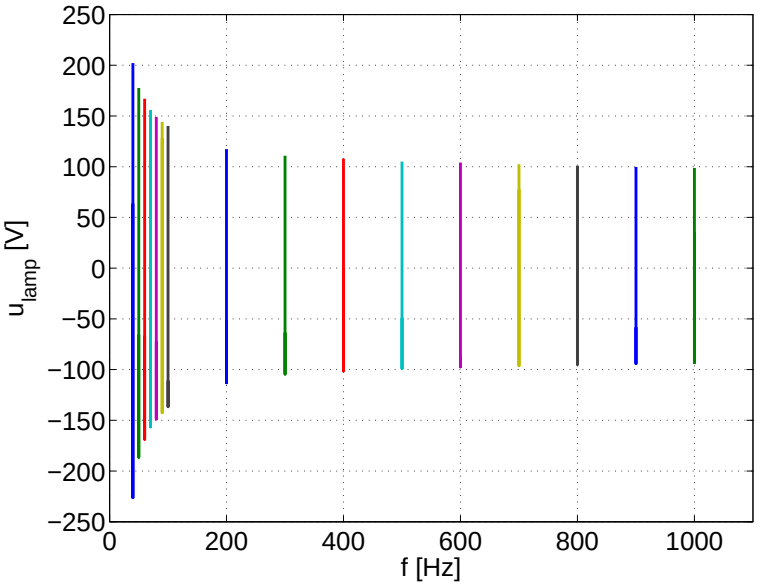

(b) $u_{lamp} = f(f)$

Figure A.2: Function of current and voltage of metal halide lamp on frequency of supply voltage.

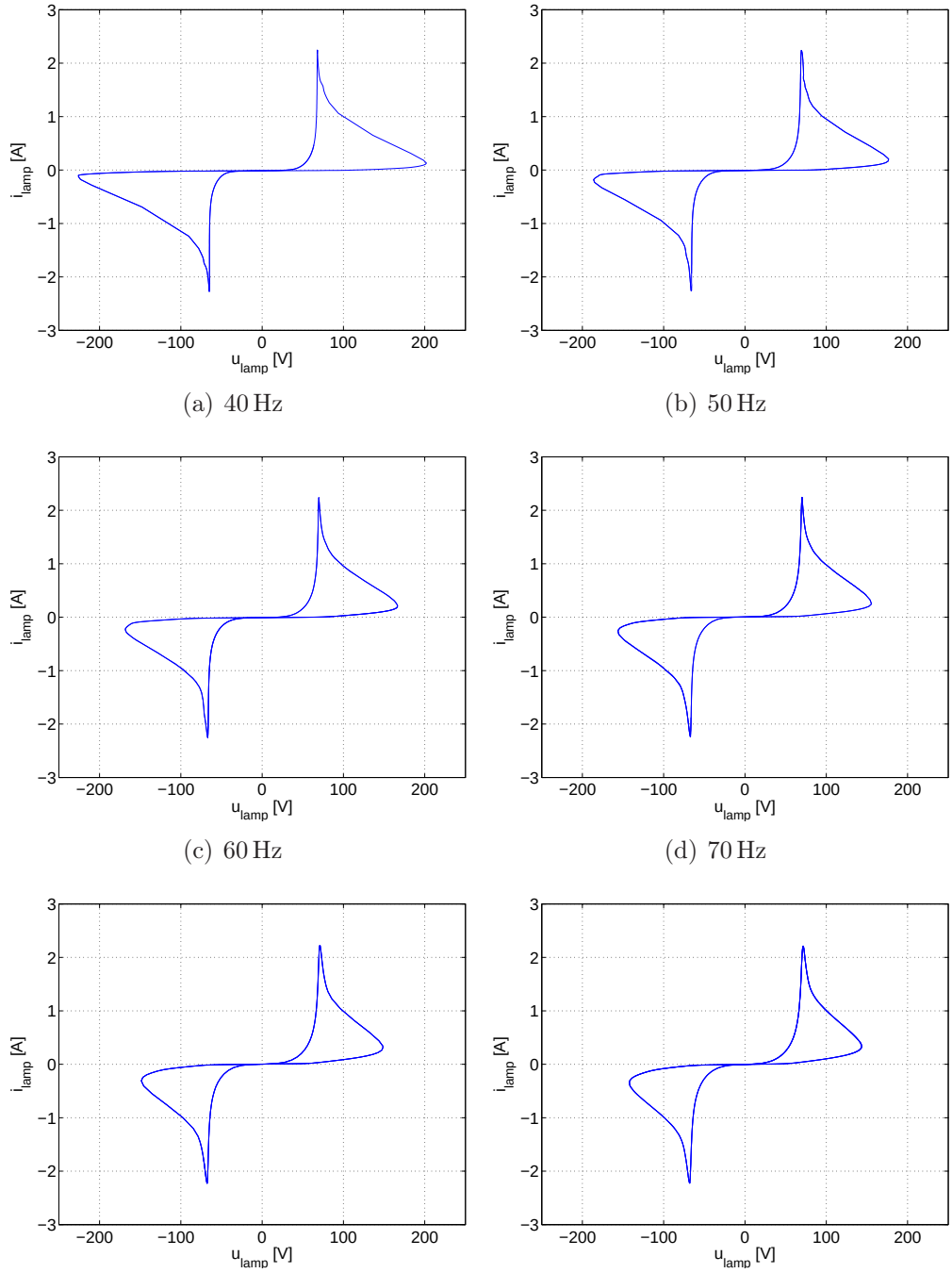

(a) 40 Hz (b) 50 Hz

(c) 60 Hz (d) 70 Hz

(e) 80 Hz (f) 90 Hz

Figure A.3: Voltage-current characteristics for frequencies of supply voltage in range 40 Hz up to 90 Hz.

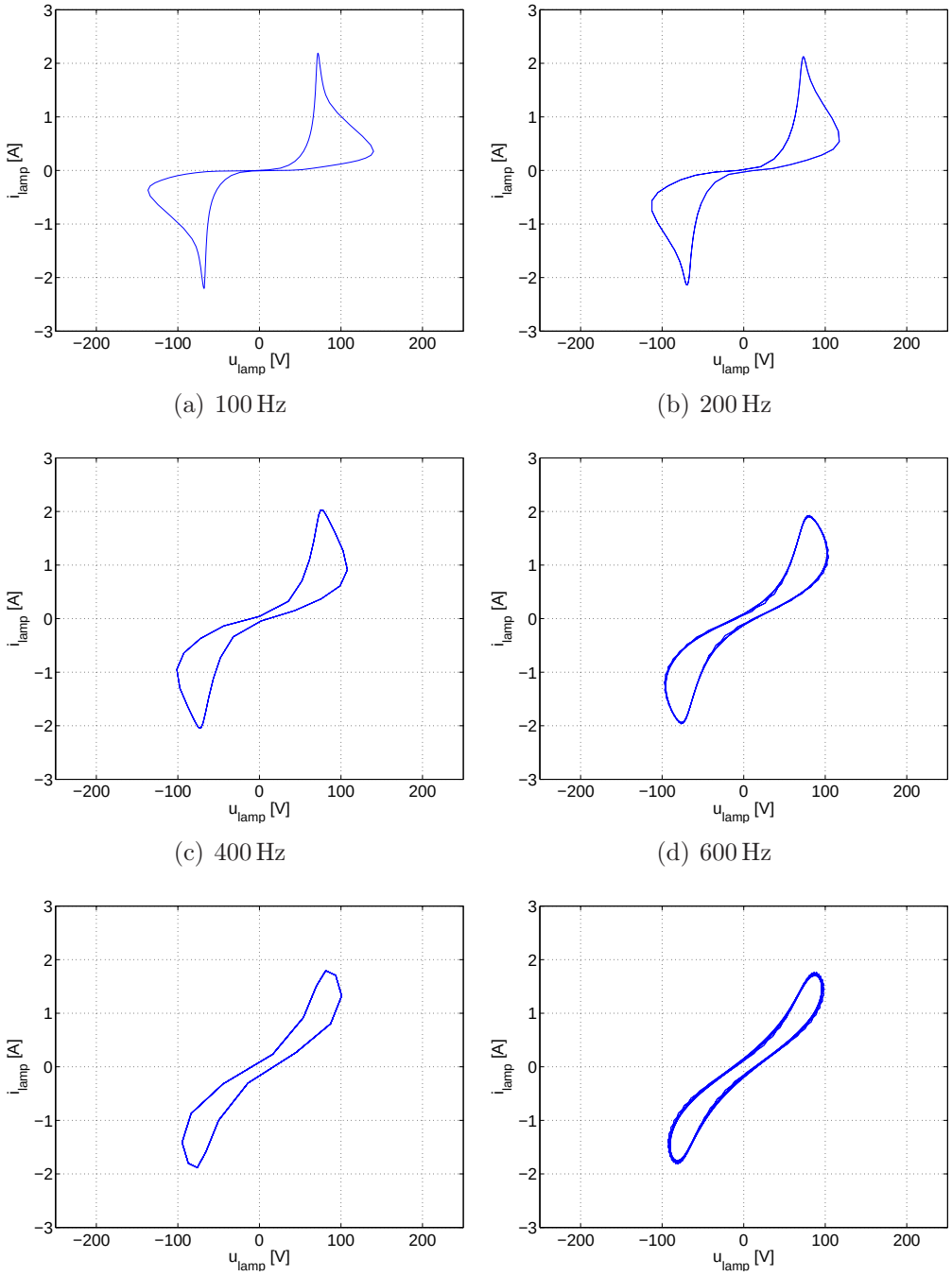

(a) 100 Hz (b) 200 Hz

(c) 400 Hz (d) 600 Hz

(e) 800 Hz (f) 1000 Hz

Figure A.4: Voltage-current characteristics for frequencies of supply voltage in range 100 Hz up to 1000 Hz.

Table A.3: Parameters for different voltage frequencies of 40–60 Hz for MHL.

Parameters for 40 Hz					
U_{net}	=	229 V	U_{lamp}	=	92 V
I_{lamp}	=	1.43 A	G_{lamp}	=	21 mS
P_{net}	=	310 W	P_{lamp}	=	76 W
Q_{net}	=	108 VAr	Q_{lamp}	=	107 VAr
S_{net}	=	328 VA	S_{lamp}	=	131 VA
R_{ball}	=	114.4 Ω	L_{ball}	=	12 mH
THD_{lamp} V	=	62.66 %	THD_{net} V	=	0 %
THD_{lamp} A	=	30.58 %	λ_{lamp}	=	0.579
Parameters for 50 Hz					
U_{net}	=	229 V	U_{lamp}	=	83 V
I_{lamp}	=	1.45 A	G_{lamp}	=	21 mS
P_{net}	=	319 W	P_{lamp}	=	80 W
Q_{net}	=	91 VAr	Q_{lamp}	=	90 VAr
S_{net}	=	331 VA	S_{lamp}	=	120 VA
R_{ball}	=	113.7 Ω	L_{ball}	=	9 mH
THD_{lamp} V	=	57.31 %	THD_{net} V	=	0 %
THD_{lamp} A	=	25.16 %	λ_{lamp}	=	0.666
Parameters for 60 Hz					
U_{net}	=	229 V	U_{lamp}	=	81 V
I_{lamp}	=	1.45 A	G_{lamp}	=	21 mS
P_{net}	=	321 W	P_{lamp}	=	82 W
Q_{net}	=	85 VAr	Q_{lamp}	=	83 VAr
S_{net}	=	332 VA	S_{lamp}	=	117 VA
R_{ball}	=	113.7 Ω	L_{ball}	=	9 mH
THD_{lamp} V	=	54.18 %	THD_{net} V	=	0 %
THD_{lamp} A	=	23.63 %	λ_{lamp}	=	0.701

Table A.4: Parameters for different voltage frequencies of 70–90 Hz for MHL.

Parameters for 70 Hz					
U_{net}	=	229 V	U_{lamp}	=	79 V
I_{lamp}	=	1.44 A	G_{lamp}	=	21 mS
P_{net}	=	321 W	P_{lamp}	=	83 W
Q_{net}	=	80 VAr	Q_{lamp}	=	78 VAr
S_{net}	=	331 VA	S_{lamp}	=	114 VA
R_{ball}	=	114.8 Ω	L_{ball}	=	8 mH
THD_{lamp} V	=	51.13 %	THD_{net} V	=	0 %
THD_{lamp} A	=	22.04 %	λ_{lamp}	=	0.729
Parameters for 80 Hz					
U_{net}	=	229 V	U_{lamp}	=	78 V
I_{lamp}	=	1.44 A	G_{lamp}	=	20 mS
P_{net}	=	320 W	P_{lamp}	=	84 W
Q_{net}	=	76 VAr	Q_{lamp}	=	74 VAr
S_{net}	=	329 VA	S_{lamp}	=	112 VA
R_{ball}	=	113.8 Ω	L_{ball}	=	8 mH
THD_{lamp} V	=	48.77 %	THD_{net} V	=	0 %
THD_{lamp} A	=	20.75 %	λ_{lamp}	=	0.749
Parameters for 90 Hz					
U_{net}	=	229 V	U_{lamp}	=	77 V
I_{lamp}	=	1.43 A	G_{lamp}	=	20 mS
P_{net}	=	320 W	P_{lamp}	=	85 W
Q_{net}	=	74 VAr	Q_{lamp}	=	72 VAr
S_{net}	=	328 VA	S_{lamp}	=	111 VA
R_{ball}	=	114.9 Ω	L_{ball}	=	7 mH
THD_{lamp} V	=	47.14 %	THD_{net} V	=	0 %
THD_{lamp} A	=	20.28 %	λ_{lamp}	=	0.763

Table A.5: Parameters for different voltage frequencies of 100–300 Hz for MHL.

Parameters for 100 Hz					
U_{net}	=	229 V	U_{lamp}	=	77 V
I_{lamp}	=	1.42 A	G_{lamp}	=	20 mS
P_{net}	=	316 W	P_{lamp}	=	84 W
Q_{net}	=	72 VAr	Q_{lamp}	=	69 VAr
S_{net}	=	324 VA	S_{lamp}	=	108 VA
R_{ball}	=	115.1 Ω	L_{ball}	=	7 mH
THD_{lamp} V	=	45.61 %	THD_{net} V	=	0 %
THD_{lamp} A	=	19.36 %	λ_{lamp}	=	0.775
Parameters for 200 Hz					
U_{net}	=	229 V	U_{lamp}	=	74 V
I_{lamp}	=	1.38 A	G_{lamp}	=	19 mS
P_{net}	=	309 W	P_{lamp}	=	86 W
Q_{net}	=	61 VAr	Q_{lamp}	=	55 VAr
S_{net}	=	315 VA	S_{lamp}	=	102 VA
R_{ball}	=	117.6 Ω	L_{ball}	=	5 mH
THD_{lamp} V	=	36.21 %	THD_{net} V	=	0 %
THD_{lamp} A	=	15 %	λ_{lamp}	=	0.84
Parameters for 300 Hz					
U_{net}	=	228 V	U_{lamp}	=	73 V
I_{lamp}	=	1.35 A	G_{lamp}	=	18 mS
P_{net}	=	304 W	P_{lamp}	=	86 W
Q_{net}	=	57 VAr	Q_{lamp}	=	48 VAr
S_{net}	=	309 VA	S_{lamp}	=	99 VA
R_{ball}	=	119.1 Ω	L_{ball}	=	5 mH
THD_{lamp} V	=	37.29 %	THD_{net} V	=	19.94 %
THD_{lamp} A	=	24.09 %	λ_{lamp}	=	0.875

Table A.6: Parameters for different voltage frequencies of 400–600 Hz for MHL.

Parameters for 400 Hz					
U_{net}	=	228 V	U_{lamp}	=	73 V
I_{lamp}	=	1.33 A	G_{lamp}	=	17 mS
P_{net}	=	298 W	P_{lamp}	=	87 W
Q_{net}	=	55 VAr	Q_{lamp}	=	43 VAr
S_{net}	=	303 VA	S_{lamp}	=	97 VA
R_{ball}	=	119.3 Ω	L_{ball}	=	4 mH
THD_{lamp} V	=	26.39 %	THD_{net} V	=	0 %
THD_{lamp} A	=	10.81 %	λ_{lamp}	=	0.897
Parameters for 500 Hz					
U_{net}	=	227 V	U_{lamp}	=	72 V
I_{lamp}	=	1.31 A	G_{lamp}	=	17 mS
P_{net}	=	292 W	P_{lamp}	=	86 W
Q_{net}	=	53 VAr	Q_{lamp}	=	38 VAr
S_{net}	=	297 VA	S_{lamp}	=	94 VA
R_{ball}	=	120 Ω	L_{ball}	=	4 mH
THD_{lamp} V	=	22.86 %	THD_{net} V	=	0 %
THD_{lamp} A	=	8.13 %	λ_{lamp}	=	0.914
Parameters for 600 Hz					
U_{net}	=	226 V	U_{lamp}	=	72 V
I_{lamp}	=	1.29 A	G_{lamp}	=	17 mS
P_{net}	=	286 W	P_{lamp}	=	86 W
Q_{net}	=	51 VAr	Q_{lamp}	=	34 VAr
S_{net}	=	291 VA	S_{lamp}	=	93 VA
R_{ball}	=	120.2 Ω	L_{ball}	=	4 mH
THD_{lamp} V	=	43.96 %	THD_{net} V	=	38.12 %
THD_{lamp} A	=	39.32 %	λ_{lamp}	=	0.93

Table A.7: Parameters for different voltage frequencies of 700–900 Hz for MHL.

Parameters for 700 Hz					
U_{net}	=	225 V	U_{lamp}	=	72 V
I_{lamp}	=	1.26 A	G_{lamp}	=	16 mS
P_{net}	=	280 W	P_{lamp}	=	86 W
Q_{net}	=	50 VAr	Q_{lamp}	=	30 VAr
S_{net}	=	285 VA	S_{lamp}	=	91 VA
R_{ball}	=	122.8 Ω	L_{ball}	=	4 mH
THD_{lamp} V	=	24.78 %	THD_{net} V	=	16.23 %
THD_{lamp} A	=	17.89 %	λ_{lamp}	=	0.942
Parameters for 800 Hz					
U_{net}	=	224 V	U_{lamp}	=	71 V
I_{lamp}	=	1.25 A	G_{lamp}	=	17 mS
P_{net}	=	276 W	P_{lamp}	=	85 W
Q_{net}	=	49 VAr	Q_{lamp}	=	27 VAr
S_{net}	=	280 VA	S_{lamp}	=	89 VA
R_{ball}	=	122.2 Ω	L_{ball}	=	4 mH
THD_{lamp} V	=	14.18 %	THD_{net} V	=	0 %
THD_{lamp} A	=	3.86 %	λ_{lamp}	=	0.953
Parameters for 900 Hz					
U_{net}	=	223 V	U_{lamp}	=	71 V
I_{lamp}	=	1.24 A	G_{lamp}	=	16 mS
P_{net}	=	271 W	P_{lamp}	=	84 W
Q_{net}	=	50 VAr	Q_{lamp}	=	25 VAr
S_{net}	=	276 VA	S_{lamp}	=	88 VA
R_{ball}	=	121.6 Ω	L_{ball}	=	3 mH
THD_{lamp} V	=	22.42 %	THD_{net} V	=	16.98 %
THD_{lamp} A	=	17.89 %	λ_{lamp}	=	0.959

Table A.8: Parameters for voltage frequency of 1 kHz for MHL.

Parameters for 1000 Hz					
U_{net}	=	221 V	U_{lamp}	=	70 V
I_{lamp}	=	1.22 A	G_{lamp}	=	16 mS
P_{net}	=	264 W	P_{lamp}	=	83 W
Q_{net}	=	50 VAr	Q_{lamp}	=	23 VAr
S_{net}	=	269 VA	S_{lamp}	=	86 VA
R_{ball}	=	122.3 Ω	L_{ball}	=	3 mH
THD_{lamp} V	=	47.52 %	THD_{net} V	=	45.37 %
THD_{lamp} A	=	45.53 %	λ_{lamp}	=	0.964

A.5 Parameters of lamp models of MHL

Table A.9: Parameters for polynomial model (5.4).

	a_2	a_1	b_3	b_2	b_1	b_0	qu
MHL150WVIS	54	0	0	387211	710	0	0.001825
MHL150WVRS	53.2	0	0	293050	670	0	0.000338
MHL150WHIS	57.3	0	0	466520	1119	0	0.000254
MHL150WVIT	87.4	0	0	535889	1235	0	0.000128
MHL150WHRS220V	54.8	0	0	327806	717	0	0.000412
MHL150WHRS230V	52.5	0	0	288961	653	0	0.000338
MHL150WHRS240V	49.7	0	0	252057	607	0	0.001
MHL150WE	14.4	0	0	219055	-1907	0	0.00033
MHL150WV040Hz	54.7	-0.067	0	216116	831	0	0.004099
MHL150WV050Hz	62	-0.028	0	257955	879	0	0.001865
MHL150WV060Hz	62.5	-0.008	0	265980	878	0	0.001563
MHL150WV070Hz	58.9	-0.006	0	249011	931	0	0.001524
MHL150WV080Hz	57	-0.009	0	244246	944	0	0.001543
MHL150WV090Hz	55.7	-0.012	0	241153	950	0	0.001507
MHL150WV100Hz	55.8	-0.007	0	242195	939	0	0.001470
MHL150WV200Hz	47.6	-0.005	0	223303	686	0	0.001077
MHL150WV300Hz	42.9	-0.007	0	239620	52	0	0.000642
MHL150WV400Hz	21.4	-0.142	0	165194	-1164	0	0.007441
MHL150WV500Hz	30	0.063	0	45116	2125	0	0.002826
MHL150WV600Hz	33	-0.005	0	351095	-2593	0	0.00021
MHL150WV700Hz	30.2	-0.018	0	395223	-3603	0	0.000286
MHL150WV800Hz	22.7	-0.0079	0	380711	-4305	0	0.000044
MHL150WV900Hz	21.1	-0.014	0	445442	-5484	0	0.000815
MHL150WV999Hz	24.5	-0.025	0	670809	-8301	0	0.000286

A.6 Content of CD-ROM

- `Text` - this directory contains text of the thesis in *.pdf and *.ps format; and all used figures in text in *.eps format;
- `Publications` - In this directory are author's publications and presentations of studied problematic.
- `Matlab` - this directory contains measured data, routines for their processing, simulation diagrams, application for identification, materials for text of the thesis *etc.* Some of names of directories don't need more explanation:
  - Experiments
    - `FL18W`
    - `FL36W`
    - `FL58W`
    - `G_filtration` - comparison of different filteres
    - `HPML`
    - `HPSL`
    - `K_functions` - functions used for data processing in experiments and in identification
    - `KEL_functions` - functions of PEM Toolbox of KEL TUL on p. 113
    - `MHL_EB`
    - `MHL_MB`
    - `MHL_MB_voltage_change`
    - `MHL_RB_freq_change`
  - `Identification`
    - `GraphicalInterface`
    - `IdenfificationStat`
  - `ModelsFromPublication`
    - `Anton_exp_2002`
    - `Anton_quad_2002`
    - `Blanco_STSM_2004`
    - `Herrick_1980`
    - `Ribarich_1998`
    - `Stamboulli_1984`

    - `Zissis_2001`
- `negVIchar` - figure of negative V-I characteristic to the text;
- `Simulation`
    - `FL`
    - `HPML`
    - `HPSL`
    - `Lamp_circ_models`
    - `MHL`
- `VirtualExperiments`
    - `MHL_coeficient_variance`
    - `MHL_coeficient_variance_diffWay`